The Biochemical Characterization of αT-Catenin Ligand Binding

by

Jonathon Alan Heier

B.S., University of Wisconsin-Madison, 2013

Submitted to the Graduate Faculty of the

School of Medicine in partial fulfillment

of the requirements for the degree of

Doctor of Philosophy

University of Pittsburgh

2021

UNIVERSITY OF PITTSBURGH

SCHOOL OF MEDICINE

This dissertation was presented

by

Jonathon Alan Heier

It was defended on

July 12, 2021

and approved by

Gerard Apodaca, Professor, Renal Electrolyte Division and Department of Cell Biology

Marijn Ford, Associate Professor, Department of Cell Biology

Yang Hong, Associate Professor, Department of Cell Biology

Lance Davidson, Professor, Department of Bioengineering

Dissertation Director: Adam Kwiatkowski, Associate Professor, Department of Cell Biology

The Biochemical and Molecular Characterization of αT-Catenin

Jonathon Alan Heier, PhD

University of Pittsburgh, 2021

Cell-cell junctions allow cells to maintain structure, organize into complex tissues and organs, and communicate both physically and chemically to function in unique environments. One such environment is the heart where cells must maintain adhesion during coordinated and constant rhythmic contraction. It is estimated that cardiomyocytes experience forces in excess of 1000nN, more than ten times that of nonmotile epithelial cells. It is not clear how these cells maintain adhesion under such extreme force. One of the cellular complexes involved in cardiomyocyte adhesion is the fascia adherens, also known as the adherens junction. The adherens junction couples adjacent cardiomyocytes and integrates the contractile myofibril network between them. The primary link between the adherens junction and the F-actin cytoskeleton is α-catenin. Two different α-catenins are expressed in the mammalian heart and, in the work presented here, I sought to understand how α-catenin functions in cardiomyocyte cell-cell adhesion. Specifically, my work addresses the properties of αT(testes)-catenin, a poorly characterized isoform with expression limited to the testes, central nervous system, and heart. Mutations in αT-catenin have been linked to cardiomyopathy and I sought to characterize its unique interactions with other adhesion and cytoskeletal proteins in the context of cardiomyocytes. I found that, in contrast to the better characterized αE(epithelial)-catenin, αT-catenin is a monomer in solution and can readily bind F-actin in the absence of tension. I also found that both αE-catenin and αT-catenin bind to β-catenin at the adherens junction with similar affinities. Finally, I showed that αT-catenin binds to vinculin by a tension-dependent mechanism, but autoinhibition of the M-region is regulated by a distinct

mechanism of intramolecular interaction involving the αT-catenin N-terminal domain. These unique properties of αT-catenin will help to define its function in cardiomyocytes and offer insight into how mutations in αT-catenin contribute to cardiomyopathy.

Table of Contents

List of Tables

List of Figures

Preface

I would first like to thank Adam for being a fantastic mentor. He has been very supportive and encouraging throughout all of my graduate school training and I have thoroughly enjoyed my time in his lab. I would also like to thank both past and present members of the Kwiatkowski lab. They have been very supportive and always made life in lab fun. I would like to thank my thesis committee and other members of the Cell Biology faculty for their insights on my work and always providing help when I needed it. Finally, I would like to thank my family and friends for their moral support throughout this process. I could not have gotten through it without them.

1.0 Introduction

The mechanisms that regulate cell-cell adhesion have been essential to the evolution of multicellular life and have allowed for the tissue specialization and organization observed across Metazoa. Cell-cell junctions allow cells to maintain structure, organize into complex tissues and organs, and communicate both physically and chemically to function in unique environments[1]. One such environment is the heart where cells must maintain adhesion during coordinated and constant rhythmic contraction[2,3]. It is estimated that cardiomyocytes experience forces in excess of 1000nN, more than ten times that of nonmotile epithelial cells[4]. It is not clear how these cells maintain adhesion under such extreme force. One of the cellular complexes involved in cardiomyocyte adhesion is the fascia adherens or adherens junction[5]. In the work presented here, I sought to understand how a component of the adherens junction, α-catenin, functions in cardiomyocyte cell-cell adhesion. Specifically, my work addresses αT(testes)-catenin, a poorly characterized isoform with expression limited to the testes, central nervous system, and heart. Mutations in αT-catenin have been linked to cardiomyopathy and I sought to characterize its unique interactions with other adhesive and cytoskeletal proteins in the context of cardiomyocytes.

1.1 Cardiomyocytes and ICD Adhesive Complexes

The heart pumps blood through the circulatory system to deliver oxygen and nutrients throughout the body. To accomplish this, the heart relies on the coordinated contractions of its muscle cells, called cardiomyocytes. Unlike skeletal muscle cells that organize into long, multinucleated syncytial fibers, cardiomyocytes function as individual cells that must physically couple and coordinate with one another to form the heart muscle. The syncytial cells of skeletal muscle allow for fast transmission of electrical signals throughout the fiber and for the contractile acto-myosin myofibril network to run continuously through the length of the muscle[6,7]. Instead of a true syncytium, individual cardiomyocytes create a functional syncytium through a specialized adhesive structure called the intercalated disc (ICD) [3,8]. This difference in cellular organization is thought to help protect the heart against cellular death, so if one or more cells fail it does not lead to failure of the entire organ[2].

The ICD mechanically couples adjacent cardiomyocytes through adherens junctions, desmosomes, and a junction containing components of each called the hybrid junction, or area composita[3,9-11]. The ICD also electrically couples cardiomyocytes through gap junctions that allow ions to pass between cells and provide electrical continuity[12] **(Figure 1.1)**. Each of these junctional complexes are essential to proper cardiac function[13]. Mutations in ICD proteins have been linked to dilated cardiomyopathy, arrhythmogenic cardiomyopathy and hypertrophic cardiomyopathy, all of which can lead to heart failure[2,3,14-16].

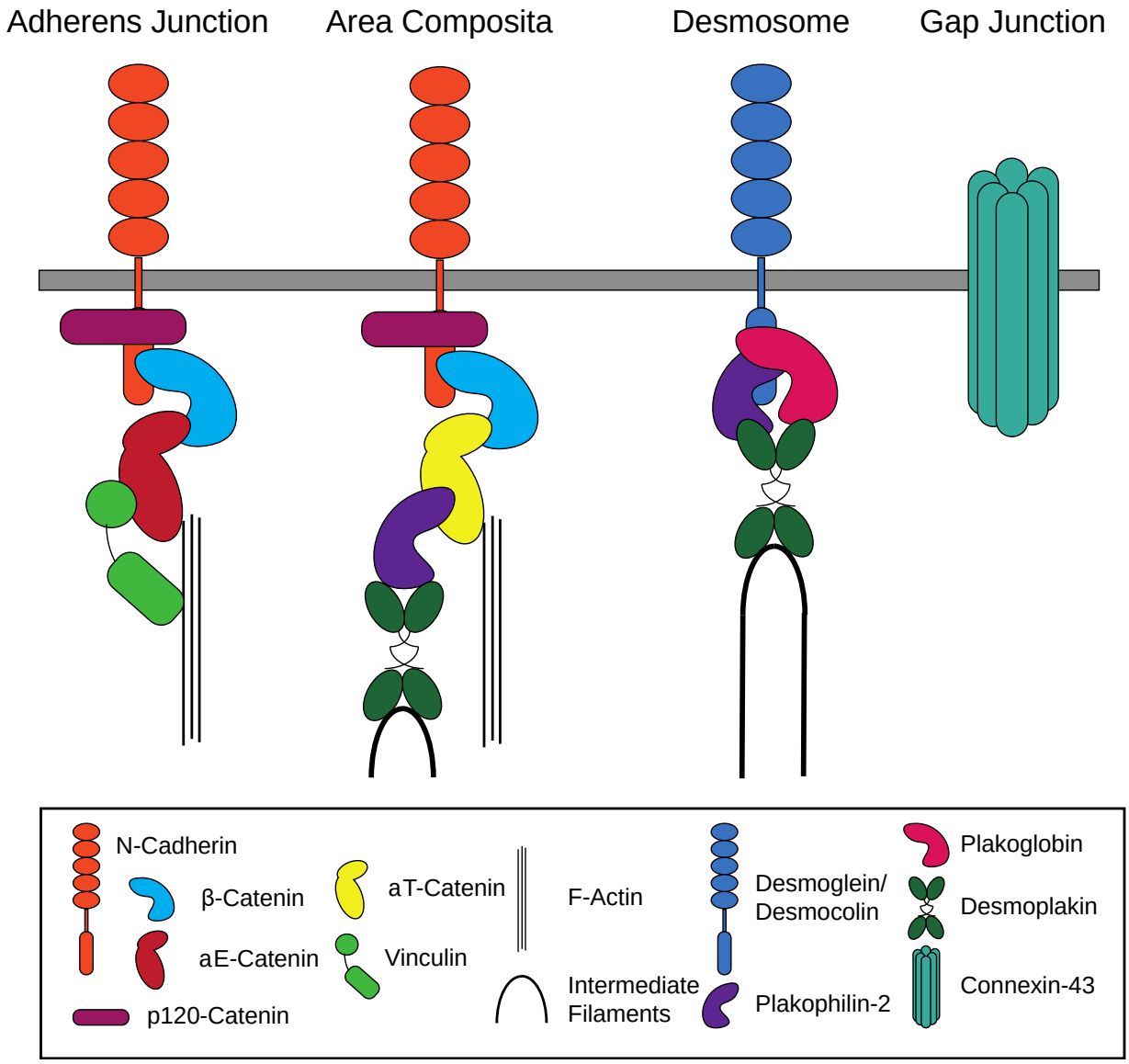

Figure 1.1 Junctional complexes that make up the intercalated disc.

Cartoon schematics of the adherens junction, area composita, desmosome and gap junction that make up the ICD in cardiomyocytes.

1.1.1 Adherens Junction

The adherens junctions(AJ) is the most ancestral cell-cell junctional complex and is found in all animals from poriferans to mammals[17,18]. AJs connect to the actin cytoskeleton and play an important role in a variety of important cellular processes such as the initiation and stabilization of adhesion between cells, cytoskeletal and transcriptional regulation, and intracellular signaling[19]. The core of the adherens junction is made of the cadherin-catenin complex[20]. Classical cadherins are single-pass transmembrane proteins with extracellular and cytoplasmic domains. The extracellular domain of the cadherin forms calcium-dependent homotypic *trans* interactions with cadherins on neighboring cells[20,21]. Classical cadherins can also form *cis* interactions with adjacent cadherins on the same cell surface to form adhesion plaques[21]. Together, *cis* and *trans* interactions create a lattice of extracellular cadherin domains to stabilize intercellular adhesions[23,24] **(Figure 1.2)**. The cytoplasmic tail domain is largely unstructured and recruits catenin proteins (discussed below) to attach the adherens junction to the F-actin cytoskeleton[22,23].

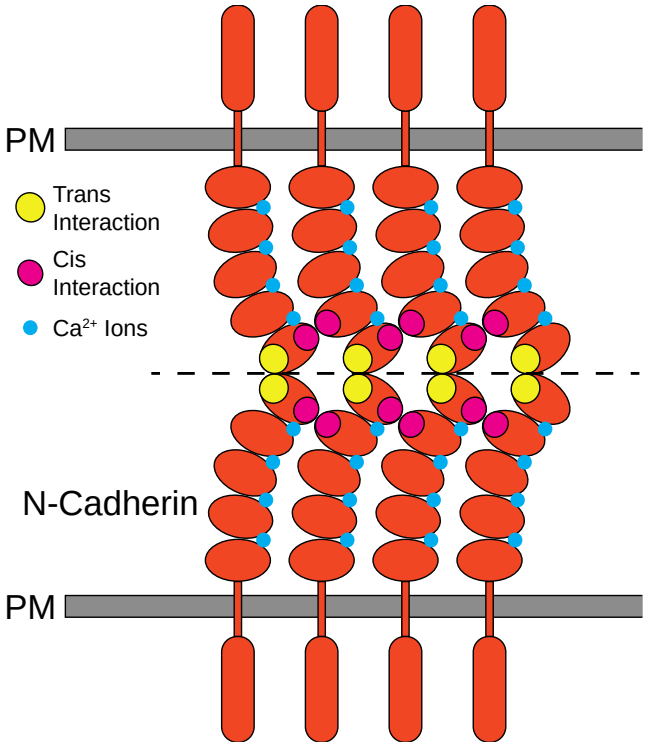

Figure 1.2 *Cis* and *trans* interactions between classical cadherins.

Cartoon Schematic of *cis* and *trans* interactions in an N-cadherin adhesion plaque.

N-cadherin is the only classical cadherin expressed in cardiomyocytes[22]. It is essential to heart development and loss of N-cadherin is embryonic lethal. In conditional knockouts, loss of N-cadherin in the developing heart prevents myocytes from forming cell-cell adhesions, causing cells to dissociate and disrupting heart tube formation[24]. N-cadherin is also required for proper heart function. Inducible knockout of N-cadherin in the adult mouse heart resulted in the disassembly of the ICD – with loss of adherens junctions, desmosomes and gap junctions – making it a linchpin of cardiomyocyte junctional assembly[25]. When N-cadherin deficient mouse hearts were rescued with E-cadherin, mice developed normally and survived to maturity but had increased rates of mortality and developed dilated cardiomyopathy. This was the result of ICD defects including vinculin localizing in the cytoplasm instead of to cell-cell contacts, and decreased

levels of the gap junction protein connexin-43, both of which have been associated with heart failure and cardiac hypertrophy[26].

The cytoplasmic tail of N-cadherin recruits two catenins in the armadillo family of proteins, p120-catenin and β-catenin[27] (**Figure 1.1**). Armadillo proteins get their name from the 42 amino acid repeat domains first discovered in the *Drosophila* β-catenin homologue Armadillo[28]. p120-catenin binds to the juxtamembrane region of the cadherin tail and plays an important role in the regulation of cadherin trafficking[29]. p120-Catenin masks an endocytic signal that is conserved across the classical cadherins[30]. Masking this signal prevents internalization to protect the cadherin from degradation. Along with this role, p120-catenin binds to cadherins during their biogenesis to aid in trafficking cadherin-catenin complexes to the membrane via kinesin transport along microtubules[31]. These mechanisms work together to regulate and maintains the population of cadherins at cell-cell junctions[32]. p120-Catenin is also involved in a variety of signaling pathways that regulate cytoskeletal organization, most notably the Rho-GTPases [33,34]. Its action on these pathways makes it a candidate for relaying outside-in signaling to regulate cellular processes like growth, polarization, migration and differentiation in response to external environmental cues[32,34].

β-Catenin, the other armadillo family catenin protein, is recruited to the distal portion of the cadherin tail. β-catenin in turn, recruits α-catenin to the adherens junction[27]. This function can also be performed by the desmosomal protein plakoglobin, a closely related protein that can also bind to the cadherin tail. Consistent with overlapping functions at the AJ, plakoglobin can compensate for the loss of β-catenin in in adult mouse heart. However, β-catenin cannot bind to desmosomal cadherins[35,36] and cannot compensate for loss of plakoglobin in mouse hearts[37]. Complete loss of β-catenin is embryonic lethal in mice and embryos are unable to complete gastrulation[38]. This is partially due to its vital signaling role during development in the Wnt

signaling pathway. In the canonical Wnt pathway, Wnt binding to the Frizzled/LRP5/LRP6 receptors causes β-catenin to accumulate in the cytoplasm, promoting translocation to the nucleus where it functions as a transcriptional activator to regulate cell fate determination, migration, cell polarity and organogenesis[39]. Mis-regulation of the Wnt pathway and overexpression of β-catenin in cardiomyocytes and cardiac fibroblasts has also been linked to cardiac injury, fibrosis and hypertrophy[40]. It is not clear if plakoglobin plays a role in the regulation of Wnt signaling.

α-Catenin is recruited by β-catenin to the cadherin tail and it serves as the primary link between the adherens junction and F-actin[41-43]. It is responsible for connecting to the cortical actin cytoskeleton as well as integrating myofibrils across cell-cell contacts in cardiomyocytes[44,45]. Three different α-catenin isoforms are expressed in mammals: αE(epithelial)-catenin, αN(neuronal)-catenin and αT(testes)-catenin[46-48]. αE-catenin is ubiquitously expressed and critical for development[49]. Knockout of αE-catenin in mice is embryonic lethal, blocking gastrulation[50]. αN-catenin is expressed in neuronal cells and is important for neural development and axon migration. Mice lacking αN-catenin develop hypomorphic brains and die around birth[51,52]. αT-catenin is expressed in the testes, heart and central nervous system. However, it is developmentally dispensable, and knockout mice develop fully and are fertile[49,53]. αE-catenin and αT-catenin are expressed in the mammalian heart and both are required for proper heart function[48,54]. In cardiac-specific αE-catenin knockout mice, the cardiomyocyte adherens junction is disrupted leading to dilated cardiomyopathy and increased incidence of rupture caused by thinning of the heart wall[11]. αT-catenin knockout mice also develop dilated cardiomyopathy at 3-6 months of age[53]. Two mutations in αT-catenin have been linked to arrhythmogenic cardiomyopathy(ACM) in humans[16,55], a disease that is associated with arrhythmias and electrical abnormalities of the heart[56]. The link between ACM and αT-catenin is not well understood.

1.1.2 Desmosome

Desmosomes are a mechanical junction found in tissues under high stress such as the heart and skin[57]. They are adapted to these high stress conditions through their attachment to the intermediate filament cytoskeleton. The name intermediate filament was coined from their average 10nm diameter that falls between 6nm actin filaments and 25nm microtubules. A variety of intermediate filaments are expressed in different cell types, including keratin in skin, neuronal filaments in neurons and desmin in myocytes[58]. Intermediate filaments can be stretched to several times their length and stiffen under strain to increase mechanical stability in tissues[58]. A variety of intermediate filaments are expressed to support different tissues, with cardiomyocytes and other muscle cells expressing desmin[59]. Desmosomes have been closely tied to the assembly and maintenance of other junctional complexes at the ICD and mutations in many desmosomal proteins have been linked to arrhythmogenic cardiomyopathy[15,56,60].

Desmosomes are thought to have evolved in the vertebrate lineage from several duplication events of adherens junction genes, so unsurprisingly they share similar structural components[1]. The desmosomal cadherins desmoglein and desmocolin are transmembrane proteins that make homotypic or heterotypic *trans* interactions with desmosomal cadherins on opposing cells[61]. Unlike classical cadherins, these *trans* interactions adopt a hyperadhesive state that does not require calcium ions under normal tissue conditions. Hyperadhesion is essential for maintaining stable contacts in response to mechanical stress, but these interactions can also revert to a weaker calcium dependent state during tissue remodeling and wound healing[57].

The tail of desmosomal cadherins recruits two armadillo proteins, plakoglobin and plakophilin. Plakoglobin and plakophilin are paralogues of β-catenin and p120-catenin, respectively[1]. In contrast to plakoglobin, plakophilin cannot bind to classical cadherins and only

binds to the tail of desmosomal cadherins. These proteins then recruit the plakin family protein desmoplakin to the desmosome to link the complex to the intermediate filament cytoskeleton[60].

Plakophilins are p120-catenin family proteins composed of an N-terminal head and 9 armadillo repeats with flexible linker regions between repeats 5 and 6[62]. Most proteins known to interact with plakophilin bind to the head domain, including the desmosomal cadherin tail and desmoplakin, but the associations of the armadillo repeats of plakophilins are not well understood[62,63]. Three different plakophilins are expressed in mammals with different expression profiles. Plakophilin-1 is expressed in the upper layers of stratified epithelia, like the epidermis[63,64]. Plakophilin-2 is expressed in simple epithelia and the lower layers of stratified epithelia. It is also expressed in non-epithelial tissues and is the primary form expressed in cardiomyocytes[65].[62] Plakophilin-3 is expressed in both simple and stratified epithelia, but is equally expressed throughout the different layers[63,64]. In addition to their structural role in adhesion, plakophilins can also shuttle into the nucleus where they are thought to play a role in cell signaling by regulating the cell cycle through the Wnt and Ras signaling pathways[65,66].

Desmoplakin is an obligate desmosomal protein that is organized into three major domains. The N-terminus contains a globular head domain that binds to plakoglobin and plakophilin. The C-terminal tail contains three plakin repeats and a GSR domain that binds intermediate filaments. These two domains are connected by a middle alpha helical rod domain[63]. Desmoplakin is expressed as two different splice variants: DP1 is 332kDa and DP2 is 260kDa. These two isoforms are identical, apart from a truncated rod domain in DP2. These two variants are coexpressed in most tissues with the exception of the heart that only expresses significant amounts of DP1[66].

Mutations in desmosomes are the primary cause of arrhythmogenic cardiomyopathy(ACM) [62]. ACM is estimated to affect as many as 1 in 1000-5000 people and is

the leading cause of sudden cardiac death in young individuals[67,68]. As this disease progresses, cardiomyocytes are replaced by fibrofatty tissue in the ventricle of the heart. Fibrotic tissue is unable to properly conduct electrical signals to coordinate contractions and results in arrhythmias, tachycardia, and electrical and physical abnormalities in the myocardium[56]. Oftentimes these symptoms are not recognized or displayed during disease progression and the first symptom is sudden cardiac death, so efforts are being made to determine viable biomarkers for diagnosis[56,69]. Mutations in a desmosome component account for as many as 50 percent of cases, and mutations in plakophilin-2 account for as many as 70% of familial cases[56,70]. It was initially thought that mutations in desmosomal components caused defects in cell-cell adhesion leading to ACM, but recent findings into the role(s) of the desmosome in cell signaling and crosstalk with other junctions have made this conclusion less clear. Desmoplakin is important for the trafficking of the gap junction protein connexin-43 to the membrane and to prevent its degradation by the lysosome once it has been delivered[71,72]. Plakophilin-2 is also linked to the proper function of Na_v 1.5, a voltage gated sodium channel important for depolarization of cardiomyocytes[73]. These results point to ACM mutations in desmosomal proteins causing defects in electrical conduction, possibly in addition to a defect in adhesion. Notably, desmosomal proteins can also associate closely with adherens junction proteins to form a hybrid junction called the area composita[10,68]. Defects in the area composita have also been linked to ACM in humans, so it is also possible that the disease results from a failure to form proper cell-cell adhesions[15,16].

1.1.3 Area Composita

In epithelial cells, adherens junctions and desmosomes form two distinct junctions whose localization is largely distinct along cell borders. In cardiomyocytes, it has been found that

components of each of these junctions are in close proximity[74] and αT-catenin can directly bind to the desmosome protein plakophilin-2[75] **(Figure 1.1)**. Adherens junctions containing αT-catenin can directly bind to F-actin and recruit Plakophilin-2 and Desmoplakin to bind intermediate filaments to make a unique junction that integrates these two cytoskeletal networks. This hybrid junction is thought to be important in reinforcing and strengthening the cell-cell adhesions in the high stress environment of cardiomyocytes[75,76].

The formation of the area composita takes place late in development. Mouse hearts have distinct junctional plaques of desmosomes and adherens junctions during embryonic development. Postnatally, these junctions begin to colocalize along the ICD[77]. αT-catenin expression also turns on perinatally suggesting the increased expression may be connected to the intermixing of these junctions and the formation of the area composita[76].

1.1.4 Gap Junction

Gap Junctions allow for the movement of ions and other small molecules to permit intercellular communication throughout the body[78]. In the heart, gap junctions carry the electrical signals necessary for proper rhythm and coordination of cardiomyocyte contraction[79]. Gap junctions are made up of integral membrane proteins called connexins that organize into hexamers called connexons. Connexons on one cell bind connexons on an opposing cell to create a pore known as the gap junction[80]**(Figure 1.1)**. Gap junctions are non-selective and allow diffusion of molecules under about 1000 Daltons. They further assemble into plaques varying is size from tens to thousands of gap junctions along lateral portions of the ICD[81,82].

Three different connexins are predominantly expressed in the mammalian heart with different expression levels depending on location: connexin-45, connexin-40 and connexin-43[79].

Connexin-45 is the predominant subunit in the pacemaker cells of the sinoatrial node and the atrioventricular node. These cells are weakly coupled to allow for proper pacemaker function[83]. Connexin-40 is highly expressed in Purkinje Fibers. These cells have rapid conductance and carry the electrical signal to the distal tip of the ventricle[84]. Ventricular cardiomyocytes express almost exclusively connexin-43 with only trace amounts of other connexins to propagate the contractile signal to the rest of the heart[79,83].

Connexin-43 is essential for proper development and heart function. Mice lacking Connexin-43 survive to term but die at birth as a result of swelling and blockage of right ventricular outflow, inhibiting gas exchange[85]. Heart specific knockout of connexin-43 results in hearts that appear physically normal and contractile, but mice die from sudden cardiac death as a result of ventricular arrhythmias by two months of age[86]. Defects in gap junction function and localization have also been associated with heart disease. Analysis of the ICD in Carvajal Syndrome patients, a disease that includes ACM, showed decreased expression of connexin-43[82]. This syndrome has been linked to mutations in desmoplakin, and desmoplakin is required for the proper delivery and maintenance of connexin-43 at the ICD[71,72]. Naxos Disease, another form of ACM caused by mutations in plakoglobin also fails to make normal gap junctions at the ICD resulting in arrhythmias[87]. These results, along with the observation that gap junctions fail to form when N-cadherin is lost at the ICD, highlight how interactions between mechanical junctions and gap junctions are crucial for proper heart function[5,82].

1.2 The α-Catenin Family of Proteins

Figure 1.3 α-Catenin domain organization.

α-catenins are organized into three major domains. The N-terminus binds β-catenin and homodimerizes in some α-catenins. The M-region binds ligands like vinculin. The C-terminus binds to F-actin.

α-Catenins are found throughout the animal kingdom, from the simplest metazoan sponges all the way to humans[17,88]. α-Catenin homologues even predate metazoans and are present in the slime mold *Dictyostelium discoidium* that lacks classical cadherins[18]. Despite the evolutionary divergence of these species, α-catenins have maintained a core structural organization[17](**Figure 1.3**). The N-terminal domain is made up of two four-helix bundles that share a common α-helix between them[89]. The N-domain binds to β-catenin and mediates homodimerization in some α-catenins[43,90,91]. The middle M-region is a series of three four-helix bundles that serves as a scaffold for other adherens junction ligands[92-95]. Many of these ligands bind to the actin cytoskeleton and help stabilize the adherens junction in response to tension[45,96]. The C-terminal domain is a five-helix bundle and binds directly to F-actin[97-100].

The first structural studies of α-catenin focused on the N-terminus of mouse αE-catenin. The structure of the N-terminal homodimerization domain, aa 82-279, was crystalized as well as a chimera of the αE-catenin N-terminus (aa 57-264) flexibly linked to β-catenin α-catenin binding site (aa118-151) [89]. This structure established that the N-terminus of αE-catenin is composed of

antiparallel four-helix bundles and that the homodimerization domain and β-catenin binding regions overlap[89]. The crystal structure of the mouse αN-catenin N-terminus (aa1-261) was resolved more than a decade later. Whereas the αE-catenin N-terminus crystalized as a homodimer[89] the αN-catenin N-terminus crystalized as a monomer but was organized as two four-helix bundles, similar to αE-catenin [101]. Further structural studies crystalized the M-fragment of αE-catenin, corresponding to the M2-M3 regions. These studies established that the M-fragment is also composed of antiparallel four-helix bundles[92,93]. The work from Pokutta and colleagues also revealed, for the first time, that the binding site for afadin in αE-catenin M-region is likely cryptic (masked) in full length αE-catenin[93].

A decade later, the binding site of another important α-catenin M-region ligand – vinculin - was mapped to the M1 region of αE-catenin and a complex was crystalized showing that M1 binds to vinculin by a helix addition mechanism[95]. This work also helped to establish that αE-catenin binding to vinculin is autoinhibited through intramolecular interactions[95]. Based in part on these findings, it was subsequently proposed that the mechanism of autoinhibition was through a network of salt bridge residues spanning the M-region, and activation (vinculin binding) required tension to break these interactions[102-104]. Six salt bridges are predicted to form between residue pairs within 4 angstroms of each other in mouse αE-catenin: Glu 277-Arg 451, Arg 326-Glu 521, Asp 392-Arg 548, Arg 383-Asp 510 and Asp 503-Arg 551[103]. In the absence of these intramolecular interactions the vinculin binding site is largely unstructured[94]. Similarly, the M-region of αN-catenin was crystalized and shares a similar domain organization and intramolecular interactions to that of αE-catenin[94].

Nearly full length structures of mouse αE-catenin[97,105] and human αE-catenin[106] have been solved. These studies showed that intramolecular interactions govern the recruitment of vinculin[97] and allosteric changes occur throughout the protein upon homodimerization[106] or binding to the cadherin/catenin complex[105]. These allosteric changes have implications for differences in F-actin binding depending on the dimerization state of αE-catenin. Crystal structures of the F-actin binding region of αE- and αN-catenin have also been solved[97,99,100]. These studies illuminated the structural basis of αE-catenin catch-bond behavior and how tension applied to F-actin strengthens the interaction[99,100].

Three α-catenins are expressed in mammals: αE-catenin, αN-catenin and αT-catenin. αE-catenin was first described in epithelia but is ubiquitously expressed throughout the body. It is the best characterized and most widely studied of the family. Canonically, it functions to link the adherens junction to the F-actin cytoskeleton, but it also plays a role in other cellular processes. αE-catenin also regulates a variety of cell signaling pathways important for development and cancer, and regulates the cytoskeleton during cell migration and morphogenesis. αN-catenin was first characterized in the nervous system and is highly expressed in the brain. It plays an important role in axon guidance, regulation of synapse formation and the proper development of the brain. αT-catenin was first discovered in the peritubular myoid cells in the testes. These are contractile cells that provide support and structure to the seminiferous tubules[107], but αT-catenin is also highly expressed in the central nervous system and heart, and is best known for its role at the ICD[48,49]. Little is known about the molecular or cellular functions of αT-catenin or how it is linked to disease in these diverse tissue types (discussed more below), but it has been shown to be an important factor required for proper heart function[53].

1.2.1 α-Catenin in disease

α-Catenins play a vital role in development and are also associated with a variety of diseases. Mouse embryos lacking αE-catenin are not viable and development is arrested prior to implantation due to defects in cell-cell adhesion[50]. It plays a critical role maintaining flexible yet strong adhesions to maintain structure during the complex cellular movements of morphogenesis[108]. When it is lost in other tissues, αE-catenin can have adverse signaling effects in addition to loss of adhesion. When αE-catenin is conditionally knocked out in the skin and brain, cell hyperproliferation was observed along with defects in cell polarity[109,110]. αE-catenin has also been linked to cancer through a myriad of signaling pathway, such as Wnt/β-catenin, NF-κB, Hippo/Yap and Hedgehog signaling[99,100]. It is a negative regulator of proliferation, and even though it has not been studied as extensively as β-catenin or E-cadherin in this role, αE-catenin has emerged as an important tumor suppressor.

The expression of αN-catenin is much more restricted than that of αE-catenin and is largely limited to the brain and the cervical spinal cord[49]. Mice lacking αN-catenin develop hypomorphic brains, particularly affecting the hippocampus and cerebellum, and die perinatally[51]. αN-catenin plays a role in developing these portions of the brain by supporting axon migration[52]. Similar to αE-catenin, αN-catenin has also been shown to play a role as a tumor suppressor. In the neural crest derived cancer neuroblastoma, decreased αN-catenin levels are correlated with poorer prognosis. Forcing its expression decreased growth of cancer cells in culture and also limited signs of cancer progression such as migration, angiogenesis, and invasion by inhibiting NF-κB signaling[111].

αT-catenin is most highly expressed in the central nervous system and the heart, but is also present in the peripheral nervous system, testes, skeletal muscle, and trace amounts in other tissue types[49]. Unlike the other two members of the mammalian α-catenin family it is dispensable for development, with knockout mice developing normally and surviving through sexual maturity. However, by 6 months of age, αT-catenin knockout mice develop dilated cardiomyopathy and ventricular arrhythmias after ischemia. This is presumably the result of reduced junctional integrity and connectivity between cardiomyocytes as plakophilin-2 and connexin-43 levels are reduced at the ICD[53]. Mutations in αT-catenin have also been linked to cardiomyopathy in humans. The N-terminal V94D mutation and the deletion of Leucine 765 in the actin binding domain both independently result in ACM[16]. ACM is typically associated with the desmosome, and mutations in αT-catenin linked to the same disorder suggest an important functional connection between the two[112].

αT-catenin has also been associated with a variety of other diseases outside of the heart. Similar to the other α-catenin family members, αT-catenin may function as a tumor suppressor. SNPs and deletions in αT-catenin have been linked to laryngeal carcinoma and hybrid neurofibroma/schwannoma[113,114]. Mono-allelic or reduced expression has also been associated with a variety of other cancer types, including in tissues with normally low expression, suggesting protein expression likely does not directly correlate with transcript number[49].

Consistent with its high expression levels in the central nervous system, αT-catenin has also been associated with neurological diseases[49]. The CTNNA3 gene that encodes αT-catenin is one of the largest genes in the human genome and is located near a common chromosomal fragile site linked to late onset Alzheimer's Disease[115,116]. It has also been linked in a number of cases to autism, with deletions in αT-catenin found in patients with sporadic autism[117-119]. Some progress

has been made in understanding the connection of αT-catenin to autism, since knockout mice show changes in signaling pathways associated with the disorder such as GABA-A receptor activation[119]. It was also found that αT-catenin may not be expressed in neurons at all, and is instead highly expressed in neurological support cells such as ependymal calls that line the ventricles of the brain and central canal of the spinal cord, and oligodendrocytes that surround neurons with myelin in the central nervous system[119,120]. It is not known whether mis-regulation of αT-catenin function is causal in these disorders, exacerbates another underlying cause or is simply associated by chance[121].

1.2.2 α-Catenin ligands

α-Catenin acts as a scaffold to recruit a wide range of proteins to the adherens junction. Many of these proteins are thought to be necessary for proper cell-cell junction formation and function. However, the composition of these protein complexes, how their recruitment is regulated and how their function may differ between α-catenin family members are all poorly understood. Most studies of α-catenin ligand interactions have focused on αE-catenin, whereas ligand interactions with other members of the mammalian α-catenin family have not been tested. In the studies presented, here we examine the interactions between the α-catenin ligands β-catenin, F-actin and vinculin.

1.2.2.1 β-catenin

α-Catenin is recruited to the cadherin tail through its interaction with β-catenin or plakoglobin[122]. The binding site for β-catenin/plakoglobin overlaps the homodimerization domain

of αE-catenin in the N-terminus, so the α/β-catenin heterodimer and αE-catenin homodimer are mutually exclusive[89]. The cadherin tail increases the affinity of the interaction between β-catenin and αE-catenin tenfold over that of β-catenin alone to the low nanomolar range (25nM for β-cat alone vs 1nM for β-cat/E-cad tail) [43]. A similar effect is observed with αN-catenin and αT-catenin, with both binding to β-catenin in complex with the cadherin tail with an affinity in the low nanomolar range[43,123].These results show that each member of the α-catenin family can associate with the adherens junction through β-catenin with similar affinities but it is not clear whether this is also the case with plakoglobin.

Note that αE-catenin binding to β-catenin independent of the adherens junction impacts cell functions by inhibiting the Wnt signaling pathway[124]. αE-catenin is able to bind β-catenin and inhibit its translocation to the nucleus to prevent Wnt-related transcription. Wnt signaling promotes cell growth and is an important in many cancers. Inhibition of this pathway is one mechanism in which αE-catenin may act as an important tumor suppressor[125].

1.2.2.2 Actin

The F-actin cytoskeleton provides necessary support and structure to the cell and anchors to cell-cell junctions[126]. Actin filaments along with myosin are the main components of myofibrils in striated muscle, and in cardiomyocytes α-catenin is required to integrate the myofibrils across the ICD[45]. α-Catenin serves as the primary link between the adherens junction and F-actin[23]. However, the strength and regulation of this linkage varies across the mammalian α-catenins.

When αE-catenin is bound to β-catenin at the adherens junction it has a very weak affinity for F-actin in the absence of tension. However, when αE-catenin is bound to itself (homodimer state) it can readily bind to F-actin with an affinity in the low micromolar range[127]. This difference

in affinity is because αE-catenin, when bound to the cadherin/β- catenin complex, forms a catch bond with F-actin and cannot fully engage with the actin filament unless under force[20,42,99]. The catch bond behavior of αE-catenin is the result of a small alpha-helix termed H0 at the N-terminus of the actin binding domain, and also gives a preferred directionality to actin binding at the junction[98,100].

The αE-catenin dimer acts away from the adherens junction to remodel the F-actin cytoskeleton. This cytoplasmic pool of αE-catenin inhibits actin nucleation by the Arp2/3 complex. When this pool is sequestered, lamellipodia and membrane dynamics are increased resulting in increased cell migration[128].

1.2.2.3 Vinculin

One of the best characterized ligands of α-catenin is vinculin. Vinculin is known to be recruited to focal adhesions in a tension dependent manner through an interaction with the protein talin[129]. Vinculin serves to stabilize the connection to actin filaments and aid in focal adhesion maturation[130]. Vinculin and α-catenin are homologous proteins and vinculin plays a very similar role in adherens junctions as it does in focal adhesions[46]. Vinculin is recruited to the adherens junction by binding to the M1 region of αE-catenin[131,132]. It is believed that vinculin adds another actin binding interface to help stabilize and reinforce the adherens junction in response to actomyosin contractile force[96].

Mice lacking vinculin are not viable and develop heart and brain defects during development[133]. Vinculin is essential for heart development and junctional organization, and when it is lost in cardiomyocytes, mice develop dilated cardiomyopathy and suffer from sudden cardiac death[134,135]. It is responsible for the integration and proper organization of myofibrils across the

ICD in cardiomyocytes and these structures are lost when vinculin cannot be recruited to the cell-cell junctions[45,136]. Vinculin plays an important role in maintaining cardiomyocyte junctions in humans and it has been found that a missense mutation in vinculin increases susceptibility to hypertrophic cardiomyopathy and disrupted ICD organization inducing interstitial fibrosis[137].

The mechanism of vinculin recruitment to αE-catenin is through a mechanosensitive conformational change of the αE-catenin M-region[95](**Figure 1.4**). When not under tension the M-region adopts a closed autoinhibited conformation[97]. The M-region is maintained in the autoinhibited conformation by a network of salt bridge residues that span between the M1, M2 and M3 regions[103]. Tension breaks these salt bridges and M1 is able to unfurl away from the rest of the M-region[102]. The vinculin head domain is then able to bind to the free M1 region where the αE-catenin α-helix is inserted into the 4-helix bundle of vinculin[138]. Once vinculin is bound, the conformation of αE-catenin is "locked" in the open conformation and even if tension is on the complex is lost, vinculin remains bound[102].

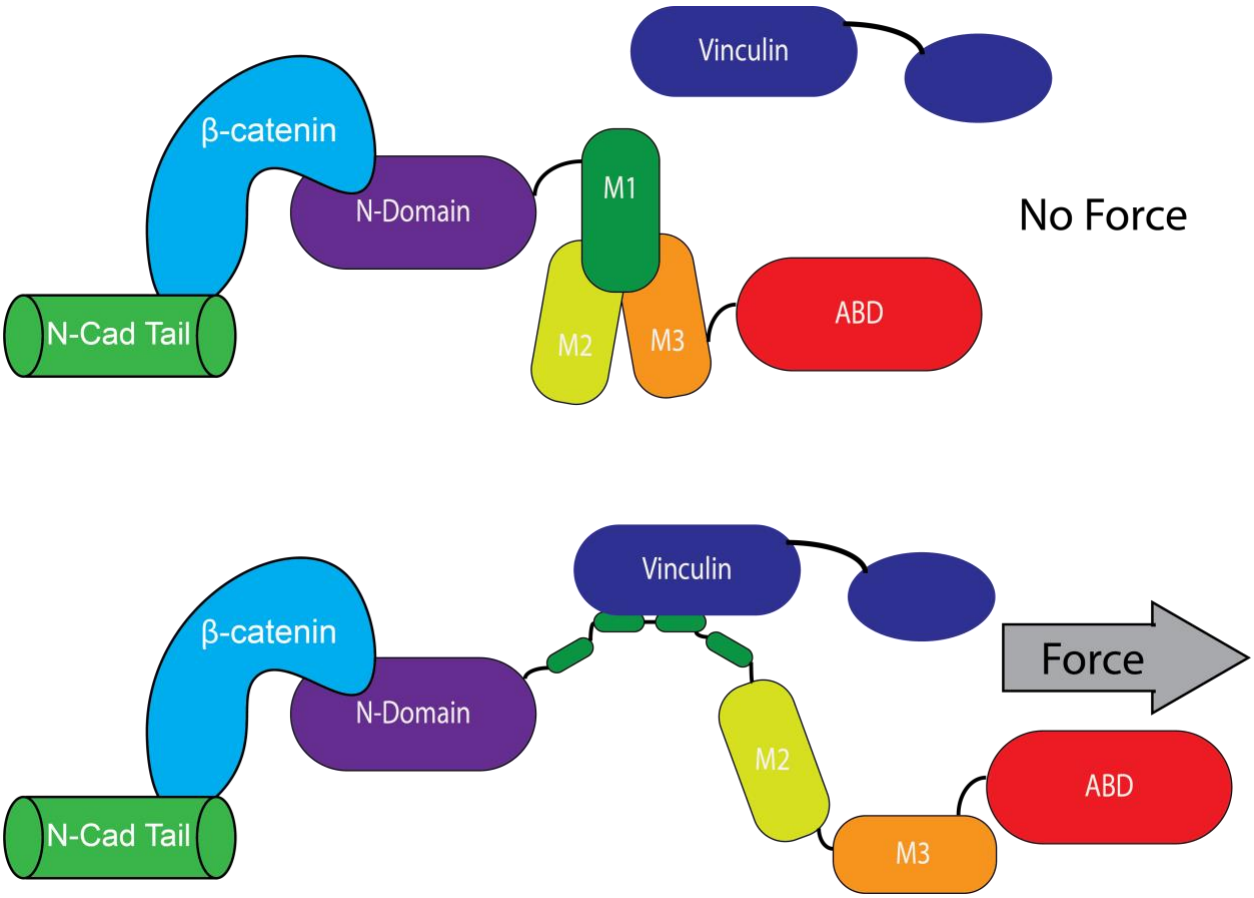

Figure 1.4 αE-catenin undergoes a conformational change in response to force to recruit vinculin.

Vinculin is also regulated by its own mechanism of autoinhibition which limits ligand binding[139]. The N-terminal head of vinculin is able to bind the C-terminal tail domain and hold it in the closed conformation[140]. This mechanism is regulated by actomyosin contractile tension and also requires multiple ligand associations to relieve autoinhibition[141]. This mechanism ensures the proper recruitment of vinculin to junctions under stress and is only activated when its necessary ligands are present[140].

It is unclear if a similar mechanism of autoinhibition of vinculin binding is present in other members of the α-catenin family. Here we show that the αT-catenin M-region is not autoinhibited in the same way that αE-catenin is despite 5 of the 6 salt bridge pairs being conserved. Instead

vinculin binding to αT-catenin is regulated by a previously undescribed intramolecular interaction between the N-Terminus and the M-region[123]. This unique mechanism of M-region autoinhibition may play an important role in how ligands are recruited to individual adherens junctions when a different α-catenin is present.

2.0 αT-catenin is a constitutive actin-binding α-catenin that directly couples the cadherin-catenin complex to actin

This text was published in the Journal of Biological Chemistry in 2016:
Wickline ED, Dale IW, Merkel CD, Heier JA, Stolz DB, Kwiatkowski AV. αT-Catenin Is a Constitutive Actin-binding α-Catenin That Directly Couples the Cadherin·Catenin Complex to Actin Filaments. *J Biol Chem*. 2016;291(30):15687-15699. doi:10.1074/jbc.M116.735423.

Contributions: I assisted in purifying recombinant proteins used for experiments throughout the paper. I repeated and verified αT-catenin WT, V94D and αE-catenin trypsin limited proteolysis experiments (Fig. 2.1D and Fig. 2.4I). I also performed and analyzed all sucrose gradient experiments (Fig. 2.2E-G and Fig. 2.4F-G). I performed the F-actin co-sedimentation experiments for αT-catenin/β-catenin and verified the results of αT-catenin WT and V94D (Fig. 2.3A-B and Fig. 2.5A-B). Finally, I helped write and edit the manuscript and responded to reviewer comments.

2.1 Overview

α-Catenin is the primary link between the cadherin/catenin complex and the actin cytoskeleton. Mammalian αE-catenin is allosterically regulated: the monomer binds the β-catenin/cadherin complex, whereas the homodimer does not bind β-catenin but interacts with F-actin. As part of the cadherin/catenin complex, αE-catenin requires force to bind F-actin strongly.

It is not known if these properties are conserved across the mammalian α-catenin family. Here we show that αT(Testes)-catenin, a protein unique to amniotes that is expressed predominantly in the heart, is a constitutive actin-binding α-catenin. We demonstrate that αT-catenin is primarily a monomer in solution and that αT-catenin monomer binds F-actin in co-sedimentation assays as strong as αE-catenin homodimer. The β-catenin/αT-catenin heterocomplex also binds F-actin with high affinity, unlike the β-catenin/αE-catenin complex, indicating that αT-catenin can directly link the cadherin/catenin complex to the actin cytoskeleton. Finally, we show that a mutation in αT-catenin linked to arrhythmogenic right ventricular cardiomyopathy (ARVC) – V94D –promotes homodimerization, blocks β-catenin binding and, in cardiomyocytes, disrupts localization at cell-cell contacts. Together, our data demonstrate that αT-catenin is a constitutively active actin-binding protein that can physically couple the cadherin-catenin complex to F-actin in the absence of tension. We speculate that these properties are optimized to meet the demands of cardiomyocyte adhesion.

2.2 Introduction

The adherens junction (AJ) mechanically couples the actin cytoskeletons of adjacent cells to establish and maintain intercellular adhesion[142-144]. The core of the AJ is the cadherin-catenin complex[145]. Classical cadherins are single-pass transmembrane proteins with an extracellular domain that mediates calcium-dependent homotypic interactions[146]. The adhesive properties of classical cadherins are driven by the recruitment of cytosolic catenin proteins to the cadherin tail: p120-catenin binds to the juxta-membrane domain and β-catenin binds to the distal part of the

tail[147]. β-Catenin, in turn, recruits α-catenin to the cadherin-catenin complex[43,89]. α-Catenin is a filamentous actin (F-actin) binding protein and the primary link between the AJ and the actin cytoskeleton[41,42,127,148].

In mammals, αE (Epithelial)-catenin is allosterically regulated: the monomer binds the β-catenin/cadherin complex, whereas the homodimer does not bind β-catenin but interacts with F-actin[127,148]. β-Catenin binding to αE-catenin sterically hinders F-actin binding[43,106], explaining how αE-catenin as part of the cadherin/catenin complex has a weak affinity for F-actin. More recently, it was shown that the cadherin-catenin complex binds strongly to F-actin under force, indicating that the αE-catenin-actin interface is dynamically regulated by tension[42]. In addition, evidence suggests that tension can regulate αE-catenin conformation: actomyosin-generated force stretches the middle (M)-domain to reveal binding sites for cytoskeletal proteins such as vinculin[95,96,103,149,150]. Thus, αE-catenin is a dynamic and multifunctional protein regulated by tension.

α-Catenin functions in adhesion and mechanical signaling must be integrated in all tissues. In cardiomyocytes, the AJ functions with the desmosome to physically link opposing cells in a specialized adhesive structure called the intercalated disc (ICD) [5]. Contractile forces place physical demands on heart junctional complexes: not only must they withstand repeated cycles of force, tension-sensing proteins within these complexes must be "tuned" to regulate signaling and maintain homeostasis[151]. Two α-catenin proteins are expressed in the mammalian heart – αE-catenin and αT (Testes)-catenin[48,75,152]. In contrast to the widely studied and well-defined mammalian αE-catenin, little is known about αT-catenin, a protein unique to amniotes that is expressed predominantly in the heart and testes[48,153]. αT-catenin is expressed in cardiomyocytes where it localizes to the ICD, and genetic ablation of αT-catenin in mice causes dilated

cardiomyopathy (DCM) [48,53,75]. Notably, two mutations in αT-catenin have been linked to arrhythmogenic right ventricular cardiomyopathy (ARVC): an amino acid (aa) change in the N-terminus (valine to aspartic acid, V94D) and deletion of one aa in the C-terminal ABD (loss of a leucine, L765del) [16]. However, the molecular properties of αT-catenin are undefined and how these mutations affect αT-catenin function in cardiomyocytes remains unclear.

Here we show that αT-catenin is a constitutive actin-binding α-catenin that can directly couple the AJ to the actin cytoskeleton. Our data also reveal that the V94D mutation linked to ARVC alters αT-catenin dimerization potential to disrupt β-catenin binding and cellular localization. We postulate that αT-catenin protein conformation and ligand binding properties are tuned to meet the specific demands of cardiomyocyte adhesion.

2.3 Results

2.3.1 αT-catenin domain stability differs from αE-catenin.

Structural studies of αE-catenin have revealed that the protein is a series of helical bundles[43,89,93,97,106]. The N-terminal (N) domain consists of two four-helix bundles (**Fig. 2.1A,** N1 and N2) and binds β-catenin and mediates homodimerization[89]. The middle (M) region is composed of three four-helix bundles (**Fig. 2.1A,** M1-M3) and binds vinculin in response to mechanical force[95,102,103,149,150,154]. A small linker region connects the C-terminal five-helix actin-binding domain (ABD) to the M region (**Fig. 2.1A**). We compared the amino acid sequence of *M. musculus* αT-catenin to *M. musculus* αE-catenin and *M. musculus* αN-catenin. αT-catenin is 58%

identical and 77% similar to αE-catenin; likewise, it is 59% identical and 77% similar to αN-catenin (**Fig. 2.1B**). αE-catenin and αN-catenin are 81% identical and 91% similar, making αT-catenin the most divergent of the mammalian family. We then analyzed sequence homology across domains between αT-catenin and αE-catenin (**Fig. 2.1C**). The region with the lowest degree of homology was N2 (39% identical and 61% similar) whereas the region with the highest was M2 (62% identical and 92% similar).

We then questioned if sequence differences affected domain organization in αT-catenin. We purified recombinant *M. musculus* αT-catenin and *M. musculus* αE-catenin from *E. coli* and used limited trypsin proteolysis to examine domain organization. As shown previously[155,156], tryptic digest of αE-catenin monomer revealed two stable fragments: the modulation domain (aa 385–651) and the β-catenin binding/homodimerization domain (aa 82-287) (**Fig. 2.1D**). Tryptic digest of αT-catenin revealed three stable fragments at 30, 25 and 18 kDa (**Fig. 2.1D**). N-terminal sequencing revealed that the 30 kDa fragment started at aa 379 and contained bundles M2 and M3 (**Fig. 2.1D**). The entire M2-M3 region forms a protease resistant fragment in mouse αE-catenin (**Fig. 2.1D**) [92,127,155] and fish αE-catenin[156]. Notably, the 18 kDa fragment started at aa 485, near the end of domain M2, and contained the entire M3 domain. This suggests that, unlike αE-catenin, the αT-catenin M2-M3 region exists in a more open, protease-sensitive state. Finally, the 25 kDa fragment started at aa 108, similar to the dimerization/β-catenin-binding domain in αE-catenin (aa 82–287), though this fragment – similar to M2-M3 – was markedly less protease-resistant than in αE-catenin. We conclude that the conformation of αT-catenin is similar to αE-catenin, though with differences in the stability of both N-terminal and middle domains that could impact function.

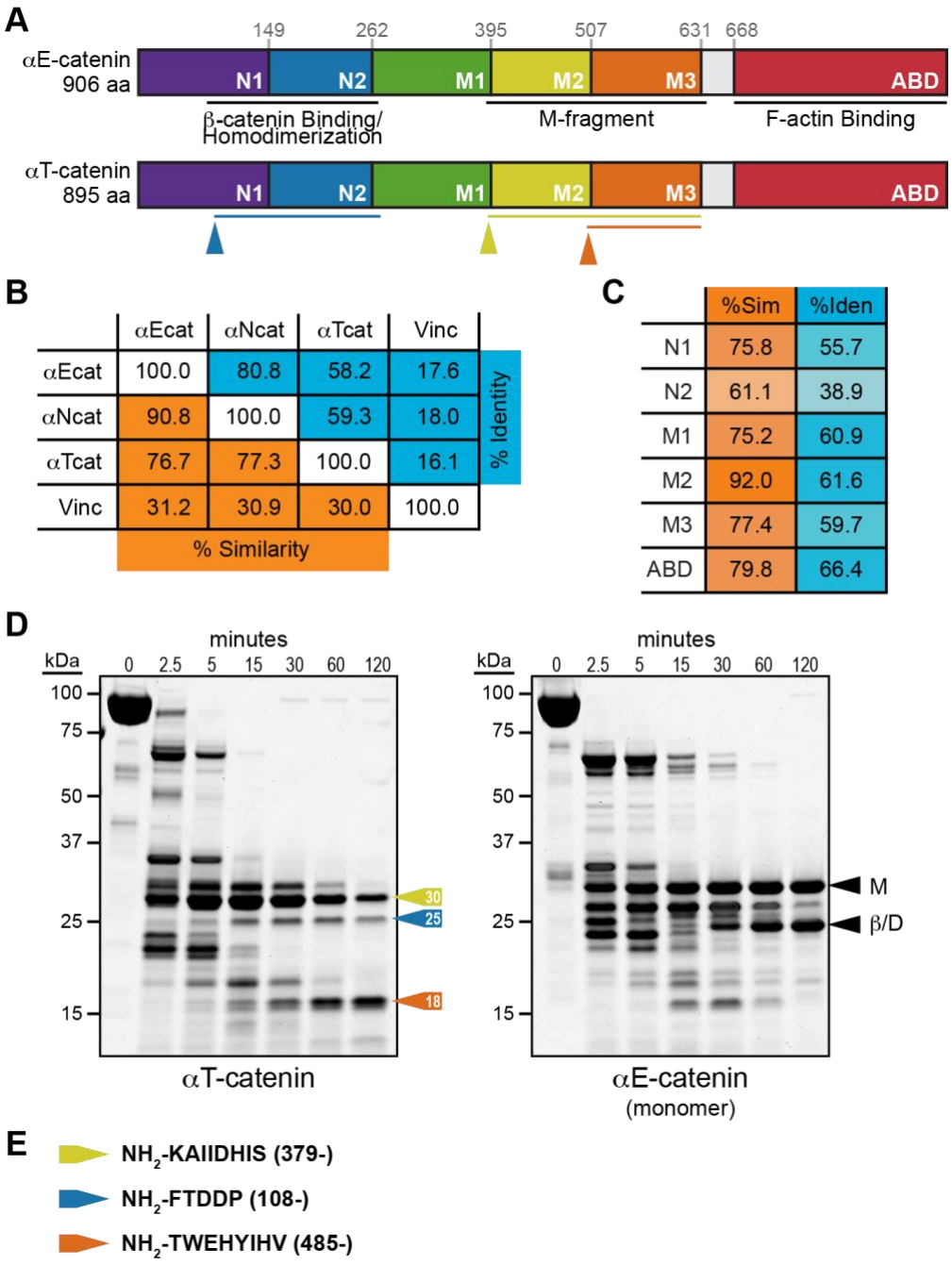

Figure 2.1 αT-catenin domain organization.

A. αE-catenin is composed of 5 four-helix bundles, a linker region and a five-helix bundle tail. Domain amino acid boundaries are marked. The 2 N-terminal four-helix bundles (N1 and N2) bind β-catenin and mediate homodimerization (protease-resistant region underlined). The middle region contains 3 four-helix bundles (M1-M3; protease-resistant M-fragment underlined). The C-terminal domain binds F-actin (actin binding

domain, ABD). αT-catenin possesses a similar domain organization based on sequence homology. Trypsin-resistant fragments (from D) are shown as color-coded lines below αT-catenin. B. Percent identity (blue) and percent similarity (orange) between M. musculus αE-catenin, αN-catenin, αT-catenin and vinculin. C. Percent identity (blue) and percent similarity (orange) between M. musculus αE-catenin and αT-catenin domains. D. Limited proteolysis of recombinant αT-catenin (left) and αE-catenin monomer (right). Coomassie-stained SDS-PAGE gel of proteins incubated for 0, 2.5, 5, 15, 30, 60 and 120 minutes at room temperature in 0.05 mg/ml of trypsin. M-fragment (M, aa 385-651) and β-catenin/dimerization (β/D, aa 82-287) fragments in αE-catenin marked with black arrows. Stable αT-catenin fragments of 30 (yellow), 25 (blue) and 18 kDa (orange) noted with colored arrows. E. Edman sequencing results of limited proteolysis fragments. Projected fragments mapped on full-length sequence (A) as color-coded lines.

2.3.2 αT-catenin is a monomer in solution

We assessed the oligomerization state of αT-catenin by chromatography. Recombinant αT-catenin protein prepared from *E. coli* was first purified by MonoQ ion exchange chromatography (IEC, **Fig. 2.2A**). Two peaks were routinely observed during elution off a MonoQ column (**Fig. 2.2A,** top chromatogram), and SDS-PAGE analysis of peak fractions revealed they both contained full-length αT-catenin (**Fig. 2.2A,** bottom gel). A similar IEC profile is observed with *M. musculus* αE-catenin (data not shown), and the two peaks correspond to the monomer (peak 1) and homodimer (peak 2) species. Both αT-catenin peak fractions were subsequently purified over a Superdex 200 (S200) size exclusion chromatography (SEC) column. The MonoQ peak 1 fraction eluted in a single, discrete peak (**Fig. 2.2B,** purple line), consistent with it being a single, likely monomeric, species. The S200 elution profile of MonoQ peak 2 was similar to peak 1, though a second, small peak was sometimes observed where a dimer species would be expected to elute (**Fig. 2.2B,** red line).

We then compared the primary S200 peak (elution volume 60-70 mls, concentrated to 25-50 μM) of αT-catenin to αE-catenin monomer and homodimer by analytical SEC. At all concentrations tested (25-50 μM), αT-catenin eluted in a single peak after both αE-catenin homodimer and monomer, suggesting that αT-catenin is a monomer (**Fig. 2.2C**). We then used SEC and sucrose density gradient centrifugation to determine the molecular mass of αT-catenin, αE-catenin monomer and αE-catenin homodimer[157]. The SEC elution profiles (**Fig. 2.2C**) were compared to known standard proteins to calculate the Stokes radius (**Fig. 2.2D**). The calculated Stokes radius of αE-catenin homodimer was similar to past observations (6.5 versus 7.4 nm; (35)) and the Stokes radii of both αE-catenin monomer and homodimer species were comparable to our previously measured radii of gyration from small angle X-ray scattering (4.5 and 6.0 nm, respectively[156]). The Stokes radius of αT-catenin was calculated to be 4.7 nm, slightly smaller than αE-catenin monomer (**Fig. 2.2D**).

We then used sucrose density gradient centrifugation to determine the sedimentation coefficients of αT-catenin, αE-catenin monomer and αE-catenin homodimer. Proteins were separated on 5-20% sucrose gradients, the average fraction peak determined and compared to a standard curve to calculate the sedimentation coefficient (**Fig. 2.2E, F**). The Svedberg coefficients were determined to be 7.0 S for αE-catenin homodimer (identical to past calculation[90]), 5.2 S for αE-catenin monomer and 5.7 S for αT-catenin. Molecular weights were then estimated based on the measured Stokes radii and sedimentation coefficients (**Fig. 2.2G**). The molecular weight of αT-catenin was calculated to be 109 kDa, similar to αE-catenin monomer (106 kDa). Finally, αT-catenin migrated as a single band by native-PAGE, faster than either αE-catenin monomer or dimer, consistent with the SEC analysis (**Fig. 2.2H**). We conclude that αT-catenin is primarily a

monomer in solution. It is important to note that these recombinant proteins are purified from *E. coli* and lack post translational modifications. A phosphorylation site at Y177 is present in the N-terminus of αE-catenin but is not within the homodimerization domain[43,158]. Phosphorylation of this residue disrupts αE-catenin binding to APC but does affect binding to β-catenin but blocking binding to APC increases the transcription of Wnt target genes[158]. There has not yet been any evidence showing post translational modifications influencing dimerization in α-catenin.

Dimerization kinetics differ significantly between mouse αE-catenin and αN-catenin at physiological temperatures[43]. αE-catenin homodimerization is significantly weaker than αN-catenin, but a kinetic block limits disassociation once an αE-catenin dimer is formed. The presence of two peaks in the MonoQ elution profile (**Fig. 2.2A**) and the minor peak in the peak 2 SEC elution (**Fig. 2.2B**) suggest that the αT-catenin might exist as a homodimer. However, if the MonoQ peak 2 elution represented a homodimer species of αT-catenin, the majority of these dimers dissociated during SEC (**Fig. 2.2B**). We were never able to purify a sufficient quantity of the potential dimer species for analysis by SEC or native-PAGE. Also, attempts to promote dimerization by incubation of the monomer at physiological (37 °C) temperatures caused the protein to aggregate and fall out of solution. Though we were unable to analyze the dimerization kinetics of wild-type (wt) αT-catenin, our analysis of the V94D mutant revealed that αT-catenin, similar to αE-catenin and αN-catenin, has dimerization potential (described below). Nonetheless, we took advantage of the lack of apparent dimerization in solution to study the behavior of αT-catenin monomer binding to F-actin.

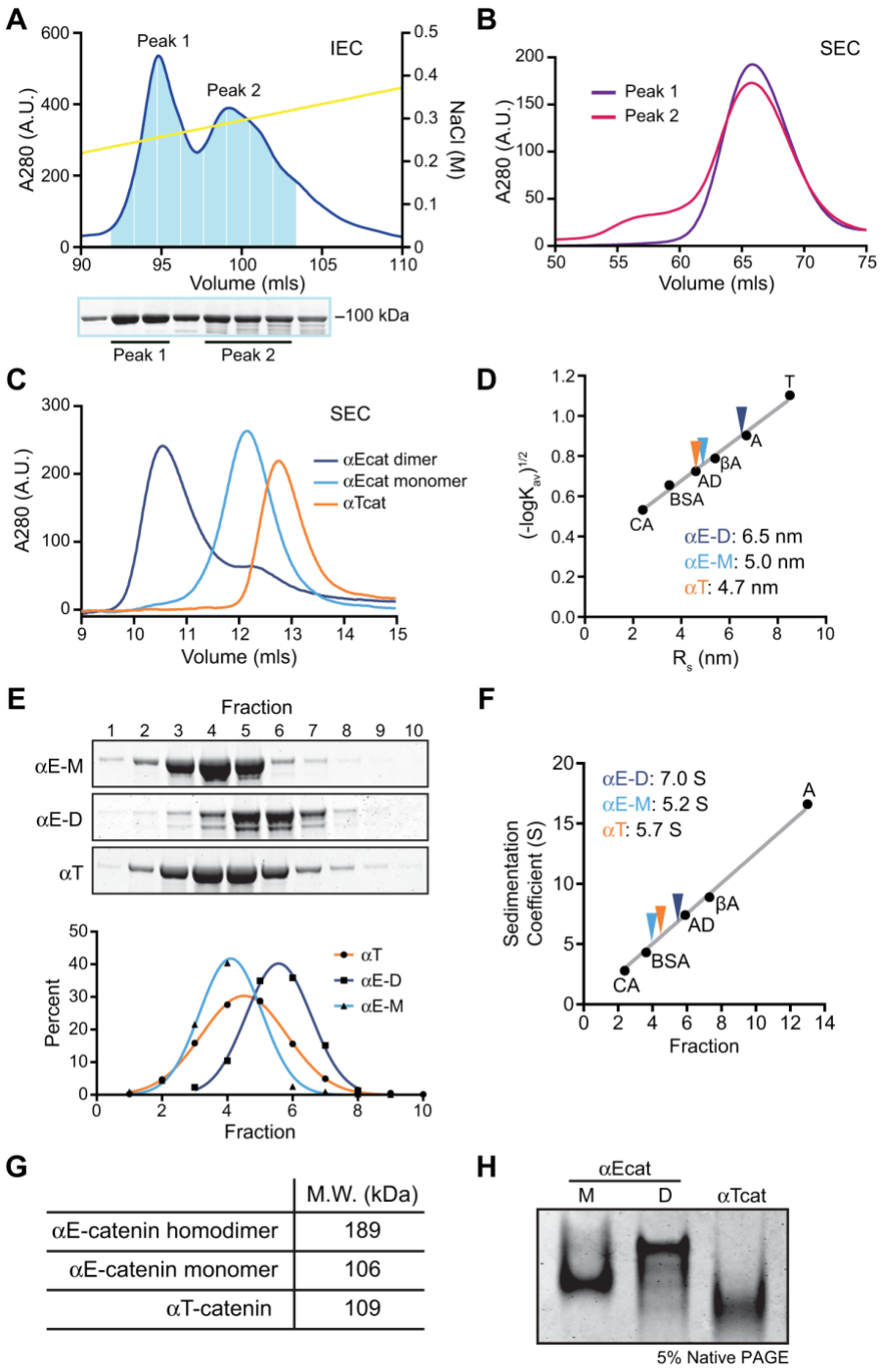

	M.W. (kDa)
αE-catenin homodimer	189
αE-catenin monomer	106
αT-catenin	109

Figure 2.2 αT-catenin is a compact monomer.

A. MonoQ anion exchange chromatography of recombinant αT-catenin (top) and Coomassie-stained SDS-PAGE of fractions (bottom). B. Superdex 200 (S200) size exclusion chromatography (SEC) of αT-catenin MonoQ peak fractions. C. Analytical S200 SEC of recombinant αE-catenin homodimer, αE-catenin monomer and αT-catenin. Elution profiles used to calculate K_{av}. D. Stokes radii of αE-catenin homodimer, αE-catenin

monomer and αT-catenin. K_{av} was calculated for standard proteins carbonic anhydrase (CA, R_s = 2.4 nm), bovine serum albumin (BSA, R_s = 3.5 nm), alcohol dehydrogenase (AD, R_s = 4.6 nm), β-amylase (BA, R_s = 5.4 nm), apoferritin (A, R_s = 6.7 nm) and thyroglobulin (T, R_s = 8.5 nm). Standard curve was created by plotting $(-\log K_{av})^{1/2}$ versus R_s. αE-catenin homodimer, αE-catenin monomer and αT-catenin R_s determined from standard curve. E. Sucrose gradient sedimentation of αE-catenin monomer (αE-M), αE-catenin dimer (αE-D) and αT-catenin (αT). Fractions were collected from 5-20% sucrose gradients and analyzed by Coomassie-stained SDS-PAGE (top). The percentage of protein in each fraction was measured, plotted and the data fit to a Gaussian curve. F. Sedimentation coefficient of αE-catenin dimer, αE-catenin monomer and αT-catenin. Standard curve was created by plotting the sedimentation coefficient (S) versus the average sucrose gradient fraction of protein standards (similar standards as D; CA = 2.8 S, BSA = 4.3 S, AD = 7.4 S, BA = 8.9 S, A = 16.6 S). αE-catenin dimer, αE-catenin monomer and αT-catenin S determined from standard curve. G. Calculated molecular weights of αE-catenin dimer, αE-catenin monomer and αT-catenin. H. Native PAGE analysis of recombinant αE-catenin dimer (αEcat D), αE-catenin monomer (αEcat M) and αT-catenin (αTcat). IEC, ion exchange chromatography; SEC, size exclusion chromatography.

2.3.3 αT-catenin monomer binds and bundles F-actin.

Mammalian αE-catenin binds and bundles F-actin[41,42,127,148,159], though in the absence of force, homodimerization is required to potentiate F-actin binding. We tested if αT-catenin monomer binds F-actin using an F-actin cosedimentation assay. Increasing concentrations of αT-catenin were incubated in the presence or absence of 2 μM F-actin, the samples centrifuged and resulting pellets analyzed. αT-catenin cosedimented with F-actin above background (**Fig. 2.3A**), and the bound protein was quantified and plotted over free protein to calculate the affinity of the interaction (**Fig. 2.3B**). BSA and αE-catenin were run as negative and positive controls, respectively (**Fig. 2.3A,** right panels). Plotted data was fit a hyperbolic function (**Fig. 2.3B**). αT-

catenin bound to F-actin with K_d of 0.4 ± 0.2 μM, similar to αE-catenin dimer (1.0 μM[159]). Thus, αT-catenin monomer is a constitutive actin-binding protein and, unlike αE-catenin, homodimerization is not required for strong F-actin binding in the absence of force[42,127,148].

To investigate if αT-catenin monomer bundles F-actin, we used transmission electron microscopy (TEM) to visualize αT-catenin incubated with actin filaments. Weak bundling of 2 μM F-actin was observed with 4 μM αT-catenin (**Fig. 2.3C, quantification in 2.5D**). In contrast, robust bundling of 2 μM F-actin was observed with 4 μM αE-catenin homodimer (**Fig. 2.3C, 2.5D**). The weak bundling observed with αT-catenin could result from either the dimer species being stabilized on the actin filament or activation of a cryptic dimerization domain, as observed in vinculin tail[160]. We conclude that αT-catenin is a poor bundler of F-actin.

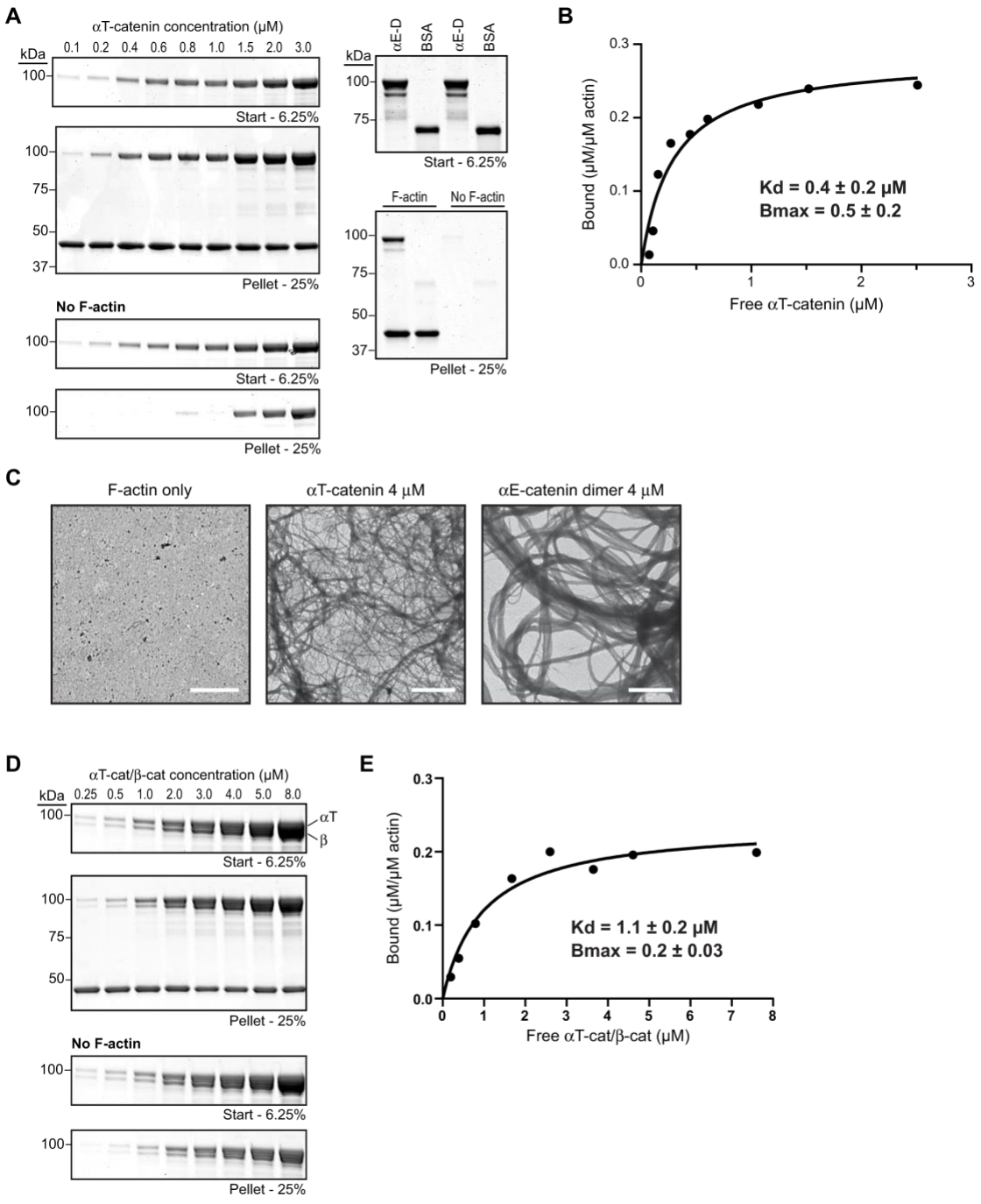

Figure 2.3 αT-catenin binds F-actin.

A. High-speed cosedimentation assay of αT-catenin with F-actin. Left panels. Increasing concentrations (0.1 – 3.0 μM) of αT-catenin were incubated with or without 2 μM F-actin, incubated for 30 minutes at RT and centrifuged. Starting (6.25% of total) and pelleted material (25% of total) were separated by SDS-PAGE and stained with Coomassie dye. Right panels. 4 μM of αE-catenin dimer and 4 μM BSA were routinely run as

positive and negative controls, respectively. B. Bound αT-catenin (μM/μM actin) from A was plotted against free αT-catenin (μM) and data fit to a hyperbolic function (black line). The average K_d and Bmax plus or minus standard deviation from four independent experiments are shown. Results from these experiments were: experiment 1, K_d = 0.3 μM, Bmax = 0.6; experiment 2, K_d = 0.8 μM, Bmax = 0.7; experiment 3, K_d = 0.3 μM, Bmax = 0.5; experiment 4 (binding results shown in A and plotted in B), K_d = 0.3 μM, Bmax = 0.3. C. Negative-stain transmission electron micrographs of 2 μM F-actin in the absence or presence of 4 μM αT-catenin or 4 μM αE-catenin homodimer. Scales bars are 2 microns. D. Increasing concentrations (0.25 – 8.0 μM) of αT-catenin/β-catenin complex were incubated with or without 2 μM F-actin, incubated for 30 minutes at RT and centrifuged. Starting (6.25% of total) and pelleted material (25% of total) was separated by SDS-PAGE and stained with Coomassie dye. E. Bound αT-catenin/β-catenin (μM/μM actin) from D was plotted against free αT-catenin/β-catenin (μM) and data fit to a hyperbolic function (black line). The average K_d and Bmax plus or minus standard deviation from three independent experiments are shown. Results from these experiments were: experiment 1 (binding results shown in D and plotted in E), K_d = 1.0 μM, Bmax = 0.2; experiment 2, K_d = 1.4 μM, Bmax = 0.2; experiment 3, K_d = 1.1 μM, Bmax = 0.2.

2.3.4 αT-catenin couples β-catenin to F-actin.

Binding to β-catenin weakens the affinity of αE-catenin for F-actin[127,148]. To test if αT-catenin can bind F-actin as part of the cadherin/catenin complex, we purified mouse β-catenin and mixed it with αT-catenin. As expected, αT-catenin bound to β-catenin with a 1:1 stoichiometry (data not shown) and we isolated the β-catenin/αT-catenin complex by SEC. Increasing concentrations of the β-catenin/αT-catenin complex were incubated in the presence or absence of F-actin, centrifuged and the pelleted material analyzed as above. Though the β-catenin/αT-catenin complex pelleted in the absence of F-actin (**Fig. 2.3D,** No F-actin panel), we were able to calculate the affinity of the complex for F-actin. The β-catenin/αT-catenin complex bound to F-actin with

a K_d of 1.1 ± 0.2 μM (**Fig. 2.3E**). Though β-catenin lowers the affinity of αT-catenin for F-actin slightly, the interaction strength is considerably stronger than that of the *D. rerio* β-catenin/αE-catenin complex (>10 μM) and similar to the strength of αE-catenin homodimer association with F-actin[156,159]. Thus, αT-catenin can bind both β-catenin and F-actin simultaneously to directly link the cadherin-catenin complex to the actin cytoskeleton. This is distinct from αE-catenin, in which force is needed to strengthen the association between the cadherin-catenin complex and F-actin[42]. Though tension may strengthen the interaction between αT-catenin and F-actin, we speculate that basal binding permits coupling between the cadherin-catenin complex and actin through αT-catenin over a range of forces.

2.3.5 αT-catenin V94D mutation creates an obligate homodimer.

Two mutations in αT-catenin have been linked to ARVC: replacement of a valine for an aspartic acid at aa 94 (V94D) in the N1 domain and deletion of a leucine at aa 765 (L765del) in the ABD[16]. Yeast two-hybrid and overexpression studies suggest the V94D mutant interferes with β-catenin binding and the L765del mutation promotes oligomerization[16]. However, it is not clear how these mutations affect the biochemical properties of αT-catenin or impact cellular function in cardiomyocytes. We used site-directed mutagenesis to make the V94D and L765del mutations in αT-catenin and attempted to purify the mutant proteins. We were unable to purify L765del – the mutation rendered the expressed protein insoluble (data not shown). However, we were successful in expressing and purifying the V94D mutant. Surprisingly, V94D eluted as a single peak off the MonoQ column rather than two as observed with wt αT-catenin (**Fig. 2.4A**). We then ran the V94D peak over an S200 SEC column where it eluted as a single peak before wt αT-catenin and similar

to the possible homodimer peak (**Fig. 2.4B**). We then compared the concentrated V94D protein (25-30 μM; concentrations greater than this precipitated out of solution) to wt αT-catenin by analytical SEC. The V94D mutant eluted as a single species before wt αT-catenin with a larger Stokes radius (**Fig. 2.2C, G**; 5.8 nm versus 4.7 nm). The V94D mutant also displayed a higher sedimentation coefficient than wt αT-catenin (**Fig. 2.4D, G;** 7.7 S versus 5.7 S). The Stokes radius and sedimentation coefficient produced a molecular weight of 183 kDa (**Fig. 2.4G**), roughly double that of wt αT-catenin. We conclude that the V94D mutation creates a stable αT-catenin homodimer.

Since full-length αT-catenin V94D is difficult to purify, we deleted the ABD (aa 660-895) in both wt and V94D αT-catenin to improve protein yield. We analyzed the SEC and sedimentation properties of the ΔABD constructs (**Fig. 2.4E-G**). Similar to the full-length construct, the V94D mutation altered the elution and sedimentation profiles of the ΔABD construct (**Fig. 2.4E, F**). The calculated molecular weight of αT-catenin V94D ΔABD was 146 kDa, compared to 90 kDa of αT-catenin ΔABD, consistent with it forming a homodimer.

We analyzed the oligomeric state of the αT-catenin ΔABD proteins by crosslinking. Increasing concentrations of αT-catenin ΔABD and αT-catenin V94D ΔABD were incubated with or without the crosslinker BS3 and the resulting products analyzed by SDS-PAGE. As expected, αT-catenin ΔABD and αT-catenin V94D ΔABD ran as 75 kDa proteins in the absence of crosslinker (**Fig. 2.4H**). In the presence of BS3, however, V94D migrated as a 150 kDa protein at all concentrations tested, indicating a crosslinked dimer. Incubation with BS3 did not affect αT-catenin ΔABD migration at low concentrations, though at higher concentrations (2 μM and 4 μM) a 150 kDa species was detected. We speculate that this could reflect a transient homodimer species. We conclude that the V94D mutation promotes dimerization of αT-catenin.

We used limited proteolysis to determine if the V94D mutation affected domain organization. Like wt αT-catenin, three fragments were resistant to trypsin cleavage in V94D (**Fig. 2.4I**). However, the β-catenin/homodimerization domain (aa 108 start, confirmed by Edman degradation sequencing) was protected relative to wt (blue arrowhead in **Fig. 2.4I**, compare to blue arrowhead in **Fig. 2.1D**), consistent with this domain being stabilized in the homodimer state.

We then questioned if the V94D homodimer could interact with β-catenin. We mixed increasing concentrations of wt or V94D αT-catenin with GST-tagged β-catenin, pulled down the β-catenin and assessed binding. Wild-type αT-catenin bound GST-β-catenin at stoichiometric levels; however, little to no V94D bound (**Fig. 2.4J**). Thus, the V94D mutation creates an obligate αT-catenin homodimer that cannot bind β-catenin.

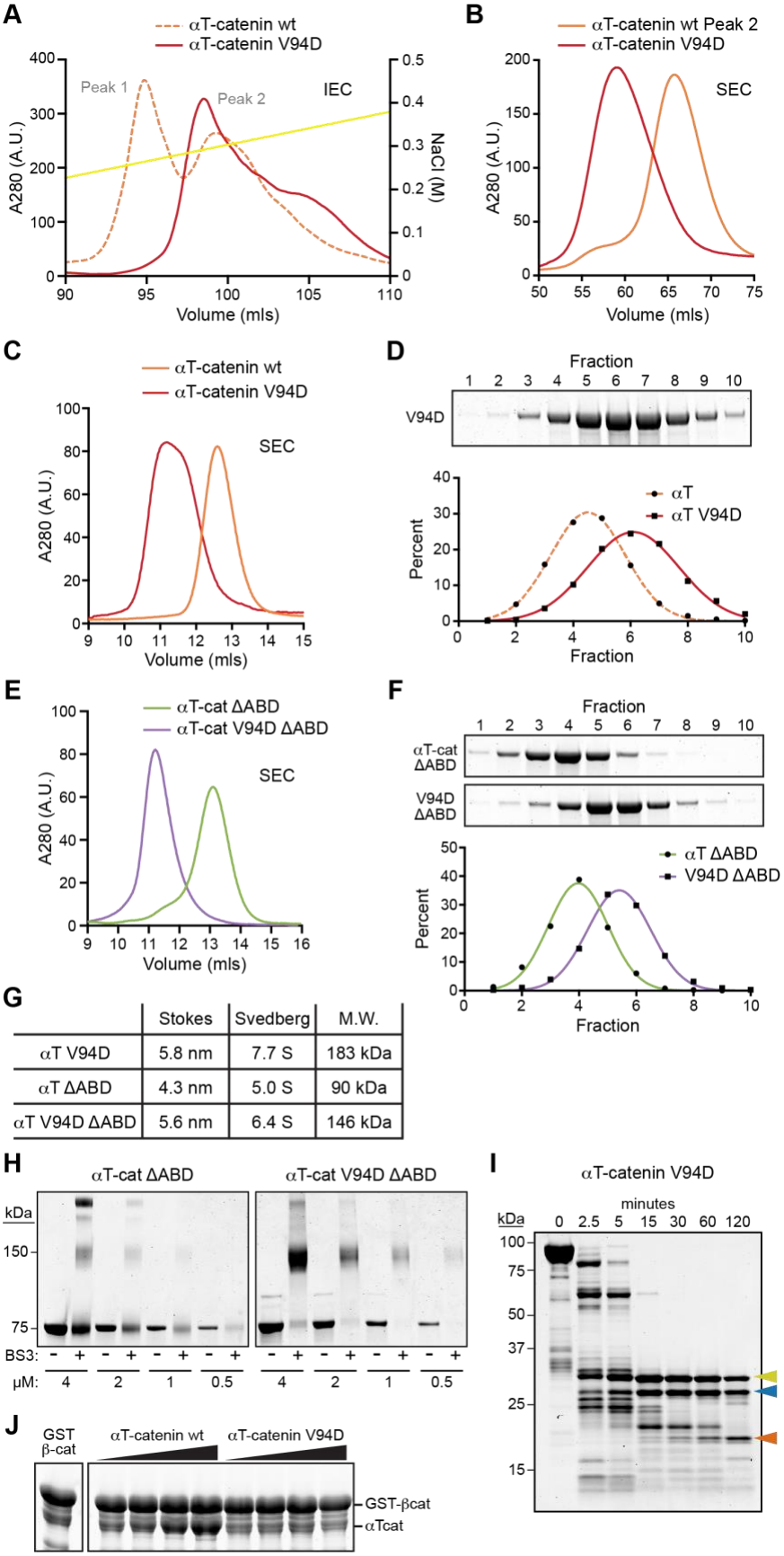

	Stokes	Svedberg	M.W.
αT V94D	5.8 nm	7.7 S	183 kDa
αT ΔABD	4.3 nm	5.0 S	90 kDa
αT V94D ΔABD	5.6 nm	6.4 S	146 kDa

Figure 2.4 . αT-catenin V94D mutation promotes homodimerization.

A. MonoQ anion exchange chromatography of αT-catenin V94D mutant (solid red line) and wt αT-catenin (dashed orange line shown as reference; chromatogram same as in Fig. 2A). B. S200 SEC of αT-catenin V94D MonoQ peak fraction and αT-catenin wt peak 2 fraction. C. Analytical S200 SEC of αT-catenin V94D and αT-catenin wt. Elution profile used to calculate R_s in G. D. Sucrose gradient sedimentation of αT-catenin V94D. Fractions were collected from 5-20% sucrose gradients and analyzed by Coomassie-stained SDS-PAGE. The percentage of V94D in each fraction was measured, plotted and the data fit to a Gaussian curve (red line). αT-catenin sedimentation profile from Fig. 2E (dashed orange line) shown for comparison. Average peak used to calculate sedimentation coefficient in G. E. Analytical S200 SEC of αT-catenin ΔABD and αT-catenin V94D ΔABD. Elution profiles used to calculate R_s in G. F. Sucrose gradient sedimentation of αT-catenin ΔABD and αT-catenin V94D ΔABD. Average peaks used to calculate sedimentation coefficients in G. G. Calculated molecular weights of αT-catenin V94D, αT-catenin ΔABD and αT-catenin V94D ΔABD. H. Cross-linking experiments with αT-catenin ΔABD and αT-catenin V94D ΔABD. Decreasing concentrations of protein (4 μM – 0.5 μM) were incubated with or without 1 mM BS3 for 30 minutes at RT, separated by SDS-PAGE and stained with Coomassie dye. I. Limited proteolysis of αT-catenin V94D. Color-coded arrows mark stable fragments mapped in Fig. 1A. J. Increasing concentrations of purified αT-catenin wt or αT-catenin V94D protein were incubated with GST-tagged full-length β-catenin for 1 hour at RT, washed, and then analyzed by SDS-PAGE. IEC, ion exchange chromatography; SEC, size exclusion chromatography.

2.3.6 αT-catenin V94D binds and bundles F-actin.

Dimerization promotes αE-catenin binding to F-actin[127,148]. We questioned if the V94D potentiates αT-catenin binding to F-actin. The V94D mutant cosedimented with F-actin (**Fig. 2.5A**) with a similar affinity to wt αT-catenin (0.4 μM ± 0.1 μM, **Fig. 2.4B**), suggesting that homodimerization does not increase the affinity of αT-catenin for F-actin.

We then tested if the V94D homodimer could bundle F-actin. We consistently observed increased bundling of 2 µM F-actin with 4 µM αT-catenin V94D relative to 4 µM wt αT-catenin (**Fig. 2.5C-D**). Though increased, the level of bundling was still less than that observed with 4 µM αE-catenin homodimer (**Fig. 2.3C, 2.5D**). We conclude that the V94D mutation promotes αT-catenin-mediated F-actin bundling.

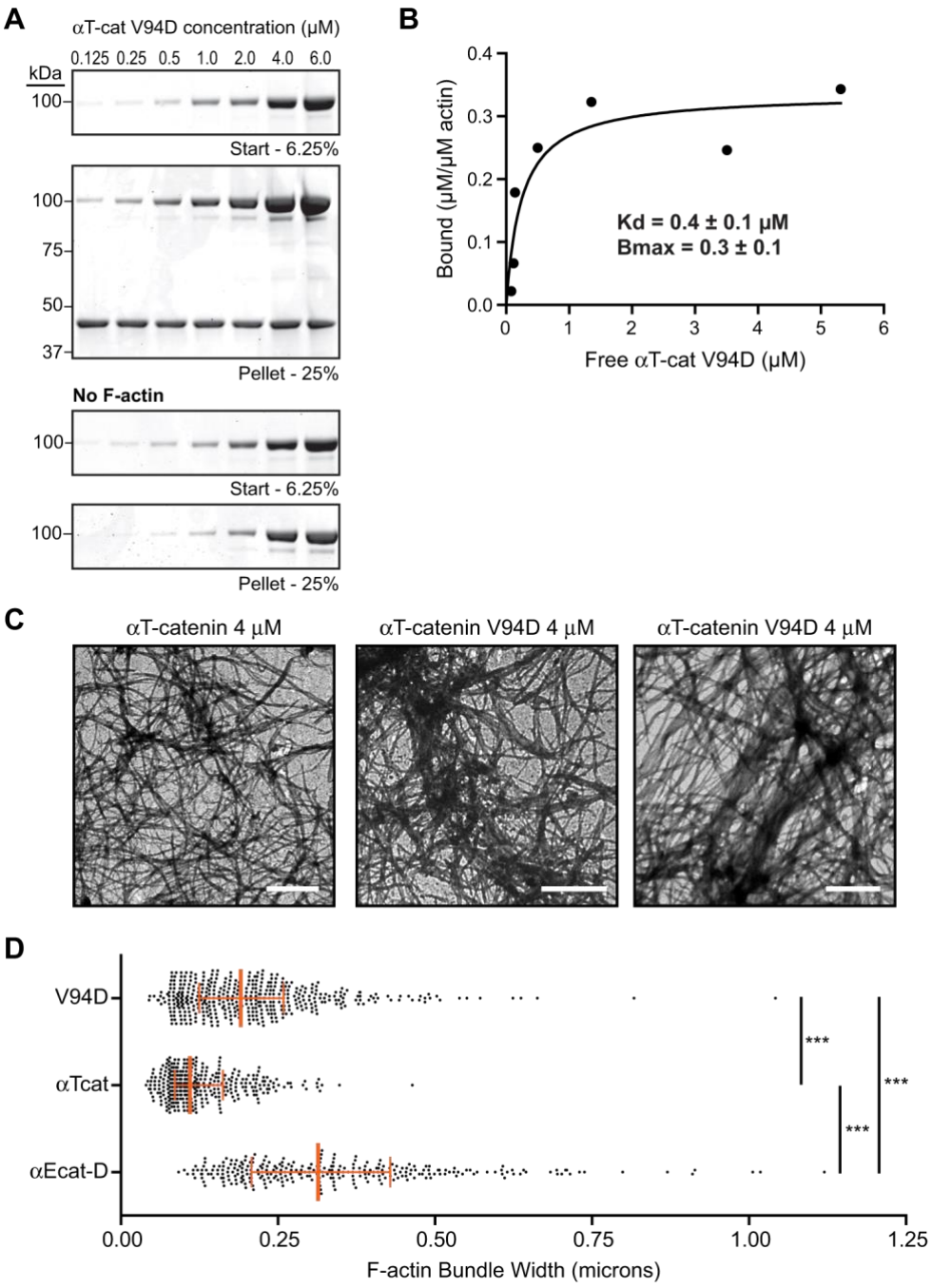

Figure 2.5 αT-catenin V94D binds F-actin and promotes bundling.

A. High-speed cosedimentation assay of αT-catenin V94D with F-actin. Increasing concentrations (0.125 – 6.0 μM) of αT-catenin V94D were incubated with or without 2 μM F-actin, incubated for 30 minutes at RT and centrifuged. Starting (6.25% of total) and pelleted material (25% of total) were separated by SDS-PAGE and stained with Coomassie dye. B. Bound αT-catenin V94D (μM/μM actin) from A was plotted against free αT-catenin V94D (μM) and data fit to a hyperbolic function (black line). The average K_d and Bmax plus or minus

standard deviation from three independent experiments are shown. Results from these experiments were: experiment 1, K_d = 0.4 µM, Bmax = 0.4; experiment 2 (binding results shown in A and plotted in B), K_d = 0.2 µM, Bmax = 0.3; experiment 3, K_d = 0.4 µM, Bmax = 0.2. C. Negative-stain transmission electron micrographs of 2 µM F-actin in the presence of 4 µM αT-catenin or 4 µM αT-catenin V94D. Scales bars are 2 microns. D. F-actin bundle width was measured in αE-catenin homodimer (αEcat-D; Fig. 3C), wt αT-catenin (αTcat) and V94D αT-catenin (V94D) samples. Scatter plot of all measurements (αEcat-D, n = 291; αTcat, n = 337; V94D, n = 449) from at least three images shown. The orange vertical line marks the median and the bars define the interquartile range. Mean and standard deviation: αEcat-D = 0.34 ± 0.17; αTcat = 0.13 ± 0.06; V94D = 0.21 ± 0.12). ***p < 0.001, One-way ANOVA with Dunn's multiple comparison test.

2.3.7 αT-catenin V94D disrupts localization in cardiomyocytes.

αT-catenin localizes to the adherens junction at the ICD in cardiomyocytes[48]. To determine if the V94D mutation disrupted αT-catenin cellular localization, we transiently expressed EGFP-tagged wt or V94D αT-catenin in neonatal mouse cardiomyocytes. EGFP-αT-catenin localized specifically to cell-cell contacts in cardiomyocytes where it colocalized with both αE-catenin and N-cadherin (**Fig. 2.6A, C; zoom in 2.6E**). In contrast, V94D was largely peripheral to cell-cell contacts (**Fig. 2.6B, D; zoom in 2.6E**) and localized to actin fibers (orange arrowheads in 2.6B and 2.6D). This was confirmed by directly measuring colocalization between N-cadherin and EGFP-αT-catenin or EGFP-αT-catenin V94D signals at AJ clusters in transfected cells using Pearson's *r* (**Fig. 2.6F**). This analysis revealed a significant reduction in colocalization between N-cadherin and EGFP-αT-catenin V94D at AJs (**Fig. 2.6F**). Thus, the V94D mutation disrupts αT-catenin subcellular localization in cardiomyocytes.

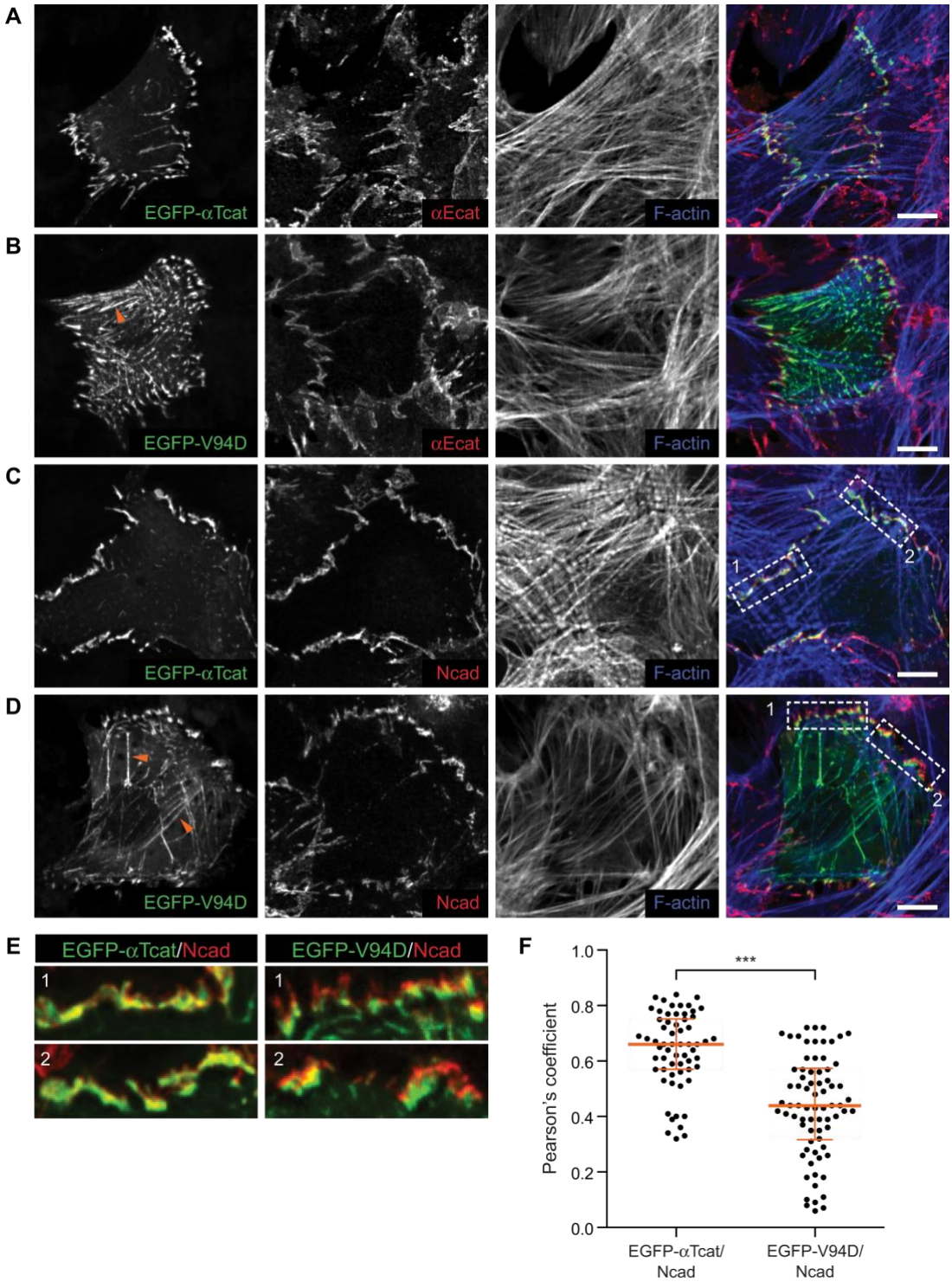

Figure 2.6 αT-catenin V94D mutation disrupts localization in cardiomyocytes.

A-E. Mouse neonatal cardiomyocytes transfected with EGFP-tagged αT-catenin or αT-catenin V94D. Cells were fixed 48 hours post-transfection and stained with Alexa-labeled phalloidin and antibodies against αE-

catenin (A–B) or N-cadherin (C–E). EGFP-αT-catenin colocalized with N-cadherin at cell-cell contacts (C; magnification of boxed contacts in E, left panels) whereas EGFP-αT-catenin V94D localization was largely adjacent to N-cadherin-rich contacts (D; magnification of boxed contacts in E, right panels). EGFP-αT-catenin V94D was also observed on actin fibers (orange arrows in B and D). Scale bars are 10 microns. F. Pearson's *r* was calculated between N-cadherin and EGFP-αT-catenin or EGFP-αT-catenin V94D signals at individual AJ clusters in transfected cells (EGFP-αTcat/Ncad, n = 61 AJ clusters; EGFP-V94D/Ncad, n = 74 AJ clusters). Scatter plot with all data points shown. The orange horizontal line marks the median and the bars define the interquartile range. Mean and standard deviation: EGFP-αTcat/Ncad = 0.64 ± 0.14; EGFP-V94D/Ncad = 0.44 ± 0.18. ***p < 0.0001, unpaired t test.

2.4 Discussion

2.4.1 αT-catenin binds F-actin strongly as a monomer.

Our *in vitro* results show that, in solution, αT-catenin binds F-actin as a monomer and in complex with β-catenin, properties that separate it from mammalian αE-catenin. αT-catenin monomer binds F-actin with a slightly higher affinity than αE-catenin homodimer (0.4 μM versus 1.0 μM) [159]. While β-catenin binding reduces the affinity of αT-catenin for F-actin, the reduction is relatively small (from 0.4 μM to 1.1 μM). We conclude that αT-catenin binding to F-actin, unlike mammalian αE-catenin, is not allosterically regulated. This would permit αT-catenin to directly couple the cadherin-catenin complex to the actin cytoskeleton in the absence of tension, though mechanical force could strengthen the αT-catenin-actin interface.

2.4.2 αT-catenin has dimerization potential.

Both *M. musculus* αE-catenin and αN-catenin homodimerize in solution, though the kinetics of dimerization differ significantly between the two mammalian α-catenins[43]. At physiological temperature, the homodimerization affinity of αN-catenin is more than 10x greater than the homodimerization affinity of αE-catenin (2 μM versus 25 μM). However, the kinetics of dissociation differ markedly: αN-catenin equilibrates quickly whereas a kinetic block limits αE-catenin dissociation[43]. The αE-catenin dimer is thus stabilized and can persist at concentrations well below the K_d of association. Our *in vitro* results suggest that αT-catenin has the ability to homodimerize. We observed a monomer and putative dimer species by IEC, though the dimer quickly dissociated upon dilution during SEC. Stronger evidence comes from our analysis of the V94D mutation, where a single amino acid change shifted the protein to the homodimer state. Crosslinking studies with the αT-catenin ΔABD constructs also provide evidence for dimerization potential in the wt protein. Unfortunately, our inability to maintain soluble αT-catenin at or near physiological temperature (37 °C) precluded a detailed analysis of dimerization kinetics. Nonetheless, our results lead us to postulate that αT-catenin has dimerization potential and that the homodimer species, similar to αN-catenin, dissociates quickly (i.e., no kinetic block).

Evidence suggests a potential role for the α-catenin homodimer in migration and cell-cell adhesion[128,159,161]. However, a physiological role for the α-catenin homodimer in cardiomyocytes and whether putative αE-catenin and αT-catenin homodimers function similarly *in vivo* is unclear. The V94D mutation, which drives αT-catenin into the dimer state *in vitro*, shifted localization from cell-cell contacts and promoted recruitment to F-actin bundles when expressed in cardiomyocytes. Actin filament crosslinking is essential for cardiomyocyte cytoskeletal

organization and function. The barbed ends of actin filaments from adjoining sarcomeres interdigitate at the Z-disc, where they are crosslinked primarily by α-actinin to form a structural lattice[162]. α-Actinin is an established α-catenin ligand[91,163] and we have detected αT-catenin in complex with α-actinin in cardiomyocyte lysates[1]. Thus, the αT-catenin homodimer could have a role in cytoskeleton organization in cardiomyocytes. Alternatively, homodimerization may serve to regulate interactions with β-catenin and/or plakoglobin along the ICD. Additional work is needed to elucidate the putative role of the αT-catenin homodimer in cardiomyocyte biology.

2.4.3 V94D mutation linked to ARVC promotes homodimerization.

The V94D mutation in αT-catenin is linked to ARVC, though the heterozygous mutation has only been documented in one individual[16]. It was previously shown that the mutation reduced both β-catenin binding and homodimerization potential in a yeast two-hybrid assay[16]. In contrast, we found that V94D promotes αT-catenin homodimerization, in effect creating an obligate homodimer species that cannot bind β-catenin. Not surprisingly, the V94D mutant disrupted cell-cell contact localization when expressed in cardiomyocytes. In the heterozygous state, it is unclear if 1) V94D interacts with wt αT-catenin to disrupt localization to cell junctions and αT-catenin-mediated adhesion, and/or 2) if the mis-localized mutant protein disrupts cytoskeletal organization. Nonetheless, to the best of our knowledge this is one of the first demonstrations of how a disease-linked mutation in α-catenin disrupts a fundamental molecular property.

[1] Wickline and Kwiatkowski, unpublished observation

2.4.4 αT-catenin domain stability.

Our limited proteolysis experiments revealed that both the β-catenin/homodimerization domain and middle domain were more protease-sensitive in αT-catenin than in αE-catenin. Notably, the N2 bundle within the β-catenin/homodimerization domain of αT-catenin is the region with the least conservation compared to αE-catenin. αT-catenin binds β-catenin (**Fig. 4D**) and plakoglobin (Kwiatkowski, unpublished observation), though the strengths of these interactions are untested. Differences in N2 could impact αT-catenin ligand binding, including self-association, to regulate molecular complex formation at cell-cell contacts.

The core M region (M1-M3) of αE-catenin is required for its function as a mechanosensor in which tension alters α-catenin conformation to promote ligand binding[95,102,149,164]. Recent structural and single molecule studies coupled with molecular dynamic simulations support a model in which mechanical force reorients M2 and M3 to release M1, which contains the vinculin binding domain[95,102,103]. A salt-bridge network between M domains is postulated to maintain αE-catenin in the autoinhibited conformation in the absence of tension[103]. Based on sequence homology, a similar salt-bridge network could exist in αT-catenin, though our limited proteolysis results showed that the αT-catenin M-fragment (M2-M3) was less stable than in αE-catenin. We speculate that increased flexibility within the αT-catenin M2 and M3 domains could reduce the force required for activation, permitting M1 release and ligand recruitment at lower tension states.

Increased flexibility between the M2 and M3 domains could also promote ligand binding within this region. Notably, αT-catenin – but not αE-catenin – was shown to bind plakophilin-2 (PKP2), a desmosomal protein that links to intermediate filaments (IFs), and the binding interface was mapped to M3[75]. αT-catenin, through association with PKP2, may function as molecular link

to integrate the actin and IF cytoskeletons at the ICD. It is possible that structural differences within core M region between α-catenins could regulate both mechanosensing and ligand binding properties.

2.4.5 αT-catenin function in cardiomyocytes

α-Catenin functions in adhesion and mechanical signaling must be integrated in all tissues. Contractile forces place physical demands on heart junctional complexes: not only must they withstand repeated cycles of force, tension-sensing proteins within these complexes must be "tuned" to regulate signaling and maintain homeostasis. Our *in vitro* studies showed that αT-catenin could directly couple the actin cytoskeleton to the cadherin/catenin in the absence of tension. We speculate that this property of αT-catenin might permit the cadherin-catenin complex to maintain a static linkage to the actomyosin network over a range of forces, such as those produced by repeated cycles of contraction and relaxation in cardiomyocytes. Our biochemical analyses also suggest that αT-catenin dimerization properties and M region stability differ from αE-catenin. How these differences impact *in vivo* function is unclear, but we speculate that they could impact molecular interactions and tension sensing. In the mammalian heart, αT-catenin may have evolved to complement αE-catenin functions in adhesion and signaling.

2.5 Experimental Procedures

2.5.1 Plasmids

DNA encoding full-length *M. musculus* αT-catenin was cloned into pGEX-TEV[159] to create a fusion between GST and αT-catenin. Site-directed mutagenesis was used to create the valine to aspartic acid mutation at amino acid 94 (V94D) in αT-catenin. The N-terminal head region (aa 1-659) of αT-catenin or αT-catenin V94D was cloned into pGEX-TEV to create the ΔABD constructs. Wild type (wt) and V94D αT-catenin were cloned into pEGFP-C1 for expression in mammalian cells.

2.5.2 Recombinant Protein Expression and Purification

GST-tagged αT-catenin, αE-catenin and β-catenin were expressed in BL21 (DE3) *E. coli* cells and purified as described[155,159] (see appendix B for detailed protocol). GST-tagged proteins bound to glutathione-agarose were equilibrated in cleavage/elution buffer (20 mM Tris pH 8.0, 150 mM NaCl, 2 mM EDTA, 1 mM DTT and 10% glycerol) and then incubated with tobacco etch virus (TEV) protease overnight at 4 °C to cleave protein from the GST tag. All proteins were purified by MonoQ anion exchange chromatography followed by Superdex 200 (S200) gel filtration chromatography in 20 mM Tris pH 8.0, 150 mM NaCl, 10% glycerol and 1 mM DTT. Eluted protein was concentrated to 20–50 μM working concentrations using a Millipore column concentrator, flash frozen in liquid nitrogen and stored at -80 °C.

2.5.3 Size Exclusion Chromatography

Analytical size exclusion chromatography (SEC) was performed at 4°C on a Superdex 200 column in 20 mM Tris pH 8.0, 150 mM NaCl and 1 mM DTT. Protein was injected at 25-30 μM.

2.5.4 Native PAGE

FPLC-purified αE-catenin and αT-catenin were diluted in cold native gel sample buffer (20 mM Tris pH 6.8, 150 mM NaCl, 300 mM sucrose, 100 mM DTT and 0.02% bromophenol blue) and loaded onto a 5% native gel (running gel: 0.4 M Tris pH 8.8, 5% acrylamide; stacking gel: 0.1 M Tris pH 6.8, 5% acrylamide). Gels were run at 80 V for 5 hours at 4 °C, stained with Coomassie blue, and imaged on a LI-COR scanner.

2.5.5 Limited proteolysis and Edman degradation sequencing

For detailed protocol see appendix C. 12 μM αT-catenin and was incubated at room temperature in 0.05 mg/mL sequence-grade trypsin (Roche) in 20 mM Tris pH 8.0, 150 mM NaCl and 1 mM DTT. Reactions were stopped with 2X Laemmli buffer at the indicated times and samples analyzed by SDS-PAGE. For N-terminal sequencing, digested peptides were blotted onto PVDF membrane, stained with 0.1% Coomassie R-250/40% methanol/1% acetic acid, destained and dried. Individual bands were excised and sequenced by Edman degradation (Iowa State University Protein Facility).

2.5.6 Stokes radius measurements

The Stokes radius (R_s) was determined by analytical size exclusion chromatography using a Superdex 200 column equilibrated with 20 mM Tris pH 8.0, 150 mM NaCl and 1 mM DTT. Standard proteins were bovine carbonic anhydrase (R_s = 2.4 nm), bovine serum albumin (R_s = 3.5 nm), yeast alcohol dehydrogenase (R_s = 4.6 nm), sweet potato β-amylase (R_s = 5.4 nm), horse spleen apoferritin (R_s = 6.7 nm) and bovine thyroglobulin (R_s = 8.5 nm). The partition coefficient, K_{av}, was calculated for all standards and α-catenin proteins used in this study. The Stokes radius was calculated from a standard curve of $(-\log K_{av})^{1/2}$ versus R_s.

2.5.7 Sucrose density gradient centrifugation

Gradients of sucrose were made by layering sucrose dissolved in 20 mM Tris pH 8.0, 150 mM NaCl from 20% to 5% in 2.5% increments in 13 x 63 mm ultracentrifuge tubes as described[165]. Each layer was frozen in a dry ice/ethanol bath before the addition of the next layer. Tubes were stored at - 80 °C until use. Tubes were thawed overnight at 4 °C to establish a gradient. 100 µl of sample was layered on top and centrifuged in a Thermo Scientific Sorvall S100-AT rotor at 70,000 rpm (200,000 g) for 4 hours at 4 °C. All α-catenin proteins were loaded at concentrations ≥ 20 µM. After centrifugation, 200 µl fractions were collected and analyzed by SDS-PAGE. Gels were imaged on a LI-COR scanner and the percentage of protein in each fraction was measured in ImageJ. Plotted data was fit to a Gaussian curve to determine the average fraction in Prism software. Standard proteins were bovine carbonic anhydrase (2.8 S), bovine serum albumin (4.3 S), yeast alcohol dehydrogenase (7.4 S), sweet potato β-amylase (8.9 S) and horse spleen

apoferritin (16.6 S). The sedimentation coefficient of α-catenin proteins was determined from a standard curve of sedimentation coefficient (Svederg units, S) versus fraction.

2.5.8 Molecular weight calculations

The molecular mass of α-catenin proteins used in this study was calculated from the measured Stokes radius and sedimentation coefficient as described[157,166].

2.5.9 Actin co-sedimentation assays

For a detailed protocol see appendix A. Chicken muscle G-actin (Cytoskeleton, Inc.) was incubated in 1X actin polymerization buffer (20 mM HEPES pH 7.5, 100 mM KCl, 2 mM $MgCl_2$, 0.5 mM ATP, 1 mM EGTA) for 1 hour at room temperature to polymerize filaments. Gel-filtered αT-catenin or αT-catenin/β-catenin heterocomplex was diluted to indicated concentrations in 1X reaction buffer (20 mM HEPES pH 7.5, 150 mM NaCl, 2 mM $MgCl_2$, 0.5 mM ATP, 1 mM EGTA, 1 mM DTT and 0.02% Thesit) with and without 2 μM F-actin and incubated for 30 minutes at room temperature. Samples were centrifuged at 50,000 rpm (>100,000 g) for 20 minutes at 4°C in an S100-AT3 rotor. Pellets were resuspended in Laemmli sample buffer, separated by SDS-PAGE and stained with Coomassie blue. Gels were imaged on a LI-COR scanner, and measured and quantified in ImageJ. To determine the amount of bound protein, background sedimentation (no F-actin pellet) was first subtracted from cosedimentation (F-actin pellet). Bound protein across samples was then normalized to the F-actin pellet. The amount of bound protein was calculated from a standard curve created from the starting material. All binding data was processed with Prism software.

2.5.10 F-actin bundling

Protein samples were prepared as for the actin cosedimentation assays and deposited on carbon grids. Samples were fixed in 2.5% glutaraldehyde, stained with 1% uranyl acetate for 1-3 minutes and examined in a JEOL JEM-1011 transmission electron microscope (TEM). To quantify bundling, a 20 micron by 20 micron grid was overlaid on images and the width of all bundles in four random squares on the grid measured using ImageJ. The data was plotted and analyzed with Prism software.

2.5.11 Crosslinking experiments

Purified αT-catenin ΔABD and αT-catenin V94D ΔABD were incubated with or without 1 mM BS3 (bis(sulfosuccinimidyl)suberate, Thermo Scientific) in 20 mM HEPES pH 7.4, 150 mM DTT and 1 mM DTT for 30 minutes at RT, separated by SDS-PAGE, stained with Coomassie dye and imaged on a LI-COR scanner.

2.5.12 GST pulldown experiments

Increasing amounts of αT-catenin or αT-catenin V94D (1-15 µg) were added to 15 µg of GST-β-catenin bound to glutathione agarose in 20 mM Tris pH 8, 150 mM NaCl and 5 mM DTT. Samples were incubated with gentle mixing for >2 hours at 4 °C and then washed 5 times in PBS + 0.05% Tween 20 and 5 mM DTT before elution in Laemmli sample buffer. Samples were separated by SDS-PAGE, stained with Coomassie dye and imaged on a LI-COR scanner.

2.5.13 Cardiomyocyte isolation and culture

All animal work was approved by the University of Pittsburgh Division of Laboratory Animal Resources. Cardiomyocytes were isolated from mouse neonates (P1-P3) as described[167]. Cardiomyocytes were plated onto collagen-coated coverslips and maintained in 78% DMEM, 17% M-199, 4% horse serum, 1% penicillin/streptomycin, 1 μM AraC and 1 μM isoproterenol. Transfections were performed 24 hours post-plating using Lipofectamine 2000 (Life Technologies).

2.5.14 Immunostaining and confocal microscopy

For a detailed protocol see appendix D. Cells were fixed in 4% paraformaldehyde (PFA) in PHEM buffer (60 mM 1,4-piperazinediethanesulfonic acid, pH 7.0, 25 mM HEPES, pH 7.0, 10 mM EGTA, pH 8.0, 2 mM $MgCl_2$, 0.12 M sucrose), washed with PBS, blocked for 1 hour at RT in PBS + 10% BSA, washed three times in PBS, incubated with primary in PBS + 1% BSA for 1 hour at RT, washed three times in PBS, incubated with secondary in PBS + 1% BSA for 1 hour at RT, washed three times in PBS, and mounted in Fluoromount G (Electron Microscopy Sciences). F-actin was stained using Alexa Fluor phalloidin (Invitrogen) and antibodies against αE-catenin (Enzo Life Sciences) or N-cadherin (Invitrogen). Cells were imaged on a Nikon Eclipse Ti inverted microscope outfitted with a Prairie swept field confocal scanner, Agilent monolithic laser launch and Andor iXon3 camera using NIS-Elements imaging software. Maximum projections of 4 micron image stacks were created for image analysis and presentation. For Pearson's r calculations, signal colocalization was measured between user-defined N-cadherin-positive AJ

clusters and EGFP signals using ImageJ. Colocalization data was plotted and analyzed with Prism software.

3.0 Distinct intramolecular interactions regulate autoinhibition of vinculin binding in αT-catenin and αE-catenin

This text was published in the Journal of Biological Chemistry in 2021:

Heier JA, Pokutta S, Dale IW, et al. Distinct intramolecular interactions regulate autoinhibition of vinculin binding in **α**T-catenin and **α**E-catenin. *J Biol Chem*. 2021;296:100582. doi:10.1016/j.jbc.2021.100582.

Contributions: I purified all proteins used in the experiments. I performed all published ITC experiments with the exception of those involving vinculin binding αT-catenin 1-659. I also performed all crosslinking and limited proteolysis experiments, in addition to the quantification of vinculin recruitment in R2/7 cells. Finally, I wrote and edited the original and revised manuscripts.

3.1 Overview

α-Catenin binds directly to β-catenin and connects the cadherin-catenin complex to the actin cytoskeleton. Tension regulates α-catenin conformation: actomyosin-generated force stretches the middle(M)-region to relieve autoinhibition and reveal a binding site for the actin-binding protein vinculin. Here we describe the biochemical properties of αT(testes)-catenin, an α-catenin isoform critical for cardiac function, and how intramolecular interactions regulate vinculin binding autoinhibition. Isothermal titration calorimetry (ITC) showed that αT-catenin binds the β-catenin/N-cadherin complex with a similar low nanomolar affinity to that of αE-catenin. Limited

proteolysis revealed that the αT-catenin M-region adopts a more open conformation than αE-catenin. The αT-catenin M-region binds the vinculin N-terminus with low nanomolar affinity, indicating that the isolated αT-catenin M-region is not autoinhibited and thereby distinct from αE-catenin. However, the αT-catenin head (N- and M-regions) binds vinculin 1000-fold more weakly (low micromolar affinity), indicating that the N-terminus regulates M-region binding to vinculin. In cells, αT-catenin recruitment of vinculin to cell-cell contacts requires the actin-binding domain and actomyosin-generated tension, indicating that force regulates vinculin binding. Together, our results show that the αT-catenin N-terminus is required to maintain M-region autoinhibition and modulate vinculin binding. We postulate that the unique molecular properties of αT-catenin allow it to function as a scaffold for building specific adhesion complexes.

3.2 Introduction

The cadherin-catenin-complex that forms the core of the adherens junction (AJ) is required for intercellular adhesion and tissue integrity[20,145,168]. Classical cadherins are single-pass transmembrane proteins with an extracellular domain that forms *trans* interactions with cadherins on adjacent cells[147,169,170]. The adhesive properties of classical cadherins are driven by the recruitment of cytosolic catenin proteins to the cadherin tail: p120-catenin binds to the juxta-membrane domain and β-catenin binds to the distal part of the tail. β-Catenin recruits α-catenin, a mechanoresponsive actin-binding protein[41-43,98,108,127,148,170]. The AJ mechanically couples and integrates the actin cytoskeletons between cells to allow dynamic adhesion and tissue morphogenesis[20].

The best characterized member of the α-catenin family of proteins is mammalian αE(epithelial)-catenin. Structurally, it is composed of 5 four-helix bundles connected to a C-terminal five-helix bundle by a flexible linker[97,105,106]. The two N-terminal four-helix bundles form the N-domain that binds β-catenin and mediates homodimerization[43,89-91]. The middle three four-helix bundles form the middle (M)-region that functions as a mechanosensor[92,93,95,103,149,171]. The C-terminal five-helix bundle forms the F-actin binding domain (ABD) [42,98-100]. F-actin binding is allosterically regulated: αE-catenin can bind F-actin readily as a homodimer, but when in complex with β-catenin, mechanical force is required for strong F-actin binding[42,100,127,148]. In addition, when tension is applied to αE-catenin, salt bridge interactions within the M-region are broken, allowing the domain to unfurl and reveal cryptic binding sites for other cytoskeletal binding proteins such as vinculin[95,102-105,149,164,172,173]. The recruitment of these proteins is thought to help stabilize the AJ in response to increased tension and further integrate the actin cytoskeleton across cell-cell contacts[45,96,149,164,172,174].

Three α-catenin family proteins are expressed in mammals: the ubiquitous αE-catenin, αN (Neuronal)-catenin and αT (Testes)-catenin[17,175]. αE-catenin and αN-catenin are 81% identical and 91% similar in amino acid sequence. αT-catenin is 58-59% identical and 77% similar to αE-catenin and αN-catenin, making it the most divergent of the family[13,17,175]. αT-catenin is predominantly expressed in the heart, testes, brain and spinal cord[48,49]. In the heart, it localizes to the intercalated disc (ICD), a specialized adhesive structure that maintains mechanical coupling and chemical communication between cardiomyocytes[5,75]. In mice, loss of αT-catenin from the heart causes dilated cardiomyopathy and mutations in αT-catenin are linked to arrhythmogenic ventricular cardiomyopathy in humans[16,53]. In addition to cardiomyopathy, αT-catenin is linked to multiple human diseases, including asthma, neurological disease and cancer[49,119,153].

Despite a growing awareness of its importance in human disease, the molecular properties and ligand interactions of αT-catenin remain poorly understood. Our previous work revealed that αT-catenin, unlike mammalian αE-catenin, is a monomer in solution that can bind to F-actin with low micromolar affinity in the absence of tension. F-actin binding is also not allosterically regulated, as the β-catenin/αT-catenin complex binds to F-actin with the same affinity as αT-catenin monomer[13]. Single molecule pulling experiments have shown the αT-catenin M-region to be mechanoresponsive as it unfurls in a force range similar to αE-catenin[176].

Here we show that αT-catenin associates with the components of the cadherin/catenin complex with an affinity similar to αE-catenin *in vitro*, revealing that they may compete with one another for binding β-catenin at the plasma membrane. We also show that the M-region of αT-catenin is not autoinhibited and can bind the vinculin N-terminus in the absence of tension with strong affinity. Unlike aE-catenin, however, when the N-terminus of αT-catenin is attached to the M-region, the affinity for vinculin drops significantly. This indicates that interdomain interactions between the N-terminus and the M-region of αT-catenin regulate its interaction with vinculin. We measured the recruitment of vinculin to cell-cell contacts and found that, despite the distinct mechanism of regulation, recruitment of vinculin is still tension dependent. Our findings indicate that the way in which tension regulates vinculin binding differs between αE-catenin and αT-catenin. We postulate that this mechanism is important for the ability of αT-catenin to build specific and distinct molecular complexes at AJs.

3.3 Results

3.3.1 αT-catenin binds tightly to the β-catenin/N-cadherin core complex

We characterized the interaction between αT-catenin and β-catenin by isothermal titration calorimetry (ITC) using purified recombinant proteins. We used the head region (comprising the N- and M-domains) of αT-catenin (aa1-659, **Fig. 3.1A**) for these experiments since it is more stable than full-length αT-catenin and yields sufficiently high protein concentrations for ITC. Past studies revealed that αE-catenin head region (aa1-651) binds β-catenin and the β-catenin•E-cadherin tail complex with a similar affinity to full-length αE-catenin[43]. We observed that the αT-catenin head binds β-catenin with a dissociation constant ~250 nM (**Fig. 3.1B, Table 3.1**). The affinity of αT-catenin for β-catenin is an order of magnitude weaker than the association of αE-catenin or αN-catenin for β-catenin (15-20 nM) [43].

Cadherin tail binding to β-catenin strengthens the affinity between β-catenin and α-catenin[43]. N-cadherin is the primary classical cadherin expressed in cardiomyocytes[25]. We tested if the N-cadherin tail ($Ncad_{cyto}$) influences the αT-catenin/β-catenin interaction by titrating β-catenin•$Ncad_{cyto}$ complex into αT-catenin head (**Fig. 1C**). The affinity of this interaction was 5-6 nM (**Table 3.1**), indicating that αT-catenin binds to the cadherin•β-catenin complex an order of magnitude more strongly than to β-catenin alone. This affinity is similar to the 1-2 nM affinity observed between the cadherin tail•β-catenin complex and αE-catenin or αN-catenin[43] and suggests that αT-catenin can effectively compete with αE-catenin for binding to the membrane-associated cadherin•β-catenin complex.

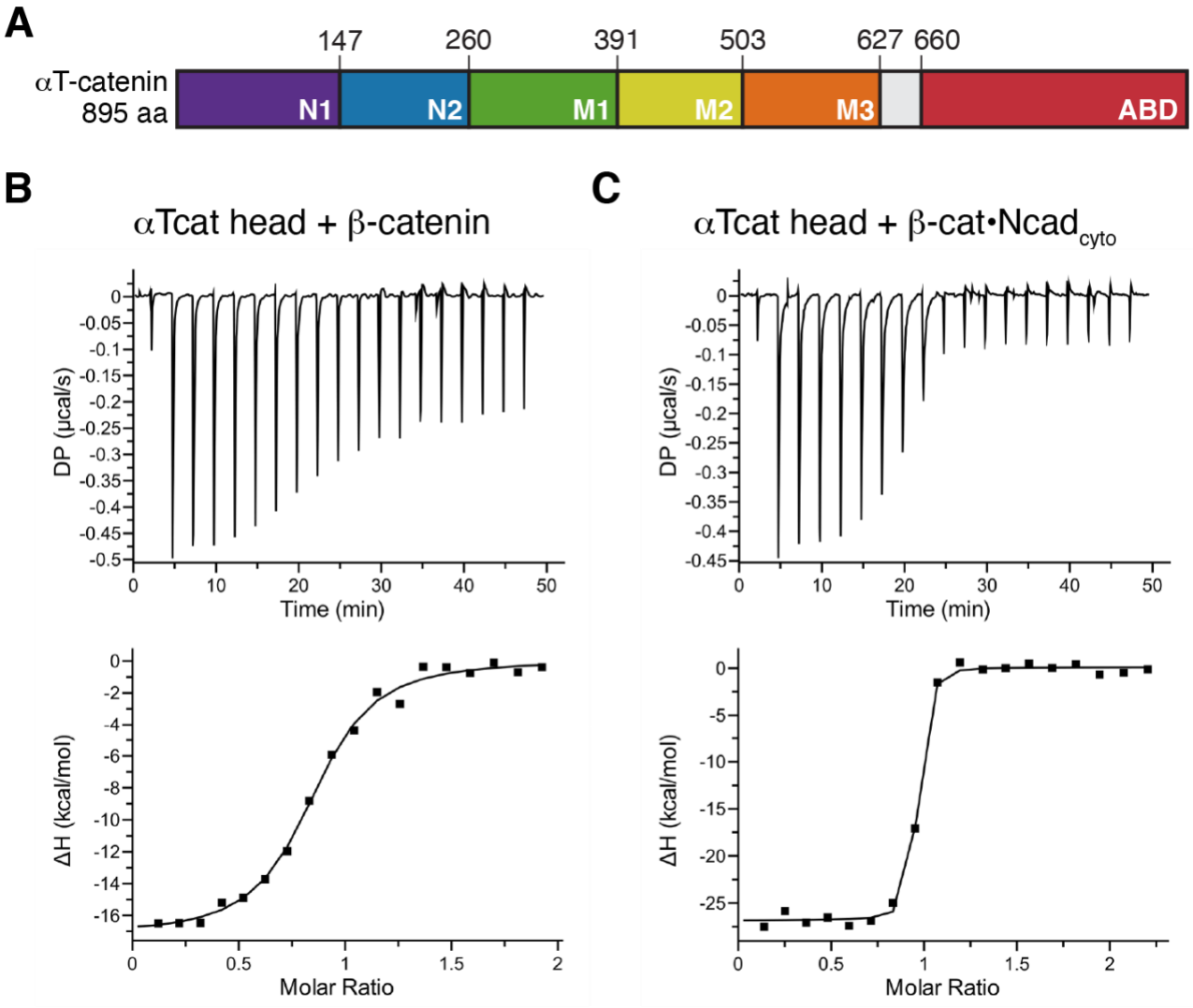

Figure 3.1 αT-catenin binds the N-cadherin•β-catenin complex with nanomolar affinity.

A. Domain organization of αT-catenin. Amino acid domain boundaries marked. B-C. αT-catenin head region (aa1-659, αTcat head) binding to β-catenin (B) or the β-catenin•N-cadherin cytoplasmic tail (β-cat•Ncadcyto) complex (C) was measured by ITC. The ratio of heat released (kcal) per mole of β-catenin or β-cat•Ncadcyto injected into αT-catenin head was plotted against the molar ratio of αT-catenin head and β-catenin or αT-catenin head and β-cat•Ncadcyto. Thermodynamic properties derived from these traces are shown in Table 1.

Table 3.1 ITC measurements of αT-catenin fragments binding to β-catenin or β-catenin•N-cadherin cytoplasmic tail complex.

Proteins	K_d (nM)	ΔH (kcal/mol)	TΔS (kcal/mol)	ΔG (kcal/mol)
αT-catenin head (1-659) + β-catenin	264.1 ± 109.1	-14.6 ± 2.1	-5.6	-9.0
αT-catenin head (1-659) + β-catenin•$Ncad_{cyto}$	5.6 ± 0.6	-27.0 ± 0.2	-15.8	-11.3
αT-catenin N1-N2 (1-259) + β-catenin•$Ncad_{cyto}$	6.9 ± 12.0	-18.9 ± 1.0	-7.8	-11.1

3.3.2 αT-catenin N-terminus is monomeric

Full-length αT-catenin is primarily a monomer in solution, though it does have homodimerization potential *in vitro*[13]. The best evidence for dimerization potential comes from a point mutation linked to arrhythmogenic ventricular cardiomyopathy in humans, V94D, that renders αT-catenin an obligate homodimer[13,16]. We analyzed the oligomerization properties of the αT-catenin N1-N2 (aa1-259, **Fig. 3.1A**) and compared them to the V94D mutant. Analytical size exclusion chromatography (SEC) of αT-catenin wild type (wt) N1-N2 and V94D N1-N2 revealed that wt N1-N2 eluted as a single monomer species (Fig. 2A, blue line) whereas the V94D mutant eluted as a dimer species (**Fig 3.2A**, red line).

We then analyzed the oligomeric state of the αT-catenin N-terminus by cross-linking. Increasing concentrations of αT-catenin N1-N2 were incubated with or without the cross-linker bis(sulfosuccinimidyl)suberate (BS3) at 4 °C or 37 °C and the resulting products analyzed by SDS-PAGE. As expected, the αT-catenin N1-N2 migrated as a 25 kDa protein in the absence of cross-linker (**Fig. 3.2B**). Incubation with BS3 did not affect migration at low concentrations, although at

higher concentrations (4 and 8 μM), larger species were detected at both temperatures. In contrast, αT-catenin V94D N1-N2 ran as 50 kDa protein in the presence of BS3 at all concentrations tested (**Fig. 3.2C**), indicating a cross-linked dimer. We conclude that the αT-catenin N-terminus, similar to full-length protein, is primarily a monomer in solution.

We then tested the ability of the αT-catenin N1-N2 to bind to the β-catenin•$Ncad_{cyto}$ complex by ITC. The affinity of this interaction was 7 nM (**Fig. 3.2D, Table 3.1**), similar to the αT-catenin head and confirming that this fragment contains the complete β-catenin binding site.

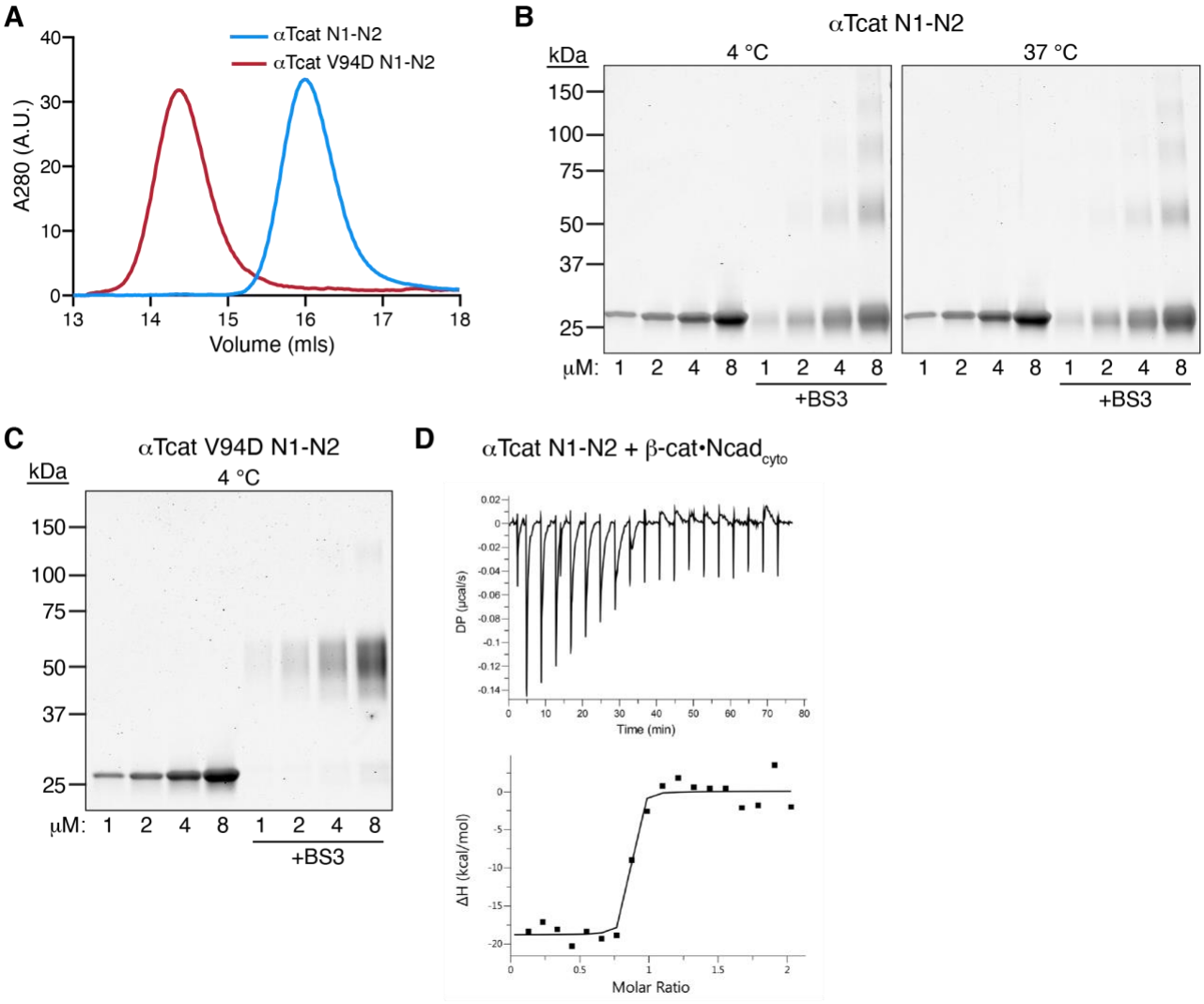

Figure 3.2 αT-catenin N1-N2 is a monomer in solution.

A. Analytical SEC of 30 μM αT-catenin N1-N2 (aa1-259, blue line) and 30 μM αT-catenin V94D N1-N2 (red line). B. Crosslinking experiments with αT-catenin N1-N2. Increasing concentrations of αT-catenin a were incubated with or without 1 mM BST at 4 °C (left panel) or 37 °C (right panel) for 30 minutes, separated by SDS-PAGE and stained with Coomassie dye. C. Crosslinking experiments with αT-catenin V94D N1-N2. Increasing concentrations of αT-catenin V94D N1-N2 were incubated with or without 1 mM BST at 4 °C for 30 minutes, separated by SDS-PAGE and stained with Coomassie dye. D. αT-catenin N1-N2 binding to β-catenin•N-cadherin cytoplasmic tail (β-cat•Ncad$_{cyto}$) was measured by ITC. Thermodynamic properties derived from this trace are shown in Table 1.

3.3.3 αT-catenin M-region binds vinculin

The αE-catenin M-region is autoinhibited with respect to vinculin binding: mechanical force is required to break an internal salt bridge network within M1-M3 to reveal the vinculin binding site in M1[103,104]. The αT-catenin M-region also recruits vinculin and force is required to unfurl M1 to promote high affinity binding[176]. However, our previous proteolysis experiments of full-length αT-catenin revealed that the M2-M3 region existed in a more open, protease-sensitive state[13]. Notably, the amino acids that form the salt bridges required for autoinhibition in the αE-catenin M-region are conserved in αT-catenin, with the exception of E277 in M1 that pairs with R451 in M2. In αT-catenin, the arginine is conserved at the corresponding residue (aa446), but the glutamic acid is replaced by a threonine at aa272[103], preventing these residues from interacting. We questioned if αT-catenin M1-M3 adopted an autoinhibited conformation.

We examined the organization and vinculin binding properties of the complete αT-catenin M-region (M1-M3, aa260-626). αT-catenin M1-M3 eluted as a single, discrete peak by SEC, identical to αE-catenin M1-M3 (aa273-651; **Fig. 3.3A**). We then probed the M-region flexibility by limited trypsin proteolysis. Tryptic digestion of αE-catenin M1-M3 revealed that it was largely protease-resistant: nearly 50% of the fragment was still intact after 120 minutes of digestion, consistent with it forming a closed, autoinhibited domain (**Fig. 3.3B**). In contrast, αT-catenin M1-M3 was completely digested after 60 minutes into three stable fragments at 23, 16 and 12 kDa (**Fig. 3.3B**). Note that both M-regions contain a similar number of lysine and arginine residues (47 in αE-catenin and 39 in αT-catenin), the majority of which are conserved. N-terminal sequencing revealed that the 23 kDa and 16 kDa fragments both started at aa379 and represented the M2-M3 and M2 bundles, respectively. The 12 kDa fragment started at aa485 and corresponded to the M3

bundle (**Fig. 3.3C**). Similar protease resistant fragments were observed from digest of full-length protein[13] and are consistent with the αT-catenin M-region adopting a more open, protease-sensitive state relative to αE-catenin, despite five of the six salt bridge residue pairs being conserved. Likewise, the isolated αT-catenin M1-M3 fragment does not appear to adopt a stable, autoinhibited conformation.

We then measured the affinity of αT-catenin M1-M3 for vinculin. We used the vinculin D1fragment (aa1-259) which contains the first two four-helix bundles and binds to αE-catenin with a similar affinity to the vinculin head domain, D1-D4[95]. As previously observed[95], the autoinhibited αE-catenin M1-M3 fragment bound weakly to vinculin D1 (**Fig. 3.3D, Table 2**). When M3 was deleted from this fragment, auto-inhibition was relieved and αE-catenin M1-M2 bound to vinculin with low nanomolar affinity, as observed previously (**Fig. 3.3E, Table 2**) [95]. In contrast, the αT-catenin M1-M3 fragment showed strong, nanomolar binding to vinculin D1 similar to αE-catenin M1-M2 (**Fig. 3.3F, Table 3.2**), indicating that αT-catenin M1-M3 binding to vinculin was not autoinhibited. Whereas binding to αE-catenin M1-M2 or M1-M3 is endothermic (entropy driven), consistent with unfolding of the M1 bundle needed for this interaction[95], binding to αT-catenin M1-M3 was exothermic, suggesting that αT-catenin M1 is unfurled in the M1-M3 fragment.

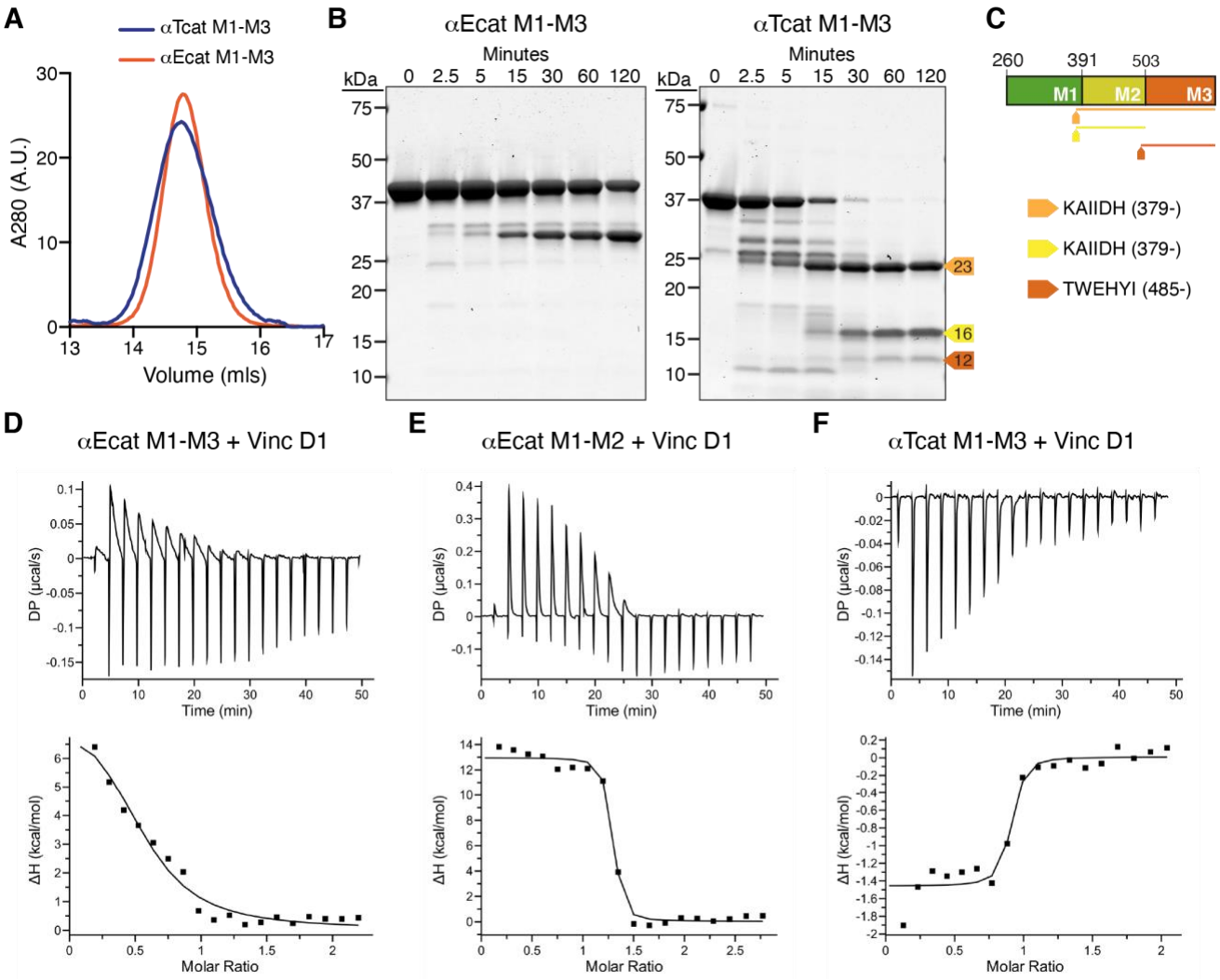

Figure 3.3 αT-catenin M1-M3 binds vinculin D1 with high affinity.

A. Analytical SEC of recombinant αT-catenin M1-M3 (aa260-626) and αE-catenin M1-M3 (aa273-651). B. Limited proteolysis of αT-catenin and αE-catenin M1-M3 fragments. Proteins incubated for 0, 2.5, 5, 15, 30, 60, and 120 min at room temperature in 0.05 mg/ml trypsin, resolved by SDS-PAGE and stained with Coomassie dye. Stable fragments of 23 (yellow-orange), 16 (yellow) and 12 kDa (orange) are marked with colored arrows. C. Edman sequencing results of limited proteolysis fragments. Protein fragments are mapped on the M1-M3 sequence as color-coded lines. D-F. Representative ITC traces of αE-catenin M1-M3 (D), αE-catenin M1-M2 (aa273-510, E) and αT-catenin M1-M3 (F) binding to vinculin D1 (aa1-259). Thermodynamic properties derived from these traces are shown in Table 2.

Table 3.2 ITC measurements of αT-catenin and αE-catenin M-domain fragments binding to vinculin D1.

Proteins	K_d (nM)	ΔH (kcal/mol)	TΔS (kcal/mol)	ΔG (kcal/mol)
αE-catenin M1-M3 (273-651) + Vinculin D1	10420 ± 4588.4	12.8 ± 5.2	19.6	-6.8
αE-catenin M1-M2 (273-510) + Vinculin D1	31.9 ± 9.1	8.7 ± 0.2	18.9	-10.3
αT-catenin M1-M3 (260-626) + Vinculin D1	60.5 ± 19.2	-2.2 ± 1.0	13.8	-9.8
αT-catenin head (1-659) + Vinculin D1	4690 ± 2740	2.3 ± 1.3	9.6	-7.3
αT-catenin head (1-659)•β-catenin + Vinculin D1	2770 ± 875	4.4 ± 0.6	11.9	-7.5
αT-catenin N2-M3 (147-626) + Vinculin D1	50.2 ± 40.4	4.0 ± 0.1	14.1	-10.1
I27-αT-catenin M1-M3 (260-626) + Vinculin D1	245.3 ± 39.7	4.8 ± 0.3	13.8	-9.0
αT-catenin N1-N2 (1-259)/M1-M3 (260-626) + Vinculin D1	50.1 ± 17.5	-3.1 ± 0.1	6.9	-10.0

3.3.4 αT-catenin N-terminus regulates vinculin binding

Recent *in vitro* single molecule stretching experiments revealed that force is required to expose the vinculin binding site in αT-catenin M1-M3[176]. However, our ITC results with the αT-catenin M1-M3 fragment indicated that tension was not required to release M1. In the stretching experiments, the αT-catenin M1-M3 fragment was flanked by a pair of titin I27 immunoglobulin-like domains and the N-terminus of the fusion protein was tethered to a substrate[176]. We questioned if N-terminal associations with M1-M3 stabilize M1 and regulate vinculin binding.

We first characterized the interaction between αT-catenin head domain and vinculin D1 by ITC. The binding shifted from exothermic to endothermic and the affinity was ~5 μM, two

orders of magnitude weaker than observed with M1-M3 (**Fig. 3.4A, Table 3.2**). This suggested that the addition of N1-N2 stabilized M1 and inhibited vinculin binding.

Recent work revealed allosteric coupling between the N-terminal domains and M-region of αE-catenin[105]. Specifically, the presence of β-catenin caused changes in the accessibility of cysteine residues in the N2-M2 interface and in M3. Since β-catenin binding alters the relative positions of the αE-catenin N1 and N2 domains[43], we tested if β-catenin binding to the αT-catenin N-region affected vinculin binding to the M-region. Vinculin D1 was titrated into a solution of purified αT-catenin head•β-catenin complex. The presence of β-catenin had little impact on the affinity (~3 μM, **Fig. 3.4B, Table 3.2**), indicating that N-terminal-mediated autoinhibition was maintained. This result is consistent with past work showing that the β-catenin•cadherin complex had no effect on αE-catenin binding to vinculin[95].

We then asked if the entire N-terminus is required to regulate M1 binding. The addition of N2 to αT-catenin M1-M3 (aa147-626) did not weaken vinculin D1 binding relative to M1-M3 (K_d = 50 nM, **Fig. 3.4C, Table 3.2**). The reaction switched from exothermic to endothermic, suggesting partial compensation of M1 stability in this fragment. Thus, all or part of N1 is required to regulate M1 interactions with vinculin. This is consistent with the observation that removing the first 56 residues of N1 from full-length αE-catenin reduces the inhibition of vinculin binding by about 50 fold[95].

We next questioned if the titin repeats attached to M1-M3 in the construct used by Pang, Le and colleagues[176] stabilized M1. We titrated vinculin D1 into a solution of the 2I27-αT-catenin M1-M3(aa259-667)-2I27 construct. Notably, the binding was endothermic and the affinity was ~250 nM, markedly weaker than observed with αT-catenin M1-M3 alone (**Fig. 3.4D, Table 3.2**). We speculate that the well-structured titin repeats promote M1 stability and may sterically occlude

vinculin D1 binding, thus reducing the affinity. The M1 stability and steric hindrance provided by the I27 repeats partially mimic the complete N-terminus and likely explain why tension is needed to promote vinculin binding in the single molecule stretching experiments whereas αT-catenin M1-M3 in solution binds vinculin readily.

Given that the entire N-terminus is required to regulate vinculin binding in αT-catenin, we asked if N1-N2 could regulate M1-M3 in *trans*. We titrated vinculin D1 into an equimolar mixture of αT-catenin N1-N2 and M1-M3. The binding reaction was similar to M1-M3 alone: exothermic with a K_d of 50 nM (**Fig. 3.4E, Table 3.2**). This result indicates that the M-region must be physically coupled to the N-terminus to stabilize M1 and regulate ligand accessibility.

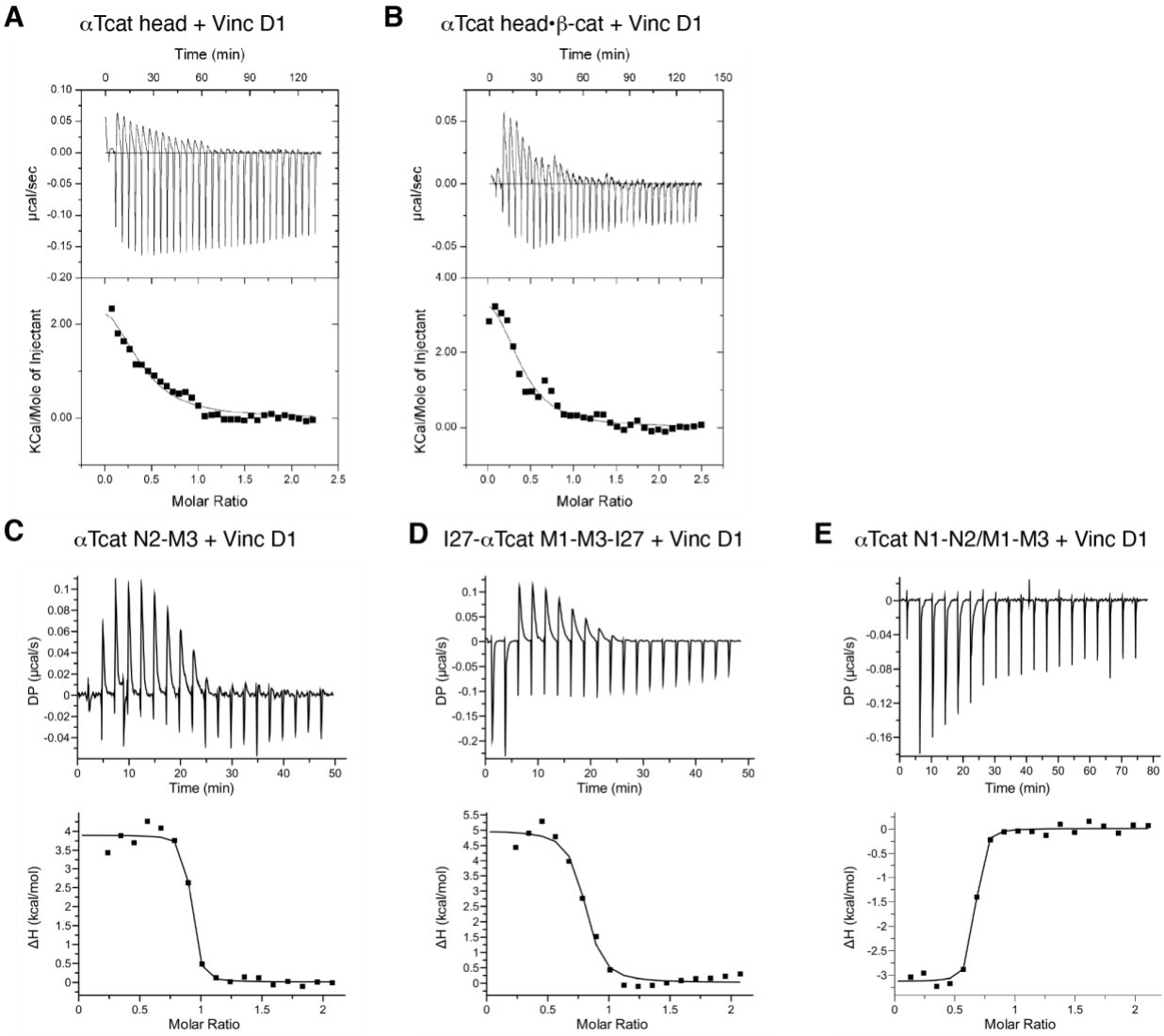

Figure 3.4 αT-catenin N-terminus regulates vinculin binding to M1-M3.

A-D. Representative ITC traces of vinculin D1 binding to αT-catenin head (A), αT-catenin head/β-catenin complex, αT-catenin N2-M3 (aa147-626), 2I27-αT-catenin M1-M3(aa259-667)-2I27 (D), and αT-catenin N1-N2/M1-M3 complex (E). Thermodynamic properties derived from these traces are shown in Table 2.

3.3.5 Tension recruits vinculin to αT-catenin

We tested the ability of αT-catenin to restore cell-cell adhesion and recruit vinculin in α-catenin-deficient R2/7 carcinoma cells[131]. We transiently expressed EGFP-αE-catenin or EGFP-

αT-catenin in R2/7 cells and analyzed cell-cell contact formation and endogenous vinculin recruitment by immunostaining. Both EGFP-αE-catenin and EGFP-αT-catenin restored cell-cell adhesion, organized F-actin along cell-cell contacts and recruited vinculin to junctions (**Fig. 3.5**). To determine if vinculin recruitment was tension dependent, we treated cells with DMSO or 50 μM blebbistatin to suppress myosin activity for 30 minutes and stained for vinculin (**Fig. 3.5, A-D**). αE-catenin and αT-catenin recruited similar levels of vinculin in DMSO controls (**Fig. 3.5, A, B and E**). Importantly, blebbistatin treatment significantly reduced vinculin recruitment to both αE-catenin and αT-catenin containing AJs (**Fig. 3.5, C, D and E**). Thus, myosin-based tension is required to recruit vinculin to αT-catenin, similar to αE-catenin.

We then examined the correlation between EGFP fusion expression and vinculin recruitment. As expected, EGFP-αE-catenin expression levels did not correlate with vinculin levels since vinculin was only recruited when αE-catenin was activated by sufficient tension[149,172]. However, we observed a strong positive correlation between EGFP-αT-catenin expression and vinculin recruitment. We observed a similar positive correlation with constitutively-open αE-catenin constructs in cardiomyocytes[45]. Together, these results suggest that while vinculin recruitment to αT-catenin is tension dependent, the force threshold for binding may be low, permitting all/most AJ-incorporated αT-catenin molecules to recruit vinculin.

Finally, we tested if actin binding was required to relieve αT-catenin autoinhibition and if removal of M3 opened the M-region to permit vinculin recruitment. We expressed EGFP-tagged truncations of αE-catenin and αT-catenin: the head domain lacking the ABD (N1-M3) or the head domain minus M3 and ABD (N1-M2). All EGFP-tagged αE-catenin and αT-catenin fragments expressed as soluble proteins of the predicted size (**Fig. 3.5N**). αE-catenin and αT-catenin N1-M3

(aa1-670 and aa1- 659. respectively) were both cytosolic and, as expected, unable to form cell-cell contacts and recruit vinculin (**Fig. 3.5, J and K**). Deletion of M3 in αE-catenin relieves autoinhibition, and αE-catenin N1-M2 (aa1-510) was able to recruit vinculin and restore cell-cell adhesion, as shown previously[131]. Here vinculin provides the necessary actin-binding activity to link the cadherin-catenin complex to F-actin through αE-catenin. In contrast, αT-catenin N1-M2 (aa1-502) was cytosolic and failed to recruit vinculin to cell-cell contacts. This suggests that, in αT-catenin, loss of M3 does not release M1 for ligand binding and underscores the importance of the N-terminus in regulating M1 binding to vinculin.

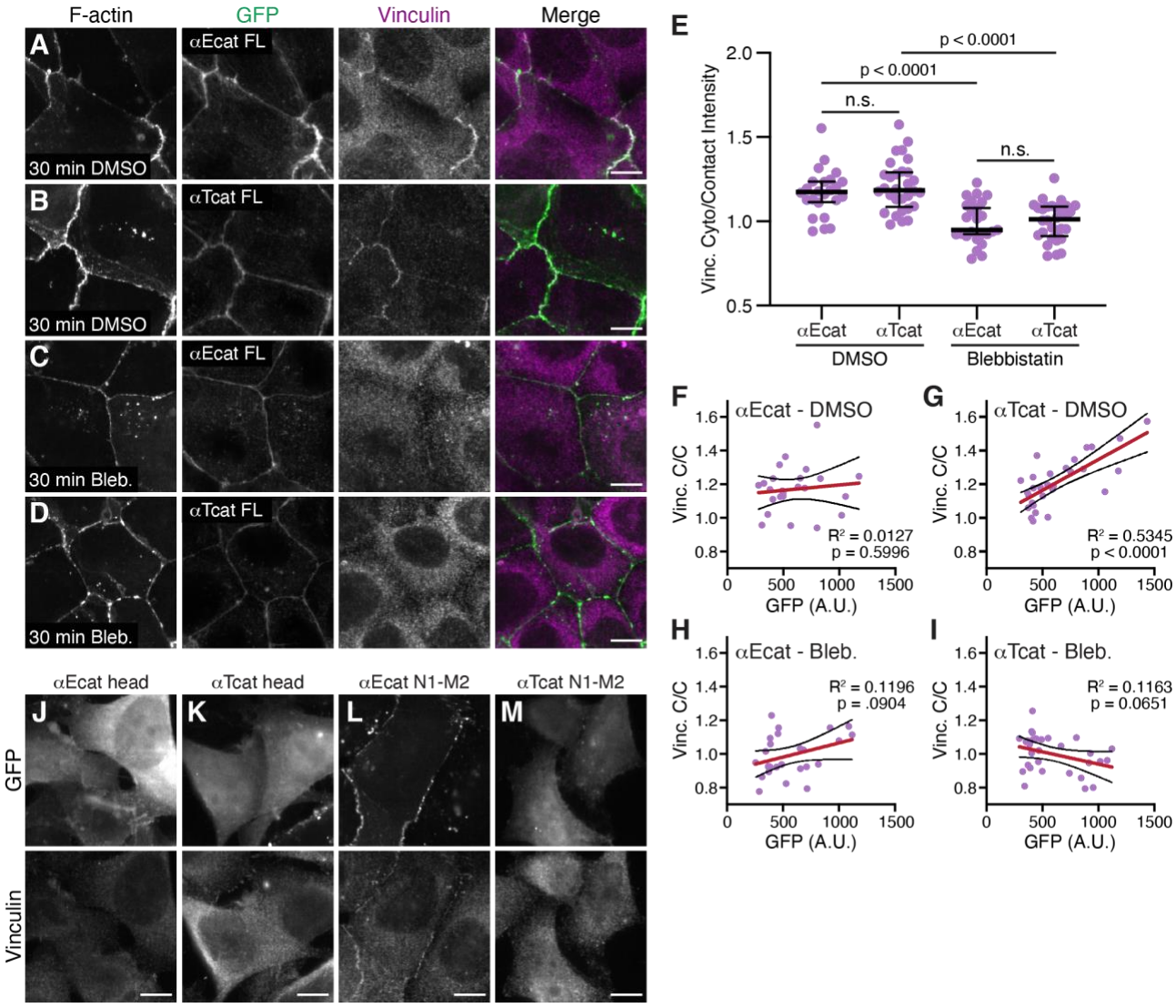

Figure 3.5 . αT-catenin recruitment of vinculin to cell-cell contacts is tension-dependent

A-D. R2/7 cells were transfected with EGFP-αE-catenin full length (αEcat FL; A and C) or EGFP-αT-catenin full length (αTcat FL; B and D) and treated for 30 mins with DMSO (A and B) or 50 µM blebbistatin (C and D) before fixation. Cells were stained for F-actin and vinculin. Individual and merged vinculin (magenta) and GFP (green) channels shown. E. Quantification of vinculin intensity at cell-cell contacts. Signal intensity at contacts was divided by the average cytoplasmic intensity and a scatter plot of all data points is shown. The black horizontal line is the median and the error bars define the interquartile range. One-way ANOVA with Tukey's comparisons; n.s. = not significant. n ≥ 24 images from two independent experiments. F-I. Vinculin contact/cytoplasmic ratio (C/C) was plotted against the average GFP intensity of each fusion construct from

the masked cell contact region. Linear regression analysis was performed to calculate the slope (red line), 95% confidence intervals (black lines surrounding slope) and R2 value. The slope deviation from zero was analyzed for significance (p value). n ≥ 24 images from two independent experiments. J-M. R2/7 cells were transfected with EGFP-tagged αE-catenin head (aa1-670, J), αT-catenin head (aa1-659, K), αE-catenin N1-M2 (aa1-510, L) and αT-catenin N1-M2 (aa1-502, M), fixed and stained for vinculin. Individual GFP (top panel) and vinculin (bottom panel) channels shown. Scale bar is 10 μm in all images. N. R2/7 cells transfected with EGFP-tagged αE-catenin or αT-catenin full-length (FL), head, or N1-M2 constructs. Cell lysates separated by SDS-PAGE and blotted for GFP (top) or GAPDH (bottom).

3.4 Discussion

3.4.1 αT-catenin forms a strong AJ core with cadherin•β-catenin

Our ITC results show that the β-catenin•N-cadherin tail complex binds with high, ~5 nM affinity to αT-catenin similar to 1-2 nM affinity previously reported between the β-catenin•cadherin tail complex and αE-catenin[43]. Thus αT-catenin forms a strong cadherin-catenin core complex like αE-catenin to link actin to the AJ. αT-catenin is co-expressed with αE-catenin in multiple mammalian tissues and, in the heart, it is enriched along the ICD with αE-catenin[48,119,153,177]. It is unknown if αE-catenin and αT-catenin bind stochastically to the cadherin•β-catenin complex in cardiomyocytes or if binding is regulated to favor one α-catenin or the other. Notably, loss of either αE-catenin or αT-catenin from the mouse heart causes dilated cardiomyopathy[11,53], suggesting that each α-catenin has a unique, critical role in ICD function and heart physiology. In addition, αE-catenin and αT-catenin (Heier and Kwiatkowski, unpublished

data) also bind plakoglobin, the desmosome-associated β-catenin homolog that is enriched at the ICD[35,64]. Plakoglobin binds the cadherin tail with an affinity similar to β-catenin and both plakoglobin and β-catenin are enriched at cardiomyocyte AJs[177]. The downstream consequences of α-catenin binding to plakoglobin or β-catenin are not clear, but recent evidence that the N-terminus and M-region of αE-catenin are allosterically coupled[105] raises the possibility that differential binding could affect downstream ligand recruitment. Future work is expected to reveal how specific cadherin•β-catenin/plakoglobin•α-catenin complexes are formed and function to regulate adhesion and signaling.

In the absence of the cadherin tail, β-catenin alone binds αT-catenin an order of magnitude weaker than αE-catenin (~250 nM versus ~20 nM). This suggest that αT-catenin does not compete with αE-catenin for binding cytosolic β-catenin. Though there is evidence of a cytosolic αE-catenin•β-catenin complex in epithelial cells[128], the physiological relevance of this interaction is not clear and a similar α-catenin•β-catenin complex in cardiomyocytes has not been reported.

αE-catenin can homodimerize and the cadherin-free, cytosolic homodimer pool regulates actin dynamics and cell motility[43,127,128,148,178]. In contrast, full-length αT-catenin is a monomer in solution and has limited dimerization potential with no evidence of homodimerization *in vivo*[13]. Our results here show that the isolated αT-catenin N-terminus is also monomeric. We speculate that limited dimerization potential and weaker affinity for β-catenin favor a cadherin-free, cytosolic pool of αT-catenin monomer. The role of such a monomer pool is unclear.

3.4.2 The αT-catenin M-region does not adopt an autoinhibited conformation in isolation

Structural, biochemical and biophysical data indicate that the αE-catenin M-region adopts an autoinhibited conformation[95,102-105,149,164,172,173]. The vinculin binding site is buried in the folded M1 domain and interactions between M1, M2 and M3 maintain the autoinhibited form. Tension breaks these interactions to release M1, allowing it to unfold and bind strongly to vinculin. More recent biophysical data suggest that the αT-catenin M-region adopts a similar conformation with force being required to free M1 for high affinity binding to vinculin[176].

Our limited proteolysis experiments with the isolated αT-catenin M-region indicate that it exists in a more open, protease-sensitive conformation. Consistent with this, ITC results revealed that the αT-catenin M-region binds vinculin with low nanomolar affinity and is not autoinhibited. αT-catenin possesses 5 of the 6 residue pairs that form the salt bridge network that mediates αE-catenin autoinhibition[103]. The E277-R451 bridge between M1 and M2 in αE-catenin is not conserved in αT-catenin, with the glutamic acid replaced by a threonine at aa272. The threonine at aa272 is conserved across the αT-catenin family. Assuming no major structural differences between the αE-catenin and αT-catenin M-regions, the T272 and R446 residues would not be able to interact. In simulations, the αE-catenin E277-R451 salt bridge is predicted to rupture quickly under external force[103,105]. Unfortunately, we lack a structure of the αT-catenin M-region to determine if a similar network regulates domain organization. However, our data demonstrate that such inter-bundle interactions within the αT-catenin M-region are insufficient for autoinhibition.

3.4.3 The N-terminus is required for αT-catenin M-region autoinhibition

The αT-catenin head fragment (N1-M3) showed weak, micromolar binding to vinculin, indicating that the N-terminus regulates M-region autoinhibition. The entire N-terminus (N1-N2) is required for autoinhibition since deleting N1 restored strong vinculin binding. Notably, replacing the N-terminus with another well-structured protein moiety, the titin I27 repeats, reduced vinculin binding and caused the binding reaction to switch from exothermic to endothermic, suggesting the M1 was stabilized. This observation explains the force-dependent vinculin binding to the αT-catenin M-region observed in recent biophysical experiments[176]. The ability of the titin I27 repeats to partially restore autoinhibition also suggests that steric, nonspecific interactions rather than specific interdomain associations (e.g., salt bridges) between the αT-catenin N-terminus and M-region promote M1 folding and M-region autoinhibition. Interestingly, the first 56 residues of αE-catenin contribute to the inhibition of vinculin binding in addition to the M3 domain[95].

3.4.4 αT-catenin recruits vinculin

Expression of EGFP-αT-catenin was sufficient to restore cell-cell contacts and recruit vinculin in α-catenin deficient R2/7 cells. Vinculin binding to αT-catenin requires actin binding by the latter and is tension-dependent, similar to αE-catenin. This is consistent with the vinculin binding site in the αT-catenin M1 domain being occluded in the absence of force. Notably, deletion of M3 in αT-catenin did not relieve autoinhibition, offering additional evidence that the intramolecular interactions required for autoinhibition in αT-catenin differ from αE-catenin.

Vinculin is recruited to αE-catenin to bolster the AJ connection to actin under mechanical load[45,149,174,179]. Neither the physiological context nor the functional role of vinculin recruitment to αT-catenin have been established *in vivo*. Loss of αE-catenin from the mouse heart disrupts AJ formation and causes a marked decrease in vinculin expression and recruitment, despite the presence of αT-catenin, resulting in cardiomyopathy[11]. The inability of αT-catenin to compensate for αE-catenin in the heart underscores how the two α-catenins, despite sharing core properties, are likely regulated by distinct mechanisms and play unique roles in junction organization and signaling.

Together, our data support a model in which the αT-catenin N-terminus functions to regulate M-region stability and autoinhibition. Our *in situ* data indicate that force is required to reveal the vinculin binding site. We speculate that it may do so by separating the M-region from the N-terminus to remove steric hinderance rather than breaking a network of internal M-region salt bridges. This could provide cadherin/β-catenin/αT-catenin complexes in cardiomyocytes with distinct mechanical properties, allowing ligand binding and allosteric signaling over a unique force scale relative to αE-catenin-containing complexes. While we have focused on vinculin binding to M1, intrinsic differences in αT-catenin M-region organization could also affect other M1 as well as M2 and M3 ligand interactions, possibly independent of force. Intramolecular and allosteric interactions are emerging as an important factor in the regulation of α-catenin conformation and molecular complex formation at the AJ. Further work is needed to define how molecular differences between the α-catenin protein family regulate mechanical adhesion and signaling.

3.5 Experimental Procedures

3.5.1 Plasmids

Full-length *M. musculus* β-catenin, αT-catenin and αE-catenin as well as αT-catenin head region (aa1-659) in pGEX-TEV were described previously[13,43,148]. The vinculin D1 construct (aa1-259) in pGEX-TEV was described in[95]. *M. musculus* αT-catenin N1-N2 (aa1-259) N1-M3 (aa 1-659), M1-M3 (aa 260-626) N2-M3 (aa 147-626) and αE-catenin M1-M3 (aa273-651), M1-M2 (aa273-510) were cloned into pGEX-TEV. The constructs encoding αT-catenin M1-M3 flanked by I27 handles in pET151/D-TOPO was kindly provided to us by Dr. Jie Yan[176].

For mammalian cell expression, full-length *M. musculus* αE-catenin and αT-catenin in pEGFP-C1 were described previously[13,148]. *M. musculus* αE-catenin fragments aa1-670 and aa1-510 and αT-catenin fragments aa1-659 and aa1-502 were cloned into pEGFP-C1.

3.5.2 Recombinant Protein Expression and Purification

For a detailed protocol see appendix B. GST-tagged and His-tagged fusion proteins were expressed in BL21-Gsold *E. coli* cells and purified as described in[13,159]. GST-tagged proteins were bound to glutathione-agarose conjugated beads while His-tagged proteins were bound to Ni-NTA beads. Bound beads were then equilibrated in cleavage buffer (20 mM Tris pH 8.0, 150 mM NaCl, 2 mM EDTA, 10% glycerol and 1 mM DTT or BME) and incubated with tobacco etch virus protease overnight at 4°C to cleave proteins from the respective tag. Proteins were then purified by MonoQ or MonoS ion exchange chromatography at 4°C, followed by S200 gel filtration

chromatography at 4°C. Purified proteins were eluted in 20 mM Tris pH 8.0, 150 mM NaCl, 10% glycerol, and 1 mM DTT, concentrated to working concentrations using a Millipore column concentrator and flash frozen in liquid nitrogen.

3.5.3 Limited Proteolysis and Edman Degradation Sequencing

For a detailed protocol see appendix C. Proteins were diluted to 12 μM in 20 mM Tris pH 8.0, 150 mM NaCl and 1 mM DTT and incubated at RT in 0.05 mg/mL sequencing grade trypsin (Roche Applied Science). Digestions were stopped with 2X Laemmli sample buffer and placed on ice until analysis. Samples were boiled and run by SDS-PAGE, then stained with 0.1% Coomassie Blue R-250, 40% ethanol, and 10% acetic acid. Gels were scanned on a LI-COR scanner. For N-terminal sequencing, digested peptides were blotted onto PVDF membrane, stained (0.1% Coomassie Blue R-250, 40% methanol, and 1% acetic acid), destained and dried. Individual bands were excised from the membrane and sequenced by Edman degradation (Iowa State University Protein Facility).

3.5.4 Crosslinking Experiments

αT-catenin protein fragments were incubated with or without 1 mM BS3 (Thermo Scientific) in 20 mM HEPES, pH 7.4, 150 mM NaCl, and 1 mM DTT for 30 min at 4°C or 37°C, separated by SDS-PAGE, stained with Coomassie dye and imaged on a LI-COR scanner.

3.5.5 Isothermal Titration Calorimetry

Proteins used for ITC were purified as described except the S200 buffer was replaced with ITC Buffer (20mM HEPES pH 8.0, 150mM NaCl, 1mM TCEP). Identical buffer was used to purify both cell and titrant samples to ensure buffer match. Only fresh, unfrozen proteins were used for ITC. Measurements were performed on a Malvern MicroCal PEAQ-ITC or MicroCal VP-ITC calorimeter (Malvern Panalytical). For experiments on the MicroCal PEAQ-ITC, titration occurred by an initial 0.5 μL injection followed by 18 x 2 μL injections of 110-150 μM β-catenin, 103-158 μM β-catenin/N-cadherin tail complex or 396-600 μM vinculin aa1-259 (D1) into the cell containing 9-55 μM of αT-catenin or αE-catenin. For experiments on the MircoCal VP-ITC, ligand was added with an initial 2 μL injection followed by 32 x 9 μL injections. The concentration of αT-catenin head or αT-catenin head•β-catenin complex in the cell varied between 22 and 56 μM. Vinculin D1 concentrations in the syringe varied between 240 and 546 μM. All calorimetry experiments were performed at 25°C. All data analysis was performed using Malvern MicroCal ITC analysis software. For baseline correction, a mean baseline value, calculated by averaging the data points at saturation, was subtracted from each data point.

3.5.6 Cell Culture

R2/7 carcinoma cells were cultured in DMEM (4.5 g/L glucose), 10% fetal bovine serum, 1mM sodium pyruvate and penicillin/streptomycin. Lipofectamine 2000 was used for all transient transfections.

3.5.7 Western Blot

R2/7 cells were lysed 48-72 hrs post-transfection in RIPA buffer (10mM Tris pH 7.5, 5mM EDTA, 0.1% Triton-X 100, 0.1% SDS, 0.1% deoxycholate, 150mM NaCl) plus protease inhibitors (Millipore). Lysate protein concentration was measured by BCA and 15 µg of each sample was separated by SDS-PAGE and transferred onto a PVDF membrane (Bio-Rad). The membrane was blocked in TBST + 5% BSA, washed in TBST and incubated with anti-GFP (1:1000, Invitrogen A11122) and anti-GAPDH (1:500, Millipore MAB374) antibodies for 1 hr at RT. The membrane was washed twice in TBST and then incubated with anti-rabbit IRDye 680 and anti-mouse IRDye 800 for 1 hr at RT, washed twice with TBST and washed once with PBS. Membranes were scanned on a Bio-Rad ChemiDoc MP imaging system.

3.5.8 Immunostaining and Confocal Microscopy

For a detailed protocol see appendix D. Cells were fixed in 4% paraformaldehyde in PHEM buffer (60 mM 1,4-piperazin- ediethanesulfonic acid pH 7.0, 25 mM HEPES pH 7.0, 10 mM EGTA pH 8.0, 2 mM MgCl and 0.12 M sucrose), washed with PBS, permeabilized with 0.2% Triton X-100 in PBS for 2 minutes and then blocked for 1 hr at RT in PBS + 10% BSA. Samples were washed three times in PBS, incubated with primary in PBS + 1% BSA for 1 hr at RT, washed three times in PBS, incubated with secondary in PBS + 1% BSA for 1 hr at RT, washed three times in PBS, and mounted in ProLong Diamond mounting medium. Cells were imaged on a Nikon Eclipse Ti inverted microscope outfitted with a Prairie swept field confocal scanner, Agilent monolithic laser launch, and Andor iXon3 camera using NIS-Elements imaging software.

3.5.9 Image Analysis

To quantify vinculin recruitment to EGFP-tagged αE-catenin and αT-catenin, a maximum projection was created from 4 planes of the z-stack (600 nm total distance) where cell-cell contacts were best in focus. IsoJ Dark thresholding was used to create a mask of the GFP channel to define the region of analysis in ImageJ. Vinculin signal intensity was then measured within the masked region. Next, three random intensity measurements of vinculin staining were taken in the cell cytoplasm and these values averaged. Finally, the vinculin intensity within the mask was divided by the cytoplasmic signal to normalize between samples and calculate the contact/cytoplasmic ratio. Colocalization data were plotted with Prism software (GraphPad). A one-way ANOVA with Tukey's comparisons was performed to determine significance; $p < 0.05$.

To examine the relationship between EGPF-αE-catenin or EGFP-αT-catenin levels and vinculin recruitment, the vinculin contact/cytoplasmic ratio was plotted against the average GFP intensity of each fusion construct within the masked cell contact region (described above). Linear regression analysis was performed to calculate the slope, 95% confidence intervals, R square value and p value using Prism software (GraphPad).

4.0 Discussion and Perspectives

4.1 Study Synopses

In these studies, I sought to characterize the molecular properties and ligand interactions of αT-catenin. Understanding these interactions will help to define the role αT-catenin plays in cardiomyocyte adhesion, identify how mutations in αT-catenin may contribute to cardiomyopathy and determine how αT-catenin functions with αE-catenin to regulate adhesion in the mammalian heart. I discovered that while αT-catenin and αE-catenin are structurally and biochemically similar, potential differences in intramolecular interactions contribute to important variations in ligand binding and ligand binding regulation. These results reveal that αE-catenin should not necessarily be used as a default for α-catenin behavior and that there may be greater diversity within the α-catenin family than previously realized.

We found that recombinant αT-catenin is primarily a monomer in solution with only limited potential to dimerize *in vitro*. In contrast, αE-catenin can readily dimerize in solution. In addition, αT-catenin monomer can bind to F-actin in the absence of tension with the same affinity as αE-catenin dimer, and binding to β-catenin does not affect this interaction. This property of αT-catenin likely means it does not interact with the F-actin cytoskeleton in the same manner as αE-catenin at adherens junctions. Note that the V94D mutation in αT-catenin associated with ACM causes it to constitutively dimerize. This mutation does not affect F-actin binding affinity but increases its ability to bundle actin fibers. Dimerization does however block αT-catenin interactions with β-catenin, causing it to mis-localize to the actin cytoskeleton near the cell

membrane and to stress fibers. This result shows that αT-catenin localization to adherens junctions is necessary for proper heart function. It also shows that if αT-catenin can dimerize *in vitro*, the process must be regulated to ensure proper localization when necessary.

αT-catenin binds to β-catenin with a 10-fold weaker affinity than that of αE-catenin (264nM vs 23nM[43]). However, when β-catenin is in complex with the N-cadherin tail this affinity strengthens to a low nanomolar affinity equal to αE-catenin (6nM vs 1nM[43]). This result shows that αT-catenin and αE-catenin associate with the adherens junction with very similar affinity and likely compete for binding to β-catenin.

Limited proteolysis revealed that the αT-catenin M-region appeared to be much more sensitive to digestion than the αE-catenin M-region and therefore the domain was more dynamic. Based on this result, we hypothesized that vinculin would bind with high affinity to the αT-catenin M-region. Indeed, the αT-catenin M-region in isolation is not autoinhibited and binds vinculin with high affinity(60nM). However, when the N-terminus of αT-catenin is connected to the M-region the high affinity interaction is lost(4.7μM) and the reaction becomes endothermic, indicating that unfolding is necessary for binging to occur. This result shows that the N-terminus is responsible for autoinhibition of vinculin binding in αT-catenin, a mechanism distinct from αE-catenin. We also showed that the salt bridge network responsible for αE-catenin M-region autoinhibition of vinculin binding[103] does not play a role in this interaction in αT-catenin. When the αT-catenin N1-M2 construct was transfected into cells, it remained autoinhibited and was unable to recruit vinculin despite all potential salt bridges being disrupted. In contrast, the same construct in αE-catenin could effectively recruit vinculin and restore cell-cell contacts. We also

show that both of αT-catenin and αE-catenin are regulated by tension, but it is still unclear whether the amount of force required to relieve autoinhibition varies.

Together, these results reveal differences in the internal mechanisms of autoinhibition and dimerization in αT-catenin compared to αE-catenin. We also identified differences in ligand interactions that likely influence the interactions between αT-catenin and the F-actin cytoskeleton. These results provide clues into how unique adherens junctions are built around αT-catenin and the role those junctions may play in cell-cell adhesion in cardiomyocytes.

4.2 Perspectives

4.2.1 αT-catenin M-region regulation and complex formation.

The mechanosensitivity of the αE-catenin M-region has been well characterized[92,95,97,103] but it is unknown whether this mechanism is conserved across the α-catenin family. We showed that the mechanism of regulation for the αT-catenin M-region still requires tension to relieve autoinhibition but is distinct from αE-catenin. M-region activation plays an important role in what ligands are recruited to the adherens junction and when they are recruited, and the ligands recruited have implications for proper adherens junction function[177,180].

Our results show a positive correlation between αT-catenin and vinculin at cell-cell contacts (**Fig 3.5G**) suggesting that αT-catenin at adherens junctions is in a more open conformation. Based on this result, αT-catenin may require less force to relieve autoinhibition of vinculin binding. Along with the fact that αT-catenin can readily bind to F-actin while bound to

β-catenin, these factors suggest that αT-catenin is active in different conditions than αE-catenin. Since αE-catenin cannot compensate for αT-catenin in the heart, their roles are distinct and likely involve recruitment of distinct ligands. One example of the specialized roles of α-catenin is myofibril integration across the ICD. Vinculin recruitment to αE-catenin is required for proper myofibril formation and αT-catenin cannot compensate despite also being able to bind vinculin[45]. Another example is plakophilin-2 recruitment to αT-catenin, which can only be recruited to αT-catenin and creates the hybrid junction integrating both the F-actin and intermediate filament cytoskeletons[75]. Both vinculin and plakophilin-2 are recruited to the M-region of α-catenin along with other proteins such as α-actinin[91] and afadin[93,181]. It is likely that these ligands are preferentially recruited to a particular α-catenin to make distinct adherens junction complexes.

To begin testing this hypothesis, we investigated the interaction between αT-catenin and afadin using recombinant proteins (see appendix B). We purified the coiled-coil region of rat afadin spanning amino acids 1417-1564. We also purified the αT-catenin M-region (aa260-626), αT-head region (aa1-659), and αT M1-ABD (aa260-895) to test 1) if afadin can bind to αT-catenin, and 2) if binding is regulated by similar intramolecular interactions as vinculin. We first used analytical size exclusion chromatography to determine if the αT-catenin M-region can bind afadin in solution. We incubated 20μM αT-catenin M1-M3 with 20μM rat afadin aa1417-1564 for one hour at room temperature and ran the protein mixture over a Superdex200 10/300 column (GE). We observed a robust complex **(Fig. 4.1A)**. Interestingly, we also found that the αT-catenin M1-M3 fragment could bind both vinculin and afadin at the same time, which has not previously been shown. We then tested the ability of vinculin and afadin to bind αT-catenin M1-ABD. We found that vinculin bound readily to αT-catenin M1-ABD, consistent with our previous

observation that the N-terminus is required for autoinhibition **(Fig. 4.1B)**. However, afadin was not readily recruited to this fragment, indicating an intramolecular interaction between the M-region and the ABD may regulate afadin binding. However, vinculin binding to M1-ABD increased afadin recruitment **(Fig. 4.1B)**. Vinculin may increase the affinity of αT-catenin M1-ABD for afadin, but SEC is unable to measure affinity with accuracy so further experiments are necessary to determine if this is the case.

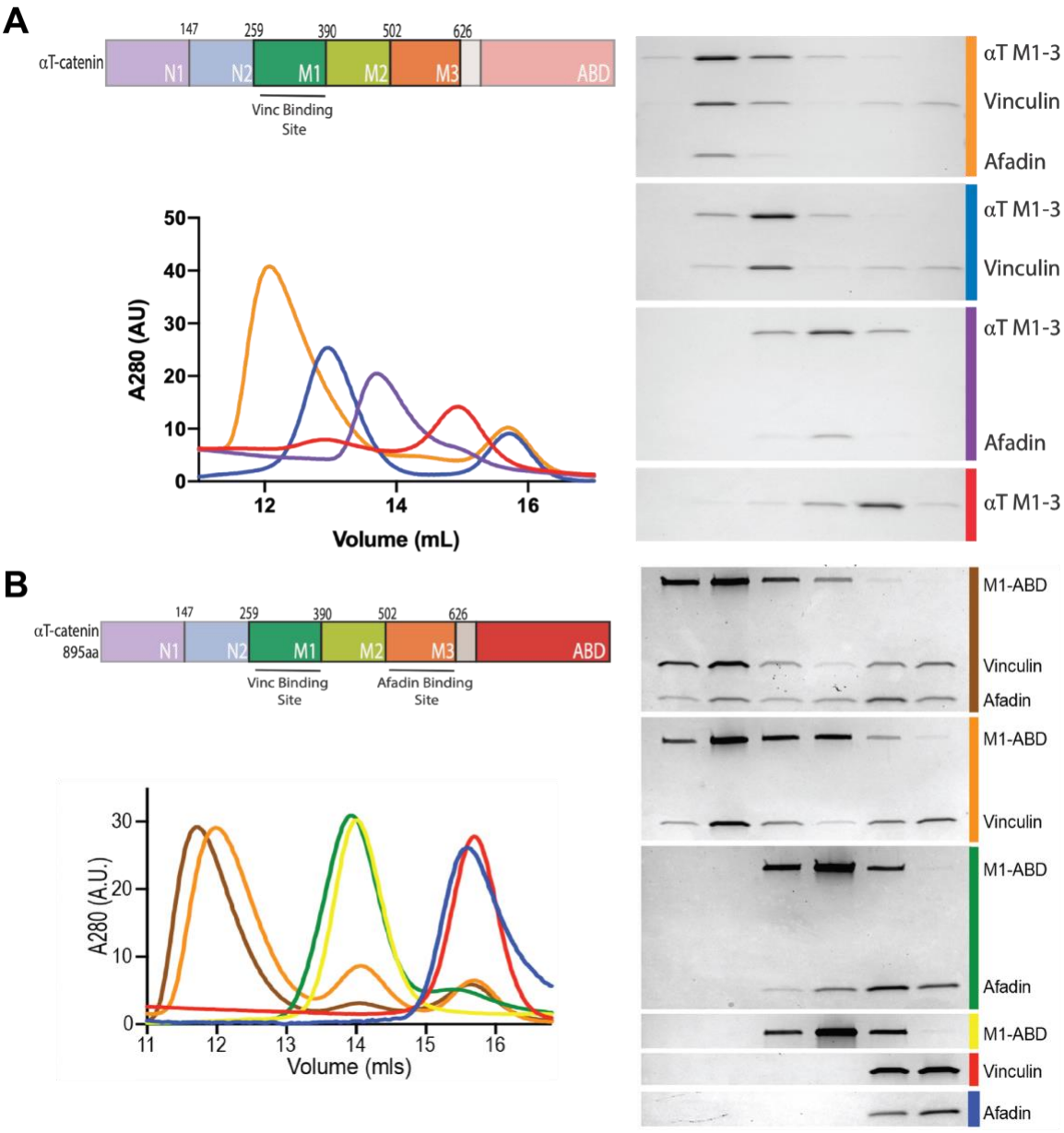

Figure 4.1 αT-catenin binds to afadin and the interaction is regulated by intramolecular interactions

A. αT-catenin, vinculin and afadin analytical size exclusion chromatograms (left) and fraction run by SDS-PAGE (right). B. αT-catenin 260-895, vinculin and afadin analytical size exclusion chromatograms (left) and fraction run by SDS-PAGE (right).

To determine the affinity of the interaction between the αT-catenin M-region and the afadin coiled coil domain we turned again to ITC. Purified afadin coiled coil domain was titrated into

αT-catenin M-region **(Fig. 4.2)**. Consistent with the SEC results, afadin readily bound the αT-catenin M-region with an affinity around 100nM in an exothermic reaction. This result indicates that, similar to vinculin, αT-catenin M-region binding to afadin is not autoinhibited. Going forward, ITC can be used with other αT-catenin fragments to better understand the intramolecular interaction that regulate this interaction. Other proteins such as vinculin can be bound to αT-catenin in the cell of the ITC to determine if they change the affinity for afadin or vice versa. These measurements will help to better understand the order of ligand recrutment to the maturing adherens junction as well as the allosteric changes that occur during ligand binding.

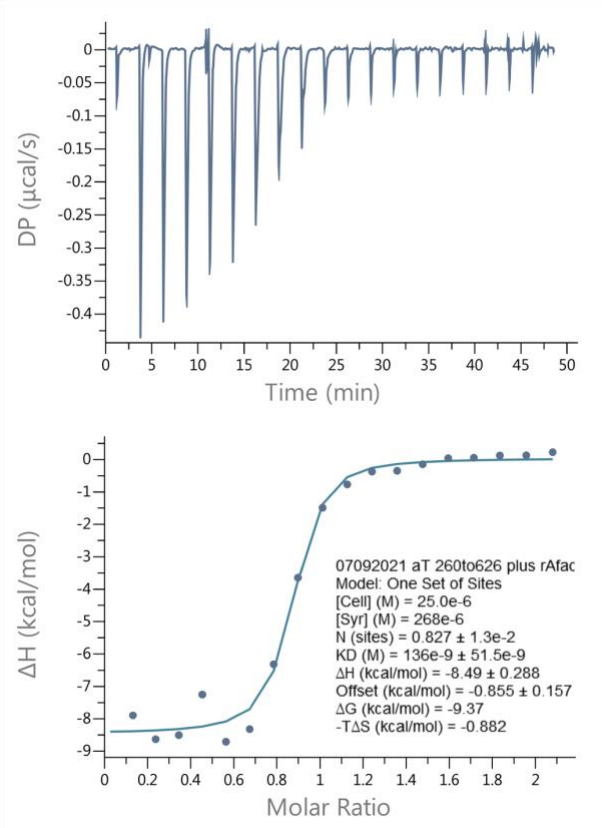

Figure 4.2 Afadin binds to αT-catenin M-region by ITC.

It is not well understood how adherens junctions are assembled, particularly at the ICD. It is possible that the non-overlapping functions of these two α-catenins is the result of the unique suite of ligands recruited to each. Understanding the difference in M-region regulation between αT-catenin and αE-catenin will help to determine how ligands are recruited to assemble adherens junctions that are properly suited to maintain adhesion in a particular environment.

4.2.2 The role of the extrajunctional pool of αT-catenin.

αE-catenin is mostly known as a junctional protein, but roughly one third of total cellular protein is cytoplasmic in epithelial cells[128]. αE-catenin has known functions outside of the adherens junction, particularly in regulating cytoskeletal organization and cell signaling. αE-catenin dimer effectively binds and bundles F-actin(**Fig. 2.3C)** and inhibits the Arp2/3 complex to promote a less branched F-actin network[127,159]. αE-catenin dimer can also be recruited to the plasma membrane independent of the cadherin through an interaction with phosphatidylinositol-3,4,5-trisphosphate. This recruitment promotes epithelial cell migration and enhanced cell-cell adhesion[178]. αE-catenin also recruits other factors to organize the F-actin cytoskeleton like mENA/VASP, zyxin, TES, EPLIN and formins[182-184] although it is not known if these proteins can be recruited to the αE-catenin dimer or if association with the cadherin complex is required.

αT-catenin shows very limited dimerization potential and is primarily a monomer in *in vitro* conditions (**Fig. 2.2**). The monomeric state of αT-catenin cannot bundle F-actin as effectively as αE-catenin dimer and in cells extrajunctional αT-catenin is unlikely to organize actin into bundles. It is also unknown whether αT-catenin can inhibit the Arp2/3 complex and alter actin filament architecture similar to αE-catenin [159]. In addition, the more open M-region of αT-catenin

may be able to readily recruit organizers of the F-actin landscape that are normally only bound to αE-catenin when it is under tension. This has the potential to make αT-catenin a cytoplasmic F-actin organizing center unique from αE-catenin. However, it is unknown if αT-catenin is recruited or able to associate with phosphatidylinositol as a monomer. These differences and how αE-catenin and αT-catenin work in tandem warrants more study to determine how they influence the F-actin cytoskeletal landscape away from the adherens junction.

αE-catenin can also regulate a variety of signaling pathways, most notably the Wnt/β-catenin pathway[125]. αE-catenin inhibits Wnt/β-catenin signaling by binding to β-catenin and preventing its translocation to the nucleus[124,185]. The αE-catenin dimerization domain overlaps with the β-catenin binding domain so these two complexes are mutually exclusive[89]. Thus, cytoplasmic β-catenin cannot bind to αE-catenin dimer to regulate Wnt signaling. αT-catenin is a monomer in solution so β-catenin would not have to compete with another αT-catenin for binding in the cytoplasm. However, this may be offset by the fact that the affinity of αT-catenin for β-catenin is 10-fold weaker than that of αE-catenin (**Table 3.1**) [43]. Note however that these measurements were calculated from proteins purified from *E. coli* and lack post translational modifications like phosphorylation that could change these interactions in mammalian cells. How the different members of the α-catenin family regulate Wnt signaling is complex and will require more study.

Another aspect of extrajunctional αT-catenin biology that has not been explored is its impact on plakophilin-2 signaling. Plakophilin-2 is a transcriptional regulator of the Wnt and Ras signaling pathway influencing the cell cycle[186] but has also been connected to the transcriptional control of calcium channels in the heart[187]. The transcriptional regulation of these channels may be a cause of ACM in patients with mutations in plakophilin-2. Since αT-catenin specifically binds

plakophilin-2, it may play are role in the regulation of these signaling pathways through a similar mechanism as αE-catenin and Wnt/β-catenin signaling. We have recently discovered that αT-catenin is a small percentage of the total α-catenin expressed in cultured neonatal mouse cardiomyocytes and may be as little as 2% (Kwiatkowski lab unpublished data). This makes it difficult to imagine that such as small percentage of protein when mutated can have a large impact on adhesion alone and result in a disease state. αT-catenin playing a role in signaling provides a mechanism by which the effect of a mutation in the protein can be amplified to result in a more severe condition like ACM.

4.2.3 αT-catenin beyond the heart.

αT-catenin being the linchpin of the *area composita* gives it a distinct functional role in cardiomyocytes. However, other cell types with αT-catenin do not contain hybrid junctions and many do not even express desmosomal proteins[49]. What is the function of αT-catenin in these diverse tissues? This has been a difficult question to address as many of the tissues where αT-catenin is expressed show no obvious phenotype when αT-catenin expression is lost[53].

αT-catenin is expressed primarily in the heart as well as the testes, skeletal muscle, and central and peripheral nervous system[49]. In the testes, αT-catenin is expressed in the peritubular myoid cells[48]. These are smooth muscle-like cells that help to transport immotile sperm by contracting to move them through the tubule[107]. In the nervous system, αT-catenin does not seem to be present in neurons but is instead expressed in support cells like the ependymal cells that line the ventricles and central canal of the spinal cord and oligodendrocytes that produce myelin in the central nervous system[119,120].

Notably, many of these cell types are contractile with the exception of the cells in the nervous system. αT-catenin could be contributing to organizing contractile F-actin network in these cells. αT-catenin could act as a scaffold for Z-disc formation in sarcomeres and in dense bodies, as α-catenin is known to bind to the Z-disc protein α-actinin[91]. Alternatively, αT-could be responsible for maintaining adhesion in high tension environments such as the heart, but neural cells are not normally under high tension and skeletal muscle does not have cell-cell junctions and instead forms long syncytial fibers.

It is also possible that αT-catenin plays a specialized role in cell signaling. αT-catenin has been shown to suppress airway hypersensitivity associated with asthma and allergic reactions, but it is unclear what cells are responsible for this reaction[153]. Knockout of αT-catenin also alters transcription of pathways associated with Alzheimers and Autism in the mouse cerebellum[119]. Decreases in αT-catenin expression have also been associated with a variety of cancers, but it is not clear whether this is the result of transcriptional changes or from the loss of cell adhesion[49]. Overall, it is not clear if there is a common niche being filled by αT-catenin across these different cell types. αT-catenin likely fills a variety of roles from adhesion to signaling to help maintain proper cell function, much like αE-catenin. Additional studies will be necessary to fully understand the role of αT-catenin throughout the body.

Appendix A Measuring protein binding to F-actin by co-sedimentation

This text was published in the Journal of Visual Experiments in 2017.

Heier JA, Dickinson DJ, Kwiatkowski AV. Measuring Protein Binding to F-actin by Co-sedimentation. *JoVE*. 2017;(123):1-8. doi:10.3791/55613.

Appendix A.1 Overview

Filamentous actin (F-actin) organization within cells is regulated by a large number of actin-binding proteins that control actin nucleation, growth, cross-linking and/or disassembly. This protocol describes a technique – the actin co-sedimentation or pelleting assay – to determine if a protein or protein domain binds F-actin and to measure the affinity of the interaction (dissociation equilibrium constant). In this technique, a protein of interest is first incubated with F-actin in solution. Then, differential centrifugation is used to sediment the actin filaments and the pelleted material is analyzed by SDS-PAGE. If the protein of interest binds F-actin, it will co-sediment with the actin filaments. The products of the binding reaction (F-actin and the protein of interest) can be quantified to determine the affinity of the interaction. The actin pelleting assay is a straightforward technique for determining if a protein of interest binds F-actin and assessing how changes to that protein, such as ligand binding, affect its interaction with F-actin.

Appendix A.2 Introduction

Actin is an essential cytoskeletal protein that plays a critical role in multiple cellular processes, including motility, contraction, adhesion and morphology[188]. Actin exists in two forms: monomeric globular actin (G-actin) and polymerized filamentous actin (F-actin). Within cells, F-actin organization is controlled by a large collection of proteins that regulate the nucleation, growth, cross-linking and disassembly of actin filaments[189-191]. However, how multiple actin-binding proteins function in concert to regulate actin network organization is still largely unclear.

Measurement of protein-protein interactions is an important approach for understanding at the biochemical level how proteins exert their effects on cell behavior. Many different assays can be used to detect interactions between purified proteins. Common approaches for soluble proteins include pull-downs, fluorescence polarization, isothermal titration calorimetry and surface plasmon resonance. Importantly, all of these assays require proteins to be soluble, and are thus difficult to adapt to a polymeric, filamentous protein such as F-actin. Here, we describe a technique – the actin co-sedimentation or pelleting assay – to determine if a protein or protein domain binds F-actin and to measure the affinity of the interaction.

The actin pelleting assay is a relatively straightforward technique that does not require specialized equipment, aside from an ultracentrifuge. All reagents can be made, assuming knowledge of basic biochemistry, or purchased. Once binding to F-actin is established, the assay can be used to measure the apparent affinity (dissociation equilibrium constant) [156]. Also, once an affinity is established, the pelleting assay is a useful tool to measure how changes to the protein of interest (*i.e.*, post-translational modifications, mutations, ligand binding) affect its interaction with F-actin[13]. The technique does have limitations (see Discussion) that the researcher should be aware of before attempting the assay.

Appendix A.3 Protocol

Appendix A.3.1 Prepare Materials

1.1) Purify the protein of interest (see section 2).

1.2) Prepare or purchase G-actin.

Note: G-actin can be isolated from multiple sources[188]; alternatively, it can be purchased. Reconstituted G-actin (in 5 mM Tris pH 8.0, 0.2 mM $CaCl_2$, 0.2 mM ATP (Adenosine triphosphate) and 0.5 mM dithiothreitol (DTT)) should be flash frozen, stored at –80 °C at >10 mg/mL in small (10-20 µL) aliquots and thawed just before use. G-actin aliquots should not be refrozen.

1.3) Prepare or purchase control protein, such as BSA (see step 4.4).

1.4) Prepare 10X Polymerization Buffer (200 mM Imidazole pH 7.0, 1 M KCl, 20 mM $MgCl_2$, 5 mM ATP, 10 mM EGTA (Ethylene glycol-bis(β-aminoethyl ether)-N,N,N',N'-tetraacetic acid). Make 10X stock, and adjust pH after addition of ATP if necessary, aliquot (25 µL is a useful volume) and store at -80°C.

1.5) Prepare 10X Reaction Buffer (200 mM Imidazole pH 7.0, 1.5 M NaCl, 20 mM $MgCl_2$, 5 mM ATP, 10 mM EGTA). Make 10X stock, adjust pH after addition of ATP if necessary, aliquot (50-100 µL is a useful volume) and store at -80°C.

Note: The composition of the Reaction Buffer is flexible and may need to be adjusted to reduce background sedimentation, limit non-specific binding and/or improve binding (steps 1.5.1 – 1.5.3).

1.5.1) Adjust the pH of the Reaction Buffer between 6 and 8 to optimize protein stability. At lower or higher pH, substitute an appropriate buffer for imidazole.

Note: Use pH 7.0 as a starting point unless a protein requires a lower or higher pH for stability. Do not use a buffer with pH below 6.0 or higher than 8.0 as this may disrupt actin. Recommended buffers (final concentration and optimal pH listed) include: 20 mM MOPS (3-(*N*-morpholino)propanesulfonic acid), pH = 6.5; 20 mM Imidazole, pH = 7.0; 10 mM HEPES (4-(2-Hydroxyethyl)piperazine-1-ethanesulfonic acid), pH = 7.5; 20 mM Tris, pH = 8.0.

1.5.2) Vary the salt concentration of the Reaction Buffer depending on the needs of the assay.

Note: Actin is an acidic protein and almost all actin-binding proteins rely to some extent on electrostatic interactions to associate with actin. Therefore, increasing salt concentration decreases actin binding in most cases. The Reaction Buffer uses a physiological level of salt (150 mM NaCl, working concentration) and this is the recommended starting point. If necessary, the salt concentration can be lowered (e.g., to 100 mM) to promote binding, or increased to limit binding.

1.5.3) Do not change the concentrations of $MgCl_2$, ATP or EGTA in the Reaction Buffer unless there is a specific reason to do so.

Appendix A.3.2 Prepare test protein for the assay

2.1) Prepare high purity protein using liquid chromatography for best results[192].

Note: If using recombinant protein, large protein tags such as GST (Glutathione-S-transferase) should be removed by protease cleavage from the target protein as they can interfere with binding. GST also causes homodimerization of fusion proteins, which can artificially increase the affinity of actin binding.

2.2) Determine protein concentration by measuring the absorbance at 280 nm. Then divide by the extinction coefficient. The extinction coefficient can be calculated from the protein sequence using sequence analysis or online tools. Alternatively, determine protein concentration using Bradford or BCA (bicinchoninic acid) methods.

Note: For initial experiments, 50-100 µL of protein at 20-40 µM is usually sufficient. This will permit analysis of binding in the low micromolar range, a useful starting point for most actin-binding proteins. A larger quantity, and often times higher concentration, of protein is needed for generating a binding curve to calculate affinity (see section 5).

2.3) Hard spin protein (50,000-100,000 x g for 10 min at 4 °C) to remove aggregates of insoluble protein just before use. If solubility is a concern, re-measure protein concentration (step 2.2) after centrifugation.

Appendix A.3.3 Prepare F-actin

3.1) Remove an aliquot of G-actin from the -80 °C freezer and thaw it quickly.

3.2) Add the 10X polymerization buffer to G-actin to a final concentration of 1X. Ensure that the G-actin concentration in 1X polymerization buffer is at least 10-20 µM, well above the critical concentration. Incubate for 1 h at RT (room temperature) to allow actin to polymerize.

3.3) After polymerization, store the F-actin in solution at 4 °C where it is stable for a few weeks. Before using the F-actin again after storage, gently invert or flick the tube several times to ensure that all actin is dissolved and uniformly distributed in solution.

Note: (Optional) Add phalloidin to achieve a 1:1 molar ratio of G-actin:phalloidin. Incubate 30 min at RT to allow phalloidin to bind the F-actin. Phalloidin stabilizes F-actin and accomplishes two things: (i) it reduces the amount of actin that does not sediment during centrifugation; and (ii) it allows F-actin to be diluted below the critical concentration (~0.5 µM), which is often necessary if varying the amount of F-actin to generate a binding curve (see section 5 on measuring affinity).

Appendix A.3.4 Pelleting Assay – Basic Protocol

Note: The basic protocol described in section 4 is used to determine if a protein of interest co-sediments with F-actin. Once binding to F-actin is established, the affinity of this interaction can be measured following the protocol described in section 5.

4.1) Prepare the reaction buffer the day of use by diluting the 10X stock to 1X and add DTT to a final concentration of 1 mM.

Note: (Optional) Add polidocanol to a final working concentration of 0.02% in the reaction buffer. Polidocanol is a surfactant that reduces non-specific background binding and helps prevent hydrophobic proteins from sticking to the ultracentrifuge tube.

4.2) Dilute the protein of interest to the desired concentrations in 1X reaction buffer in ultracentrifuge tubes. Keep samples volumes low (40-60 µL) to avoid using large amounts of protein by using ultracentrifuge tubes with small minimum volumes (*e.g.*, 7 x 20 mm tubes that hold 0.2 mL).

Note: Since many actin-binding proteins have an affinity for F-actin in the micromolar range, testing a protein of interest at 2 and 10 µM is recommended. If binding is not observed at 10 µM, it is unlikely that binding will be observed at higher concentrations. If the added protein makes up more than 10-20% of the final reaction volume, it may be necessary to dialyze the protein into the reaction buffer before doing the experiment.

4.3) Add F-actin to the desired final concentration.

Note: 2 µM is a useful concentration for initial experiments because it is well above the critical concentration (thus maintaining actin in the filamentous state) and it will produce a visible pellet when analyzed by SDS-PAGE (4.10).

4.4) Prepare the following controls in ultracentrifuge tubes to make the assay informative.

4.4.1) Prepare sample(s) containing the protein of interest without F-actin. Ensure that the concentration of protein in these samples matches the concentration in the "plus F-actin" samples.

These samples will determine the amount of protein that is aggregated or stuck to the sides of the ultracentrifuge tube in the absence of F-actin.

4.4.2) Prepare negative control samples containing a control protein that does not bind F-actin at the same or similar concentration(s) used for the protein of interest, with and without F-actin. This is an important control because proteins can become "trapped" in actin filaments and pellet with F-actin even though they do not bind F-actin.

Note: The amount of trapping can vary depending on F-actin source, buffer conditions, *etc*., and thus this control should be included in all experiments. Ideally, the control protein should have molecular weight similar to the protein of interest (*e.g.*, for αE-catenin (~100 kDa), BSA (66 kDa) is an appropriate control). Commercially available gel filtration standards make excellent control proteins since they cover a range of sizes and tend not to contain aggregates.

4.4.3) Optionally, prepare positive control samples containing a protein that binds F-actin, with and without F-actin. Ensure that the concentration(s) are similar to those of the protein of interest. This control is helpful in that it demonstrates that the experimental conditions (*e.g.*, prepared F-actin, reaction buffer, centrifugation) permit F-actin binding.

Note: Since the pelleting assay can fail to detect weak F-actin interactions (see Discussion), it is recommended that the known F-actin binding protein have a moderate-to-weak affinity for F-actin (in the low micromolar range). Purified F-actin binding proteins are commercially available.

4.5) Incubate all samples for 30 min at RT.

Note: Longer incubation times are okay, assuming the protein of interest is stable, though likely unnecessary. If the protein of interest is not stable at RT, then samples can be incubated at 4 °C. In this case, longer incubation times may be necessary.

4.6) Load the samples into the centrifuge rotor. Position the tubes within the rotor to assist in resuspending the pellet after centrifugation. For this, mark all centrifuge tubes (*e.g.*, with a sample number) and place all tubes in the rotor in the same position (*e.g.*, number facing out).

4.7) Centrifuge at 100,000 x g for 20 min at 4 °C in an ultracentrifuge.

4.8) After centrifugation, remove 3/4 of the supernatant (*e.g.*, 45 µL if the starting volume was 60 µL) from each tube and mix with 1/3 volumes of 4X sample buffer (15 µL in this case) in a separate microcentrifuge tube.

4.8.1) Remove the remaining supernatant with a gel-loading tip, taking care not to disturb the pellet (which may be visible as a glassy spot).

Note: It is important to remove the supernatant from the tubes as soon as possible after completion of the centrifuge run to limit protein dissociation post-separation. Also, do not wash the pellet with reaction buffer for the same reason.

4.9) Add 4/3 volumes of 1X sample buffer to each pellet (*e.g.*, 80 µL if the starting volume was 60 µL).

Note: This makes the dilution the same as for the supernatant (step 4.8, 1/3 volumes of 4X sample buffer added) permitting direct comparison between pellet and supernatant samples and determining the percentage of protein that pelleted.

4.9.1) Add sample buffer to all tubes and incubate for at least 5 min at RT. Allow the pellet to sit in the sample buffer to improve sample recovery.

4.9.2) Triturate the sample 8-10X with a p200 pipette tip to resuspended the pellet, by continuously washing the pellet area of the tube. Gently scrape the pipette tip over the pellet during the trituration to help with resuspension.

Note: Take care to avoid introducing air into the sample during the trituration, as this will cause the sample buffer to bubble and reduce sample recovery.

4.9.3) Transfer the resuspended samples to microfuge tubes after trituration.

4.10) Analyze the supernatant and pellet samples by SDS-PAGE and Coomassie staining[193] by loading 10-15 µL of sample per lane, this is sufficient to visualize proteins. Proteins that co-sediment with F-actin will be enriched in the "plus F-actin" pellet samples over the "no F-actin" pellet samples (**Fig. 1A**).

Note: Standard Coomassie blue staining is sufficient for detection if protein concentrations are in the 0.1 – 10 µM range. Colloidal Coomassie[9] or western blotting can be used for increased sensitivity if lower protein concentrations are used to measure higher-affinity interactions.

4.11) Image Coomassie-stained gels using a scanner or imaging system (step 5.12).

Appendix A.3.5 Pelleting Assay – Quantification

Note: If specific binding to F-actin is observed, it can be useful to measure the affinity of the interaction. This is accomplished by making a few changes and additions to the protocol outlined in section 4. For an excellent guide to designing and interpreting binding assays, see Pollard[194]. A flow chart (**Fig. 2**) is provided for assistance with the analysis and quantification.

5.1) Determine the concentration range to test. The concentration range will depend on the protein, and should span from a concentration below the apparent Kd (e.g., 1 µM) to concentrations high enough to saturate binding.

Note: It is critical that binding reach saturation in multiple samples at the high end of the concentration range to generate an accurate binding curve (**Fig. 1C**). As noted above, many actin-binding proteins have an affinity for F-actin in the low micromolar range (1-5 µM). For a protein with a Kd of 0.5-1 µM, a useful starting concentration range would be 0.1 µM – 10 µM.

5.2) Hard spin (step 2.3) the protein of interest to remove aggregates. Serially dilute the protein to make a concentration series, containing 7-8 samples, at 2X the final concentration to be tested. For example, if the range to test is 0.1 µM – 8 µM, prepare the following dilutions in 1X Reaction Buffer: 16, 8, 4, 2, 1, 0.5 and 0.2 µM.

Note: As mentioned in step 4.2, if the added protein makes up more than 10%-20% of the first dilution (the 16 µM sample in the example above), it may be necessary to either concentrate the

protein further or dialyze the protein into 1X Reaction Buffer. Be sure to prepare enough of each dilution for “plus F-actin” and “no F-actin” samples.

5.3) Prepare samples in ultracentrifuge tubes as in section 4. Add F-actin to appropriate samples and bring up to volume with 1X Reaction Buffer. For example, for 50 µL reactions using 2 µM F-actin, each sample would comprise 25 µL 2X protein, 10 µL 10 µM F-actin and 15 µL 1X reaction buffer. Include control samples (4.4.2 & 4.4.3).

Note: For negative and positive controls, use one concentration within the range to be tested (step 5.1), ideally near the middle to high end of the range (e.g., 4 µM if the concentration range is 0.1 to 10 µM).

5.4) Incubate all samples for 30 min at RT.

5.5) After 30 min, remove 1/5 of each sample (e.g., 10 µL of 50 µL reaction) and mix with 20 µL of water and 10 µL of 4X sample buffer. These are the “Total” samples and will be used to generate a standard curve.

5.6) Load the samples into the ultracentrifuge rotor. Centrifuge at 100,000 x g for 20 min at 4 °C.

5.7) Optionally, after centrifugation, remove 3/4 of the supernatant (e.g., 30 µL if the centrifuged volume was 40 µL) from each tube and mix with 4X sample buffer (10 µL in this case) in a separate microfuge tube. Remove the remaining supernatant with a gel-loading tip, taking care not to disturb the pellet.

Note: When measuring the binding affinity, it is not necessary to run the supernatant. Nonetheless, it can be useful to save the supernatant, especially when testing a new protein.

5.8) Remove the supernatant if not analyzing (5.7).

5.9) Resuspend the pellet in 1 volume of 1X sample buffer (e.g., 40 µL if the centrifuged volume was 40 µL).

5.9.1) Add sample buffer to all tubes and incubate for at least 5 min at RT.

5.9.2) Triturate the sample 8-10X with a p200 pipette tip, continually washing the pellet area of the tube. Gently scrape the pipette tip over the pellet during the trituration to help with resuspension.

5.10) Transfer the resuspended protein to a microcentrifuge tube. These are the "Pellet" samples.

5.11) Analyze Total and Pellet samples by SDS-PAGE[193]. Run all samples on one gel if possible; if not, run the pellet samples on one gel and the total samples on a second gel.
Note: Given the number of samples, a large gel system is recommended for analysis. If running samples on two or more gels, it is important that all gels be stained identically – same Coomassie solution and identical time in stain/destain.

5.12) Image Coomassie-stained gels using an imaging system that measures protein band intensities over a wide (two to three log) and linear range. Ensure that images are collected with no saturated pixels.

Note: Laser-based imaging systems offer the best sensitivity and signal-to-noise ratios.

5.13) Using ImageJ or similar analysis program, measure protein band intensities and calculate the amount of bound protein.

Note: For all sample measurements, use the selection tool in ImageJ to draw a region of interest (ROI) around each band and measure (Analyze > Measure) the area and mean gray value. Calculate the background for each gel by measuring the mean gray value from an area without sample. Subtract the background mean gray value from each ROI mean gray value and then multiply by the area to obtain the integrated density value for each band.

5.13.1) Measure protein of interest band intensities from the Total samples (**Fig. 2A**).

5.13.2) Generate a standard curve by plotting band intensity (integrated density measurements) versus protein mass (**Fig. 2B**).

5.13.3) Measure the amount of protein of interest that co-sedimented with F-actin (co-sedimented protein, **Fig. 2C**).

5.13.4) Measure the amount of protein of interest that sedimented in the absence of F-actin (background sedimentation, **Fig. 2D**).

5.13.5) Subtract the background sedimentation from the co-sedimented protein (i.e., subtract the values from step 5.13.4 from step 5.13.3) to determine the amount of protein that bound to F-actin.

5.13.6) Measure the amount of F-actin in each pellet (**Fig. 2E**). Determine the average amount of F-actin per sample and then divide each sample by the average to determine the ratio of F-actin in each sample relative to the average (numbers below bands).

5.13.7) For each sample, divide the amount of bound protein (calculated in step 5.13.5) by the F-actin actin pellet ratio (5.13.6) to adjust for differences in the pellet. This value is the normalized bound protein.

5.13.8) Use the standard curve (step 5.13.2) to calculate the amount (mass) of normalized bound protein (step 5.13.7) in each sample.

Note: The protein removed initially (the "Total" sample) as well as the amount loaded (which, unless entire pellet was loaded, will be some fraction of the pellet) must be accounted for when calculating the total amount of protein that pelleted.

5.13.9) Determine the concentration of bound protein in each sample from the total mass of protein in the pellet (calculated in step 5.13.8) and volume of the sample. Subtract this value from the starting concentration to determine the amount of free protein. Divide the concentration of bound protein by the concentration of actin (μM/μM of actin) and plot versus the concentration of free protein to generate a binding curve (**Fig. 1C**).

Note: Since F-actin is not a single uniform species it is difficult to extrapolate the molar concentration of F-actin from the G-actin concentration. Use the starting G-actin concentration to determine the amount of bound protein (μM/μM of actin) and estimate the apparent concentration of binding sites in the reaction. The concentration of binding sites is usually less than the concentration of actin monomers in the reaction, because not all of the actin polymerizes and because a single actin binding protein molecule can make contact with multiple monomers on the actin filament.

5.14) Determine the affinity (K_d) and Bmax by nonlinear least squares regression from the binding curve using a statistical program.

Note: Scatchard plots are discouraged for analyzing binding data, partly because they can obscure whether binding is saturated and they can distort experimental error[194].

Appendix A.4 Representative Results

We examined αE-catenin homodimer binding to F-actin in the co-sedimentation assay. Since past experiments have shown that the affinity of αE-catenin homodimer for F-actin is around 1 μM and the Bmax near 1[159], we performed the assay with a low concentration of F-actin (0.2 μM rather than 2 μM; see Discussion). Since 0.2 μM is below the critical concentration, phalloidin was added to stabilize F-actin polymerized from rabbit skeletal muscle G-actin (step 3.3). Increasing concentrations of αE-catenin homodimer (0.125 – 12.0 μM) were incubated in the presence or absence of 0.2 μM F-actin, the samples centrifuged and resulting pellets analyzed (**Fig. 1A**). As expected, αE-catenin homodimer cosedimented with F-actin above background (**Fig. 1A**,

compare F-actin pellet samples to No F-actin pellet samples). BSA was run as a negative control (**Fig. 1B**). Bound protein was quantified and plotted over free protein to calculate the affinity of the interaction (**Fig. 1C**). The plotted data best fit a Hill equation, and the calculated K_d was 2.9 μM, the Bmax was 0.2 and the Hill coefficient (h) was 4.8. Thus, αE-catenin homodimer binds F-actin cooperatively with a low micromolar affinity, consistent with previous work (Kd of 2.9 μM versus ~1.0 μM) [159].

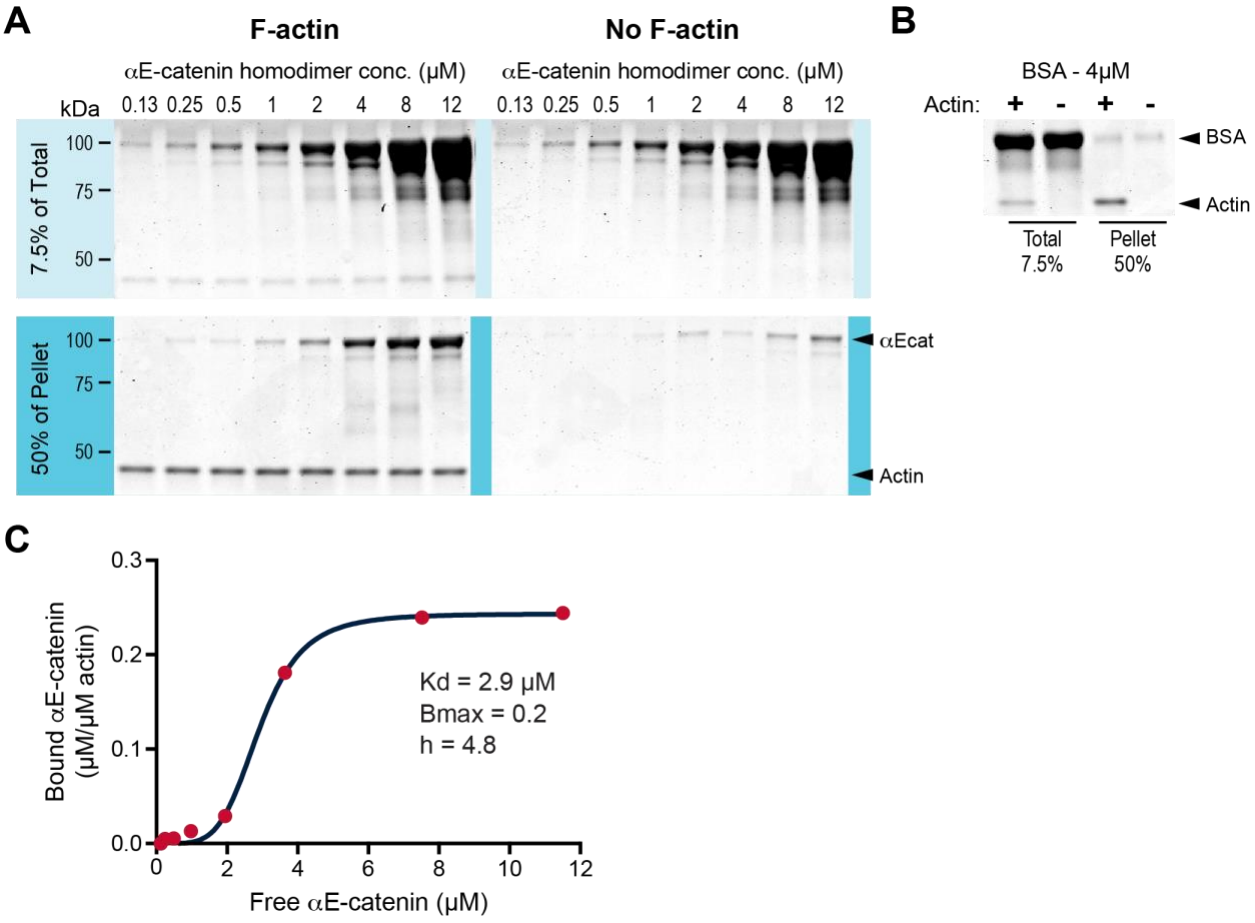

Appendix Figure 1 High-speed F-actin co-sedimentation assay.

A. Increasing concentrations (0.125 – 12.0 μM) of αE-catenin homodimer were incubated with (left panels) or without (right panels) 0.2 μM F-actin stabilized with phalloidin, incubated for 30 min at RT and centrifuged. Total (7.5% of the starting material) and pelleted material (50% of the pelleted material) were separated by SDS-PAGE and stained with Coomassie dye. B. 4 μM BSA was run as a negative control. Total and pellet samples, with (+) or without (-) F-actin, were separated by SDS-PAGE and stained with Coomassie dye. C. Bound αE-catenin (μM/μM actin) from A was plotted against free αE-catenin (μM) and data fit to a Hill equation (red line). K_d, Bmax and Hill coefficient (h) listed.

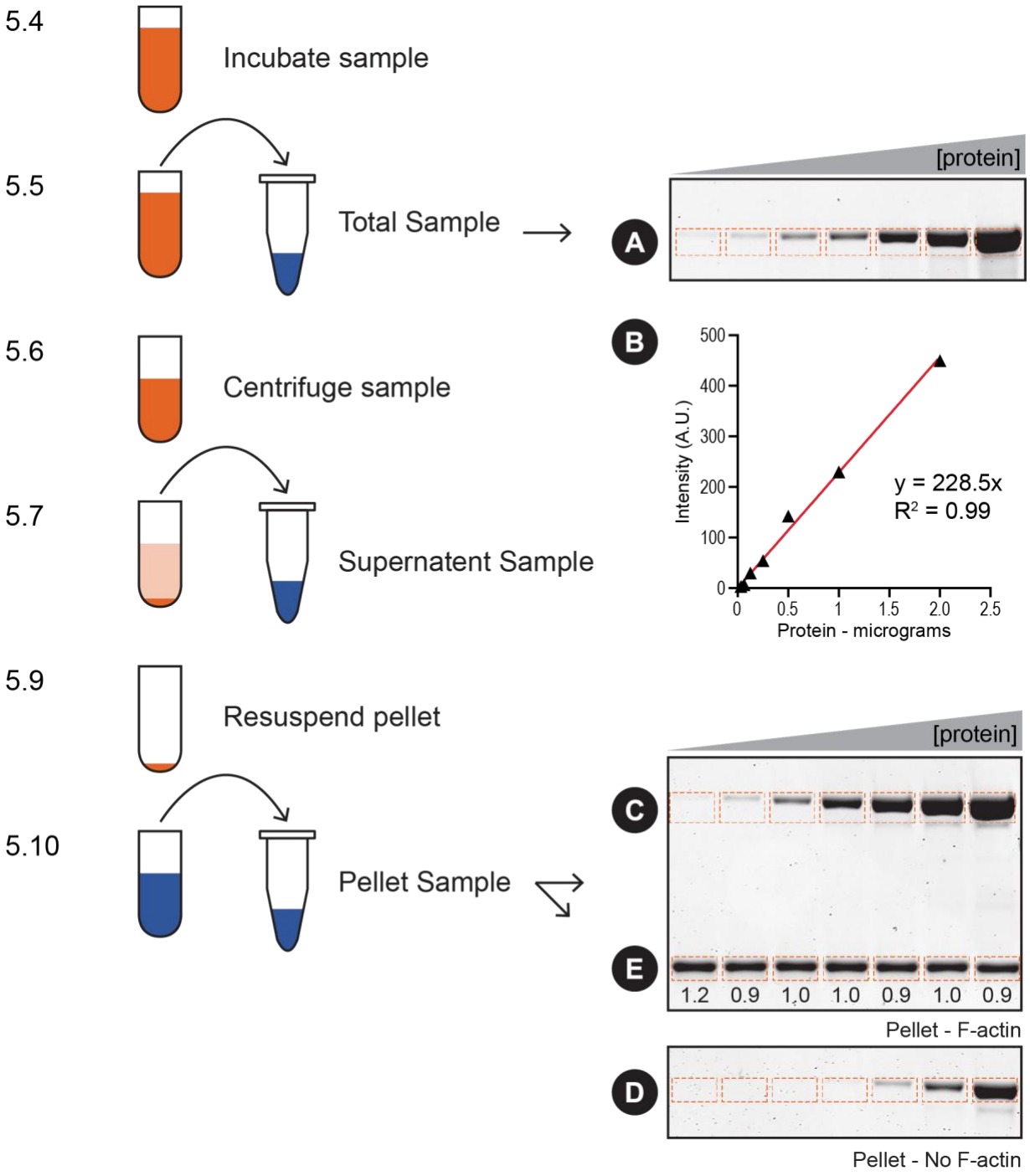

Appendix Figure 2 Actin pelleting quantification – flow chart.

The schematic outlines key steps in section 5 with examples of Total and Pellet samples (A, C-E) and standard curve (B) used for quantification. 5.13 steps: 1) Measure the amount of protein of interest in the Total samples (A). 2) Generate a standard curve by plotting band intensity versus protein mass (B). 3) Measure the amount of protein of interest that co-sedimented with F-actin (C). 4) Measure the amount of protein of

interest that pelleted in the absence of F-actin (D). 5) Subtract D from C to determine the amount of protein bound to F-actin. 6) Measure the amount of F-actin in each pellet (E), calculate the average amount of F-actin per sample and then divide each sample by the average (numbers below show ratio). 7) For each sample, divide the amount of bound protein (calculated in step 5) by the F-actin pellet ratio (calculated in step 6) to adjust for differences in the pellet. 8) Use the standard curve (B) to calculate the amount (mass) of normalized bound protein in each sample (step 7). 9) Determine concentration of free protein and bound protein to create a binding curve.

Appendix A.5 Discussion

The actin co-sedimentation assay is a straightforward technique that can quickly determine if a protein binds F-actin. With some modifications, the technique can also be used to measure the affinity of the interaction. In addition to points raised in the protocol above, the following issues should be considered when designing, conducting and interpreting the assay.

Appendix A.5.1 Protein of interest

Freshly prepared or frozen protein can be used in the assay. If frozen protein is used, it is highly recommended that results be compared with fresh (never frozen) protein to ensure that freezing is not affecting F-actin binding.

Appendix A.5.2 G-actin source

Many pelleting experiments use G-actin isolated from muscle because of its relative abundance. There are three main actin isotypes in mammals – alpha, beta and gamma – that are

remarkably similar (>90% sequence identity). Nonetheless, there are functional differences between the isotypes[195,196]. If possible, the G-actin isotype used in the binding assay should match the *in vivo* isotype. For example, if testing a protein expressed in skeletal muscle, alpha-actin is the best choice; if examining a protein expressed in fibroblast, beta-actin is recommended.

Appendix A.5.3 Phalloidin use

Since phalloidin binds F-actin it can interfere or even block the binding of some F-actin binding proteins (e.g., phalloidin blocks cofilin from binding to actin filaments[197]). Thus, phalloidin should be used with caution, and results compared to non-phalloidin-treated samples when possible.

Appendix A.5.4 High background

It is not uncommon for proteins to sediment in the absence of F-actin (**Fig. 1A**, no F-actin pellet samples). However, high levels of background sedimentation can mask true actin co-sedimentation and make it difficult, if not impossible, to determine if a protein binds F-actin or measure the affinity of the interaction. Adding polidicanol to the reaction buffer (step 4.1) can reduce background significantly and is an easy solution. If that doesn't reduce background, adjusting the reaction buffer, salt concentration and/or incubation temperature may help.

Appendix A.5.5 Binding curve

To generate a binding curve, it is necessary to vary the concentration of either the protein of interest or F-actin over a series of reactions. In practice, it is easier and preferable to maintain F-actin at a fixed concentration and vary the concentration of the protein of interest. Maintaining F-actin at a fixed concentration (e.g., 2 μM) in the pelleting assay limits non-specific trapping at higher concentrations of F-actin and prevents depolymerization at lower (< 0.5 μM) concentrations of F-actin. Depolymerization can be prevented using phalloidin, though this introduces a potential complicating factor into the system (see step 3.3 and above). Maintaining F-actin at a fixed concentration also allows one to compare (and normalize) the F-actin pellet across samples and identify failed experiments (where the F-actin pellet is highly variable, preventing analysis across concentrations). Finally, maintaining F-actin at a fixed concentration allows one to determine if binding to the actin filament is cooperative (**Fig. 1C**).

Appendix A.5.6 Saturated binding

As in all binding experiments, it is critical that binding to F-actin is saturated and that the concentration of protein plus F-actin plateaus (**Fig. 1C**). Without a plateau, it is not possible to calculate an accurate dissociation equilibrium constant. Thus, it is important to plan carefully the dilution series to be tested and always include higher concentrations of protein (at least 5-10 fold higher than the expected Kd).

Appendix A.5.7 Binding analysis

In order for the measured dissociation constants to be conclusive, the assay should be performed using an F-actin concentration such that the concentration of binding sites on F-actin for the protein of interest is much lower than the affinity. To check whether this criterion was met, estimate the concentration of binding sites from Bmax. For example, if [F-actin] was 2 μM and Bmax = 0.5, then [binding sites] ≈ 1 μM. The K_d should be greater than [binding sites] by at least 5-10 fold. If the measured K_d is of the same order of magnitude as [binding sites], then it is possible that the observed binding curve represents a titration of high-affinity binding sites rather than a true binding isotherm. If this is observed, repeat the assay using a 10-fold lower F-actin concentration to measure an accurate affinity. For high-affinity interactions, phalloidin stabilization (step 3.3) may be necessary in order to achieve an F-actin concentration low enough to measure affinity accurately.

Finally, there are fundamental limitations with the co-sedimentation assay that researchers should be aware of when performing and evaluating the assay. Most importantly, the co-sedimentation assay does not produce a true equilibrium constant. The products of binding (protein plus F-actin) are separated from the reactants during centrifugation, whereupon the products can then dissociate to create a new equilibrium. As a result, the co-sedimentation assay can miscalculate or fail to detect low affinity interactions. Since many actin-binding proteins have a low (micromolar) affinity for F-actin, a negative result (i.e., no detectable binding) in the assay does not necessarily mean a protein does not bind F-actin. As an alternative, TIRF microscopy-based single filament binding assays are more sensitive and more accurate for determining a dissociation constant (for reviews on this technique, see[198,199]). Nonetheless, despite these

limitations the pelleting assay is an effective tool within the means of most researchers to determine if a protein binds F-actin and to measure the affinity of the interaction.

Appendix B Protein Purification Protocol

Appendix B.1 Protein Induction

1.1) Grow an overnight culture of BL21 cells or other bacterial strain transformed with a pGEX (or similar) bacterial expression plasmid containing the protein of interest. Start 30mL of culture per liter of induction.

1.2) Seed 1 liter of LB ampicillin with 30mL of starter culture. Incubate at 37°C and 220 RPM until OD reaches 0.6-0.8.

1.3) When OD is reached, add 0.5mM IPTG to induce protein production. Lower the temperature to 30°C and incubate for 4 hours. For large or difficult to induce proteins the temperature can be lowered to 18°C and incubated overnight.

1.4) Pellet the cells by centrifuging at 5000g for 15 minutes.

1.5) Resuspend the pellet in 10mL of resuspension buffer (see appendix B.5) and freeze in liquid nitrogen. Frozen cell suspensions can be kept at -80°C for >5 years.

Appendix B.2 Protein Purification

2.1) Thaw frozen cell suspension quickly by placing conical tubes in beaker filled with cold water.

2.2) To suspension add: Protease Inhibitors (Kept at 100x=10ul per 1mL), DNAse, EDTA, and DTT. Example: Conical tube with 30mL of solution would need:

(a) Protease Inhibitors 100X (Roche): 300 uL

(b) DNAse (Sigma; 50ug/ul final conc): 300 uL

(c) EDTA (Sigma; 2mM Final Conc): 120 uL of .5M EDTA

(d) DTT (Sigma; 5mM Final Conc): 150 uL of 1M DTT

2.3) Lyse cells in EmulsiFlex homogenizer. Cells should be run through system three times between 15,000 and 20,000 PSI.

2.4) Centrifuge cell suspension at 20,000g for 30 minutes at 4°C.

2.5) Incubate post-centrifuged suspension with 5 ml bed volume of glutathione agarose beads (for every 2L of culture) equilibrated with PBSTR Wash Buffer (appendix B.5). Do not exceed 5mL bed volume per 2L culture or 5mL bed volume per 50mL tube. Incubate at 4°C for 30 minutes with gentle mixing.

2.6) Following binding incubation (Step 2.5), pellet beads by spinning gently in centrifuge (1 minute at 2000rpm with a slow deceleration). Wash beads 3 times with ice cold PBSTR Wash Buffer.

2.7) Wash beads 1 time with ice cold cleavage buffer (appendix B.5) and combine tubes.

2.8) Incubate beads with TEV Protease in 10mL Cleavage Buffer overnight at 4ºC with gentle agitation.

Appendix B.3 FPLC Protocol

Appendix B.3.1 Cation/Anion Column Preparation – AKTA Purifier FPLC

3.1) Fill a 500mL flask with 400mL of MonoQ A buffer (appendix B.5). Fill a 250mL flask fill with 200mL of MonoQ B buffer.

3.2) Perform a pump wash to equilibrate with buffer.

3.3) Set pump to 4ml/min and alarm pressure to 4MPa. Equilibrate the ion exchange column with 1 column volume MonoQ A buffer.

3.4) Using the gradient setting, increase the concentration of monoQ B to 100% over 1 minute. Allow the concentration of MonoQ B to remain at 100% for 1 column volume to elute any proteins from the column.

3.5) Decrease the gradient to 0% MonoQ B over 1 minute and re-equilibrate with 1 column volume of MonoQ A.

Appendix B.3.2 Sample Preparation and Loading

3.6) Filter TEV Incubated protein through column into 50mL tube. There should be no more than 15mL of flow through in the tube.

3.7) Fill tube to 45mL with MonoQ A buffer and add EDTA to a final concentration of 2mM.

3.8) Filter the sample into a new tube through a 0.22μM filter to remove and aggregates.

3.9) Transfer the filtered sample to the loop and place the caps on the end. Use a 5mL syringe and the MonoQ A buffer remove any bubbles present.

3.10) Attach the loop to the FPLC loading port.

Appendix B.4 Running the FPLC

Appendix B.4.1 Ion Exchange Column

4.1) Select the appropriate column and set the sample injection volume to the volume in the loop.

4.2) A typical program will inject the sample and wash the column with 2 column volumes of MonoQ A buffer to remove unbound protein. A gradient will then be applied increasing the concentration of monoQ B buffer to 40% over 5 column volumes while collecting 1.5 mL fractions. The majority of proteins will elute in this range.

4.3) Stop fractionation and increase the concentration of MonoQ B buffer to 100% over 1 column volume to elute any other bound proteins. Rinse the column with 2 column volumes of MonoQ A buffer to re-equilibrate the column.

Appendix B.4.2 Size Exclusion Column

4.4) Prepare a 500mL flask with 400mL of S200 buffer (appendix B.5) and perform a pump wash to equilibrate.

4.5) Attach the 5mL loop to the FPLC and flush with 10mL of S200 buffer. Load the sample from the ion exchange column using a 5mL syringe.

4.6) A typical size exclusion program will equilibrate the column with 1 column volume of S200 buffer then inject the sample and elute with 1 column volume of S200 buffer while collecting 1mL fractions.

4.7) Purified proteins can then be concentrated and used in experiments or frozen in liquid nitrogen and stored at -80ºC for later use.

Appendix B.5 Buffers

Resuspension Buffer: 20mM Tris pH 8.0, 200mM NaCl

PBSTR Wash Buffer: 1x PBS, 300mM NaCl, 0.05% Tween20, 5mM DTT

Cleavage Buffer: 20mM Tris pH 8.0, 150mM NaCl, 1mM EDTA, 10% Glycerol, 5mM DTT

MonoQ A Buffer: 20mM Tris pH 8.0, 1mM DTT

MonoQ B Buffer: 20mM Tris pH 8.0, 1M NaCl, 1mM DTT

S200 Buffer: 20mM Tris pH 8.0, 150mM NaCl, 10% Glycerol, 1mM DTT

Appendix C Limited Proteolysis

1.1) Aliquot sequence-grade trypsin (Roche) in molecular biology grade H_2O to get 1 µg/µL. 25 µg trypsin + 25 µL H_2O = 1 µg/µl. Aliquot in 5 µL / vial and flash freeze aliquots in liquid nitrogen.

1.2) Dilute protein of interest to 12 µM with proteolysis buffer (20mM Tris pH 8.0, 150mM NaCl, 1mM DTT). 100µL is required per protein tested.

1.3) Dilute trypsin to 0.25µg/mL in proteolysis buffer.

1.4) Add 12µL of protein and 3µL of diluted trypsin. Incubate samples for 0', 2.5', 5', 15', 30', 60', 120' at room temperature. For the 0' sample add water instead of trypsin.

1.5) To stop reaction add 15µL of 2X Laemmli Sample Buffer and Boil for 2 minutes.

1.6) Load 15µL onto 4-20% gradient SDS-PAGE gel and stain with Coomassie.

Appendix D PHEM Fix and Immunostaining

Appendix D.1 PHEM Fix Preparation

Final	Stock	Volume
60 mM PIPES pH 7.0	0.5 M	60 ml
25 mM HEPES pH 7.0	1 M	12.5 ml
10 mM EGTA pH 8.0	0.1 M	50 ml
2 mM $MgCl_2$	1 M	1 ml
0.12 M Sucrose	1.2 M	50 ml
4% Paraformaldehyde		20 g
		500 ml

1.1) Dissolve paraformaldehyde in 300 ml water. Add few drops of 10 N NaOH and stir while heating in fume hood. When dissolved, let cool to room temperature.

1.2) Add PIPES, HEPES, EGTA, $MgCl_2$ and Sucrose. Adjust pH to 7.3-7.4, then adjust final volume of 500 ml with water. Aliquot and freeze at –20 °C in non-defrosting freezer. Aliquots are good for about 1 year.

1.3) Thaw at 37 °C and dispose of any unused portion (DO NOT refreeze). Note: after prolonged periods of freezing, it may be necessary to heat for 20-30 minutes and vortex to get paraformaldehyde into solution. If it does not go into solution, discard.

Appendix D.2 Fixation/Staining

1.4) Replace media with warm fixative (37 °C) and fix for 10 minutes at room temperature.

1.5) Wash 2X in PBS, 5 min/wash. Fixed cells can be stored for weeks at 4 °C in PBS + 0.02% azide. However, if staining cells transfected with a fluorescent protein, it's best to stain soon after fixation (1-2 days).

1.6) When ready to stain, permeabilize cells with PBS + 0.2% Triton X-100 for 2 min at RT. Timing is important and can vary between cells lines, but 2 min works for most cell types.

1.7) Wash 2X in PBS, 5 min/wash. Block coverslips in PBS + 10% BSA 1 hour at RT, or overnight at 4 °C. Rinse 1X in PBS.

1.8) Primary antibody staining. Dilute antibodies in PBS + 1% BSA and stain for 1 hr at RT or ON at 4 °C. Hardier cells (e.g. MDCK epithelial cells, fibroblasts) can be stained upside down to conserve antibody; delicate cells types (e.g. neurons) should be stained right side up. Coverslips should be stained on parafilm in a humidified chamber (moistened Kimwipes in a closed plastic container works well).

1.9) Wash coverslips 2X in PBS, 5 min/wash.

1.10) Secondary antibody staining. Dilute antibodies in PBS + 1% BSA. Stain for 45 min to 1 hr at RT. Do not stain overnight. If using phalloidin to stain for F-actin, add to secondary mix (use 1:200 – 1:500).

1.11) Wash 2X in PBS, 5 min/wash. If you want to DAPI stain, you can do a quick (5 min) stain here, followed by 2 more washes.

1.12) Mount coverslips in favorite fixing media. Seal/adhere coverslips with nail polish if necessary. Allow sufficient time to dry, clean coverslips with diluted Windex and image.

Bibliography

1. Green KJ, Roth-Carter Q, Niessen CM, Nichols SA. Tracing the Evolutionary Origin of Desmosomes. *Current Biology*. 2020;30(10):R535-R543. doi:10.1016/j.cub.2020.03.047.

2. Noorman M, van der Heyden MAG, van Veen TAB, et al. Cardiac cell–cell junctions in health and disease: Electrical versus mechanical coupling. *Journal of Molecular and Cellular Cardiology*. 2009;47(1):23-31. doi:10.1016/j.yjmcc.2009.03.016.

3. Sheikh F, Ross RS, Chen J. Cell-Cell Connection to Cardiac Disease. *Trends in Cardiovascular Medicine*. 2009;19(6):182-190. doi:10.1016/j.tcm.2009.12.001.

4. McCain ML, Lee H, Aratyn-Schaus Y, Kleber A, Parker KK. Cooperative coupling of cell-matrix and cell–cell adhesions in cardiac muscle. *Proc Natl Acad Sci USA*. June 2012:1-6. doi:10.1073/pnas.1203007109/-/DCSupplemental.

5. Vite A, Radice GL. N-Cadherin/Catenin Complex as a Master Regulator of Intercalated Disc Function. *Cell Communication & Adhesion*. 2014;21(3):169-179. doi:10.3109/15419061.2014.908853.

6. Horsley V, Pavlath GK. Forming a Multinucleated Cell: Molecules That Regulate Myoblast Fusion. *Cells Tissues Organs*. January 2004:1-12. doi:10.1159/000075028.

7. Oren-Suissa M, Podbilewicz B. Cell fusion during development. *Trends in Cell Biology*. November 2007:1-10. doi:10.1016/j.tcb.2007.09.004.

8. Ehler E. Cardiac cytoarchitecture-why the “hardware” is important for heart function! *BBA - Molecular Cell Research*. 2016;1863(Part B):1857-1863. doi:10.1016/j.bbamcr.2015.11.006.

9. Rayns DG, Simpson FO, Ledingham JM. Ultrastructure of Desmosomes in Mammalian Intercalated Disc; Appearances After Lanthanum Treatment. *Journal of Cell Biology*. July 1969:1-5.

10. Franke WW, Borrmann CM, Grund C, Pieperhoff S. The area composita of adhering junctions connecting heart muscle cells of vertebrates. I. Molecular definition in intercalated disks of cardiomyocytes by immunoelectron microscopy of desmosomal proteins. *European Journal of Cell Biology*. 2006;85(2):69-82. doi:10.1016/j.ejcb.2005.11.003.

11. Sheikh F, Chen Y, Chen Y, et al. alpha-E-catenin inactivation disrupts the cardiomyocyte adherens junction, resulting in cardiomyopathy and susceptibility to wall rupture. *Circulation*. 2006;114(10):1046-1055. doi:10.1161/CIRCULATIONAHA.106.634469.

12. Rohr S. Role of gap junctions in the propagation of the cardiac action potential. *Cardiovasc Res*. April 2004:1-14. doi:10.1016/j.cardiores.2003.11.035.

13. Wickline ED, Dale IW, Merkel CD, Heier JA, Stolz DB, Kwiatkowski AV. αT-Catenin Is a Constitutive Actin-binding α-Catenin That Directly Couples the Cadherin·Catenin Complex to Actin Filaments. *J Biol Chem*. 2016;291(30):15687-15699. doi:10.1074/jbc.M116.735423.

14. Maeda M, Holder E, Lowes B, Valent S, Bies RD. Dilated cardiomyopathy associated with deficiency of the cytoskeletal protein metavinculin. *Circulation*. 1997;95(1):17-20. doi:10.1161/01.cir.95.1.17.

15. Calore M, Lorenzon A, De Bortoli M, Poloni G, Rampazzo A. Arrhythmogenic cardiomyopathy: a disease of intercalated discs. *Cell Tissue Res*. May 2015:1-10. doi:10.1007/s00441-014-2015-5.

16. van Hengel J, Calore M, Bauce B, et al. Mutations in the area composita protein αT-catenin are associated with arrhythmogenic right ventricular cardiomyopathy. *European Heart Journal*. 2012;34(3):201-210. doi:10.1093/eurheartj/ehs373.

17. Zhao Z-M, Reynolds AB, Gaucher EA. The evolutionary history of the catenin gene family during metazoan evolution. *BMC Evolutionary Biology*. 2011:1-13.

18. Dickinson DJ, Nelson WJ, Weis WI. A Polarized Epithelium Organized by **β**- and **α**-Catenin Predates Cadherin and Metazoan Origins. *Science*. March 2011:1-5. doi:10.1126/science.1198904.

19. Hartsock A, Nelson WJ. Adherens and tight junctions: Structure, function and connections to the actin cytoskeleton. *Biochimica et Biophysica Acta (BBA) - Molecular Cell Research*. March 2008:1-10. doi:10.1016/j.bbamem.2007.07.012.

20. Mège RM, Ishiyama N. Integration of Cadherin Adhesion and Cytoskeleton at Adherens Junctions. *Cold Spring Harb Perspect Biol*. 2017;9(5):a028738–19. doi:10.1101/cshperspect.a028738.

21. Takeda H, Shimoyama Y, Nagafuchi A, Hirohashi S. E-cadherin functions as a cis-dimer at the cell-cell adhesive interface *in vivio*. *Nature Structural Biology*. March 1999:1-3.

22. Zuppinger C, Eppenberger-Eberhardt M, Eppenberger HM. N-Cadherin: Structure, Function and Importance in the Formation of New Intercalated Disc-Like Cell Contacts in Cardiomyocytes. *Heart Failure Reviews*. October 2000:1-7.

23. Perez TD, Nelson WJ. Cadherin Adhesion: Mechanisms and Molecular Interactions. *Handbook of Experimental Pharmacology*. 2004:1-19. doi:10.1007/978-3-540-68170-0_1.

24. Radice GL, Rayburn H, Matsunami H, Knudsen KA, Takeichi M, Hynes RO. Developmental Defects in Mouse Embryos Lacking N-Cadherin. *Developmental Biology*. December 1996:1-15.

25. Kostetskii I, Li J, Xiong Y, et al. Induced Deletion of the N-Cadherin Gene in the Heart Leads to Dissolution of the Intercalated Disc Structure. *Circulation Research*. February 2005:1-9. doi:10.1161/01.RES.0000156274.72390.2c.

26. Luo Y, Ferreira-Cornwell MC, Baldwin HS, et al. Rescuing the N-cadherin knockout by cardiac-specific expression of N- or E-cadherin. *Development*. January 2001:1-11.

27. Gul IS, Hulpiau P, Saeys Y, van Roy F. Evolution and diversity of cadherins and catenins. *Experimental Cell Research*. 2017;358(1):3-9. doi:10.1016/j.yexcr.2017.03.001.

28. Peifer M, Berg S, Reynolds AB. A Repeating Amino Acid Motif Shared by Proteins with Diverse Cellular Roles. *Cell*. March 1994:1-3. doi:10.1016/0092-8674(94)90353-0.

29. Peifer M, Yap AS. Traffic control: p120-catenin acts as a gatekeeper to control the fate of classical cadherins in mammalian cells. *Journal of Cell Biology*. October 2003:1-4. doi:10.1083/jcb.200310090.

30. Nanes BA, Chiasson-MacKenzie C, Lowery AM, et al. p120-catenin binding masks an endocytic signal conserved in classical cadherins. *Journal of Cell Biology*. October 2012:1-16. doi:10.1083/jcb.201205029.

31. Chen X, Kojima S-I, Borisy GG, Green KJ. p120 catenin associates with kinesin and facilitates the transport of cadherin–catenin complexes to intercellular junctions. *Journal of Cell Biology*. October 2003:1-11. doi:10.1083/jcb.200305137.

32. Pieters T, van Roy F, van Hengel J. Functions of p120ctn isoforms in cell-cell adhesion and intracellular signaling. *Frontiers in Bioscience*. January 2012:1-26.

33. Braga VMM, Yap AS. The challenges of abundance: epithelial junctions and small GTPase signalling. *Current Opinion in Cell Biology*. September 2005:1-9. doi:10.1016/j.ceb.2005.08.012.

34. Anastasiadis PZ. p120-ctn: A nexus for contextual signaling via Rho GTPases. *Biochimica et Biophysica Acta (BBA) - Molecular Cell Research*. December 2006:1-13. doi:10.1016/j.bbamcr.2006.08.040.

35. Choi H-J, Gross JC, Pokutta S, Weis WI. Interactions of Plakoglobin and Beta-Catenin with Desmosomal Cadherins. *J Biol Chem*. October 2009:1-13.

36. Valenta T, Hausmann G, Basler K. The many faces and functions of **β**-catenin. *EMBO J*. 2012;31(12):2714-2736. doi:10.1038/emboj.2012.150.

37. Zhou J, Qu J, Yi XP, et al. Upregulation of **γ**-catenin compensates for the loss of **β**-catenin in adult cardiomyocytes. *American Journal of Physiology Heart and Circulatory Physiology*. December 2007:1-7. doi:10.1152/ajpheart.00576.2006.

38. Haegel H, Larue L, Ohsugi M, Fedorov L, Harrenknecht K, Kemler R. Lack of **β**-catenin affects mouse development at gastrulation. *Development*. September 1995:1-9.

39. Komiya Y, Habas R. Wnt signal transduction pathways. *Organogenesis*. June 2008:1-8.

40. Zhao Y, Wang C, Wang C, et al. An essential role for Wnt/β-catenin signaling in mediating hypertensive heart disease. *Scientific Reports*. June 2018:1-14. doi:10.1038/s41598-018-27064-2.

41. Rimm DL, Koslov ER, Kebriaei P, Cianci CD, Morrow JS. **α**(E)-Catenin is an actin-binding and -bundling protein mediating the attachment of F-actin to the membrane adhesion complex. *Proc Natl Acad Sci USA*. September 1995:1-5.

42. Buckley CD, Tan J, Anderson KL, et al. The minimal cadherin-catenin complex binds to actin filaments under force. *Science*. 2014;346(6209):1254211-1254211. doi:10.1126/science.1254211.

43. Pokutta S, Choi H-J, Ahlsen G, Hansen SD, Weis WI. Structural and thermodynamic characterization of cadherin·β-catenin·α-catenin complex formation. *J Biol Chem*. 2014;289(19):13589-13601. doi:10.1074/jbc.M114.554709.

44. Liang X, Gomez GA, Yap AS. Current perspectives on cadherin-cytoskeleton interactions and dynamics. *Cell Health and Cytoskeleton*. January 2015:1-14. doi:10.2147/CHC.S76107.

45. Merkel CD, Li Y, Raza Q, Stolz DB, Kwiatkowski AV. Vinculin anchors contractile actin to the cardiomyocyte adherens junction. *Molecular Biology of the Cell*. September 2019:1-12. doi:10.1091/mbc.E19-04-0216).

46. Herrenknecht K, Ozawa M, Lenter M, Kemler R. The Uvomorulin-Anchorage Protein a-Catenin Is a Vinculin Homologue. *Proc Natl Acad Sci USA*. July 1991:1-5.

47. Hirano S, Kimoto N, Shimoyama Y, Hirohashi S, Takeichi M. Identification of a Neural a-Catenin as a Key Regulator of Cadherin Function and Multicellular Organization. *Cell*. July 1992:1-9.

48. Janssens B, Goossens S, van Roy F. aT-Catenin: a novel tissue-specific b-catenin-binding protein mediating strong cell-cell adhesion. *Journal of Cell Science*. August 2001:1-12.

49. Chiarella SE, Rabin EE, Ostilla LA, Flozak AS, Gottardi CJ. αT-catenin: A developmentally dispensable, disease-linked member of the α-catenin family. *Tissue Barriers*. 2018;0(0):1-12. doi:10.1080/21688370.2018.1463896.

50. Torres M, Stoykova A, Huber O, et al. An **α**-E-catenin gene trap mutation defines its function in preimplantation development. *Proc Natl Acad Sci USA*. January 1997:1-6.

51. Park C, Falls W, Finger JH, Longo-Guess CM, Ackerman SL. Deletion in Catna2, encoding **α**N-catenin, causes cerebellar and hippocampal lamination defects and impaired startle modulation. *Nature Genetics*. June 2002:1-6. doi:10.1038/ng908.

52. Uemura M, Takeichi M. **α**N-Catenin Deficiency Causes Defects in Axon Migration and Nuclear Organization in Restricted Regions of the Mouse Brain. *Developmental Dynamics*. August 2006:1-8. doi:10.1002/dvdy.20841.

53. Li J, Goossens S, van Hengel J, et al. Loss of αT-catenin alters the hybrid adhering junctions in the heart and leads to dilated cardiomyopathy and ventricular arrhythmia following acute ischemia. *Journal of Cell Science*. 2012;125(4):1058-1067. doi:10.1242/jcs.098640.

54. Vite A, Li J, Radice GL. New functions for alpha-catenins in health and disease: from cancer to heart regeneration. *Cell Tissue Res*. 2015;360(3):773-783. doi:10.1007/s00441-015-2123-x.

55. Christensen AH, Benn M, Tybjaerg-Hansen A, Haunso S, Svendsen JH. Screening of Three Novel Candidate Genes in Arrhythmogenic Right Ventricular Cardiomyopathy. *Genetic Testing and Molecular Biomarkers*. March 2011:1-6. doi:10.1089/gtmb.2010.0151.

56. Elliott PM, Anastasakis A, Asimaki A, Green KJ, van Tintelen JP. Definition and treatment of arrhythmogenic cardiomyopathy: an updated expert panel report. *European Journal of Heart Failure*. July 2019:1-10. doi:10.1002/ejhf.1534.

57. Hatzfeld M, Keil R, Magin TM. Desmosomes and Intermediate Filaments: Their Consequences for Tissue Mechanics. *Cold Spring Harb Perspect Biol*. May 2017:1-22. doi:10.1101/cshperspect.a029157.

58. Herrmann H, Aebi U. Intermediate Filaments: Structure and Assembly. *Cold Spring Harb Perspect Biol*. October 2016:1-22. doi:10.1101/cshperspect.a018242.

59. Paulin D, Li Z. Desmin: a major intermediate filament protein essential for the structural integrity and function of muscle. *Experimental Cell Research*. October 2004:1-7. doi:10.1016/j.yexcr.2004.08.004.

60. Green KJ, Jaiganesh A, Broussard JA. Desmosomes: Essential contributors to an integrated intercellular junction network. *F Research*. December 2019:1-16. doi:10.12688/f1000research.20942.1.

61. Broussard JA, Getsios S, Green KJ. Desmosome regulation and signaling in disease. *Cell Tissue Res*. 2015;360(3):501-512. doi:10.1007/s00441-015-2136-5.

62. Delmar M, McKenna WJ. The Cardiac Desmosome and Arrhythmogenic Cardiomyopathies. *Circulation*. September 2010:1-15. doi:10.1161/CIRCRESAHA.110.223412.

63. Delva E, Tucker DK, Kowalczyk AP. The Desmosome. *Cold Spring Harb Perspect Biol*. July 2009:1-17. doi:10.1101/cshperspect.a002543.

64. Kowalczyk AP, Green KJ. Structure, Function, and Regulation of Desmosomes. *Progress in Molecular Biology and Translation Science*. February 2015:1-20. doi:10.1016/B978-0-12-394311-8.00005-4.

65. Schmidt A, Jager S. Plakophilins—hard work in the desmosome, recreation in the nucleus? *European Journal of Cell Biology*. February 2005:1-16. doi:10.1016/j.ejcb.2004.12.020.

66. Al-Jassar C, Bikker H, Overduin M, Chidgey M. Mechanistic Basis of Desmosome-Targeted Diseases. *Journal of Molecular Biology*. 2013;425(21):4006-4022. doi:10.1016/j.jmb.2013.07.035.

67. Corrado D, Basso C, Judge D. Cardiomyopathy Compendium: Arrythmogenic Cardiomyopathy. *Circulation*. September 2017:1-19. doi:10.1161/CIRCRESAHA.117.309345.).

68. Virani SS, Alonso A, Benjamin EJ, Tsao CW. **Heart Disease and Stroke Statistics— 2020 Update**. *Circulation*. February 2020:1-458. doi:10.1161/CIR.0000000000000757.

69. Beffagna G, Occhi G, Nava A, Towbin JA, Danieli GA, Rampazzo A. Regulatory mutations in transforming growth factor-h3 gene cause arrhythmogenic right ventricular cardiomyopathy type 1. *Cardiovasc Res*. January 2005:1-8. doi:10.1016/j.cardiores.2004.10.005.

70. van Tintelen JP, Entius MM, Bhuiyan ZA, et al. Plakophilin-2 Mutations Are the Major Determinant of Familial Arrhythmogenic Right Ventricular Dysplasia/Cardiomyopathy. *Circulation*. March 2006:1-9. doi:10.1161/CIRCULATIONAHA.105.609719.

71. Patel DM, Dubash AD, Kreitzer G, Green KJ. Disease mutations in desmoplakin inhibit Cx43 membrane targeting mediated by desmoplakin–EB1 interactions. *Journal of Cell Biology*. September 2014:1-19. doi:10.1083/jcb.201312110.

72. Kam CY, Dubash AD, Magistrati E, et al. Desmoplakin maintains gap junctions by inhibiting Ras/MAPK and lysosomal degradation of connexin-43. *Journal of Cell Biology*. August 2018:1-17. doi:10.1083/jcb.201710161&domain=pdf.

73. Sato PY, Coombs W, Lin X, et al. Interactions Between Ankyrin-G, Plakophilin-2, and Connexin43 at the Cardiac Intercalated Disc. *Circulation*. June 2011:1-9. doi:10.1161/CIRCRESAHA.111.247023.

74. Borrman C, Grund C, Kuhn C, Hofmann I, Pieperhoff S, Franke WW. The area composita of adhering junctions connecting heart muscle cells of vertebrates. II. Colocalizations of desmosomal and fascia adhaerens molecules in the intercalated disk. *European Journal of Cell Biology*. 2006;85(6):469-485. doi:10.1016/j.ejcb.2006.02.009.

75. Goossens S, Janssens B, Bonne S, et al. A unique and specific interaction between aT-catenin and plakophilin-2 in the area composita, the mixed-type junctional structure of cardiac intercalated discs. *Journal of Cell Science*. 2007;120(12):2126-2136. doi:10.1242/jcs.004713.

76. Pieperhoff S, Schumacher H, Franke WW. The area composita of adhering junctions connecting heart muscle cells of vertebrates. V. The importance of plakophilin-2 demonstrated by small interference RNA-mediated knockdown in cultured rat cardiomyocytes. *European Journal of Cell Biology*. July 2008:1-13. doi:10.1016/j.ejcb.2007.12.002.

77. Pieperhoff S, Franke WW. The area composita of adhering junctions connecting heart muscle cells of vertebrates – IV: Coalescence and amalgamation of desmosomal and adhaerens junction components – Late processes in mammalian heart development. *European Journal of Cell Biology*. June 2007:1-15. doi:10.1016/j.ejcb.2007.04.001.

78. Goodenough DA, Paul DL. Gap Junctions. *Cold Spring Harb Perspect Biol*. June 2009:1-19. doi:10.1101/cshperspect.a002576.

79. Severs NJ, Bruce AF, Dupont E, Rothery S. Remodelling of gap junctions and connexin expression in diseased myocardium. *Cardiovasc Res*. September 2008:1-11. doi:10.1093/cvr/cvn133.

80. Goodenough DA, Goliger JA, Paul DL. Connexins, Connexons, and Intercellular Communication. *Annual Reviews*. January 1996:1-30.

81. Sohl G, Willecke K. Gap junctions and the connexin protein family. *Cardiovasc Res*. April 2004:1-5. doi:10.1016/j.cardiores.2003.11.013.

82. Lambiase PD, Tinker A. Connexins in the heart. *Cell Tissue Research*. May 2015:1-10. doi:10.1007/s00441-014-2020-8.

83. Verheule S, Kaese S. Connexin diversity in the heart: insights from transgenic mouse models. *Frontiers in Pharmacology*. June 2013:1-14. doi:10.3389/fphar.2013.00081/abstract.

84. Ideker RE, Kong W, Pogwizd S. Purkinje Fibers and Arrhythmias. *Pacing Clinical Electrophysiology*. March 2010:1-4. doi:10.1111/j.1540-8159.2008.02232.x.

85. Reaume AG, de Sousa PA, Kulkarni S, et al. Cardiac Malformation in Neonatal Mice Lacking Connexin43. *Science*. March 1995:1-7. doi:10.1126/science.7892609.

86. Gutstein DE, Morley GE, Tamaddon H, et al. Conduction Slowing and Sudden Arrhythmic Death in Mice With Cardiac-Restricted Inactivation of Connexin43. *Integrative Physiology*. February 2001:1-7.

87. Kaplan SR, Gard JJ, Protonotarios N, Brousse N, Fontaine G, Saffitz JE. Remodeling of myocyte gap junctions in arrhythmogenic right ventricular cardiomyopathy due to a deletion in plakoglobin (Naxos disease). *Heart Rhythm*. May 2004:1-9. doi:10.1016/j.hrthm.2004.01.001.

88. Miller PW, Clarke DN, Weis WI, Lowe CJ, Nelson WJ. The Evolutionary Origin of Epithelial Cell–Cell Adhesion Mechanisms. In: *Functional Organization of Vertebrate Plasma Membrane*. Vol 72. Current Topics in Membranes. Elsevier; 2013:267-311. doi:10.1016/B978-0-12-417027-8.00008-8.

89. Pokutta S, Weis WI. Structure of the Dimerization and b-catenin-binding region of a-catenin. *Molecular Cell*. March 2000:1-11.

90. Koslov ER, Maupin P, Pradhan D, Morrow JS, Rimm DL. **α**-Catenin Can Form Asymmetric Homodimeric Complexes and/or Heterodimeric Complexes with b-Catenin. *J Biol Chem*. October 1997:1-7.

91. Nieset JE, Redfield AR, Jin F, Knudsen KA, Johnson KR, Wheelock MJ. Characterization of the interactions of a-catenin with a-actinin and b-catenin/plakoglobin. *Journal of Cell Science*. March 1997:1-10.

92. Yang J, Barford D, Tonks NK, Dokurno P. Crystal structure of the M-fragment of a-catenin: implications for modulation of cell adhesion. *European Molecular Biology Organization*. 2001:1-12.

93. Pokutta S, Drees F, Takai Y, Nelson WJ, Weis WI. Biochemical and Structural Definition of the l-Afadin- and Actin-binding Sites of α-Catenin. *J Biol Chem*. 2002;277(21):18868-18874. doi:10.1074/jbc.M201463200.

94. Hirano Y, Amano Y, Yonemura S, Hakoshima T. The force-sensing device region of α-catenin is an intrinsically disordered segment in the absence of intramolecular stabilization of the autoinhibitory form. *Genes Cells*. 2018;7:357–16. doi:10.1111/gtc.12578.

95. Choi H-J, Pokutta S, Weis WI. αE-catenin is an autoinhibited molecule that coactivates vinculin. *Proc Natl Acad Sci USA*. May 2012:1-6. doi:10.1073/pnas.1203906109/-/DCSupplemental.

96. Thomas WA, Boscher CC, Chu Y-S, et al. **α**-Catenin and Vinculin Cooperate to Promote High E-cadherin-based Adhesion Strength. *J Biol Chem*. 2013;288(7):4957-4969. doi:10.1074/jbc.M112.403774.

97. Ishiyama N, Tanaka N, Abe K, Takeichi M, Ikura M. An Autoinhibited Structure of a-Catenin and Its Implications for Vinculin Recruitment to Adherens Junctions. *J Biol Chem*. May 2013:1-14.

98. Ishiyama N, Sarpal R, Wood MN, et al. Force-dependent allostery of the a-catenin actin-binding domain controls adherens junction dynamics and functions. *Nature Communications*. November 2018:1-17. doi:10.1038/s41467-018-07481-7.

99. Mei L, de los Reyes SE, Reynolds MJ, Leicher R, Liu S, Alushin GM. Molecular mechanism for direct actin force-sensing by **α**-catenin. *eLife*. October 2020:1-32. doi:10.7554/eLife.62514.

100. Xu X-P, Pokutta S, Torres M, et al. Structural basis of **α**E-catenin-F-actin catch bond behavior. *eLife*. October 2020:1-21. doi:10.7554/eLife.60878.

101. Shibahara T, Hirano Y, Hakoshima T. Structure of the free form of the N-terminal VH1 domain of monomeric α-catenin. *FEBS*. June 2015:1-7. doi:10.1016/j.febslet.2015.05.053.

102. Yao M, Qiu W, Liu R, et al. Force-dependent conformational switch of alpha-catenin controls vinculin binding. *Nature Communications*. 2014;5:1-11. doi:10.1038/ncomms5525.

103. Li J, Newhall J, Ishiyama N, et al. Structural Determinants of the Mechanical Stability of **α**-Catenin. *J Biol Chem*. July 2015:1-14.

104. Barrick SK, Li J, Kong X, Ray A, Tajkhorshid E, Leckband DE. Salt bridges gate **α**-catenin activation at intercellular junctions. *Molecular Biology of the Cell*. January 2018:1-12. doi:10.1091/mbc.E17-03-0168).

105. Terekhova K, Pokutta S, Kee YS, et al. Binding partner- and force- promoted changes in αE-catenin conformation probed by native cysteine labeling. *Scientific Reports*. October 2019:1-13. doi:10.1038/s41598-019-51816-3.

106. Rangarajan ES, Izard T. Dimer asymmetry defines α-catenin interactions. *Nature Structural & Molecular Biology*. 2013;20(2):188-193. doi:10.1038/nsmb.2479.

107. Mayerhofer A. Human testicular peritubular cells: more than meets the eye. *Reproduction*. April 2013:1-10. doi:10.1530/REP-12-0497.

108. Maiden SL, Hardin J. The secret life of **α**-catenin: Moonlighting in morphogenesis. *Journal of Cell Biology*. November 2011:1-10. doi:10.1083/jcb.201103106.

109. Vasioukhin V, Bauer C, Degenstein L, Wise B, Fuchs E. Hyperproliferation and Defects in Epithelial Polarity upon Conditional Ablation of a-Catenin in Skin. *Cell*. February 2001:1-13.

110. Lien W-H, Klezovitch O, Fernandez TE, Delrow J, Vasioukhin V. aE-Catenin Controls Cerebral Cortical Size by Regulating the Hedgehog Signaling Pathway. *Science*. 2006;311(5767):1606-1609. doi:10.1126/science.1123513.

111. Qiao J, Rellinger EJ, Kim KW, et al. Identification of α-N-catenin as a novel tumor suppressor in neuroblastoma. *Oncotarget*. August 2019:1-13.

112. Austin KM, Trembley MA, Chandler SF, et al. Molecular mechanisms of arrhythmogenic cardiomyopathy. *Nature Reviews Cardiology*. August 2019:1-19. doi:10.1038/s41569-019-0200-7.

113. Fanjul-Fernandez M, Quesada V, Cabanillas R, et al. Cell-cell adhesion genes CTNNA2 and CTNNA3 are tumour suppressors frequently mutated in laryngeal carcinomas. *Nature Communications*. October 2013:1-9. doi:10.1038/ncomms3531.

114. Stahn V, Nagel I, Fischer-Huchzermeyer S, et al. Molecular Analysis of Hybrid Neurofibroma/Schwannoma Identifies Common Monosomy 22 and α-T-Catenin/CTNNA3 as a Novel Candidate Tumor Suppressor. *The American Journal of Pathology*. 2016;186(12):3285-3296. doi:10.1016/j.ajpath.2016.08.019.

115. Miyashita A, Arai H, Asada T, et al. Genetic association of CTNNA3 with late-onset Alzheimer's disease in females. *Human Molecular Genetics*. November 2007:1-16. doi:10.1093/hmg/ddm244.

116. Smith JD, Meehan MH, Crean J, McCann A. Alpha T-catenin (CTNNA3): a gene in the hand is worth two in the nest. *Cell and Molecular Life Sciences*. July 2011:1-6. doi:10.1007/s00018-011-0728-0.

117. O'Roak BJ, Vives L, Girirajan S, et al. Sporadic autism exomes reveal a highly interconnected protein network of de novo mutations. *Nature*. April 2012:1-7. doi:10.1038/nature10989.

118. Bacchelli E, Ceroni F, Pinto D, et al. A CTNNA3 compound heterozygous deletion implicates a role for aT-catenin in susceptibility to autism spectrum disorder. 2014;6(1):1-11. doi:10.1186/1866-1955-6-17.

119. Folmsbee SS, Wilcox DR, Tyberghein K, et al. αT-catenin in restricted brain cell types and its potential connection to autism. *Journal of Molecular Psychiatry*. April 2016:1-13. doi:10.1186/s40303-016-0017-9.

120. Zhang Y, Chen K, Sloan S, et al. An RNA-Sequencing Transcriptome and Splicing Database of Glia, Neurons, and Vascular Cells of the Cerebral Cortex. *Journal of Neuroscience*. December 2014:1-19. doi:10.1523/JNEUROSCI.1860-14.2014.

121. Busby V, Goossens S, Nowotny P, Janssens B, van Roy F, Lovestone S. aT-Catenin Is Expressed in Human Brain and Interacts With the Wnt Signaling Pathway But Is Not Responsible for Linkage to Chromosome 10 in Alzheimer's Disease. *NeuroMolecular Medicine*. April 2004:1-14.

122. Aberle H, Butz S, Stappert J, Weissig H, Kemler R, Hoschuetzky H. Assembly of the cadherin-catenin complex in vitro with recombinant proteins. *Journal of Cell Science*. August 1994:1-9.

123. Heier JA, Pokutta S, Dale IW, et al. Distinct intramolecular interactions regulate autoinhibition of vinculin binding in **α**T-catenin and **α**E-catenin. *J Biol Chem*. 2021;296:100582. doi:10.1016/j.jbc.2021.100582.

124. Daugherty RL, Serebryannyy L, Yemelyanov A, et al. α-Catenin is an inhibitor of transcription. *Proc Natl Acad Sci USA*. April 2014:1-6. doi:10.1073/pnas.1308663111.

125. Sun Y, Zhang J, Ma L. **α**-Catenin: A tumor supressor beyond adherens junctions. *Cell Cycle*. July 2014:1-6. doi:10.4161/cc.29765.

126. Dominguez R, Holmes KC. Actin Structure and Function. *Annual Reviews*. June 2011:1-20. doi:10.1146/annurev-biophys-042910-155359.

127. Drees F, Pokutta S, Yamada S, Nelson WJ, Weis WI. α-Catenin Is a Molecular Switch that Binds E-Cadherin-β-Catenin and Regulates Actin-Filament Assembly. *Cell*. 2005;123(5):903-915. doi:10.1016/j.cell.2005.09.021.

128. Benjamin JM, Kwiatkowski AV, Yang C, et al. αE-catenin regulates actin dynamics independently of cadherin-mediated cell–cell adhesion. *J Cell Biol*. 2010;189(2):339-352. doi:10.1083/jcb.200910041.

129. Lee SE, Chunsrivirot S, Kamm RD, Mofrad MRK. Molecular Dynamics Study of Talin-Vinculin Binding. *Biophysical Journal*. July 2008:1-10. doi:10.1529/biophysj.107.124487.

130. Burridge K, Chrzanowska-Wodnicka M. Focal Adhesions, Contractility, and Signaling. *Annual Reviews*. June 1996:1-58.

131. Watabe-Uchida M, Uchida N, van Roy F, Takeichi M. a-Catenin-Vinculin Interaction Functions to Organize the Apical Junctional Complex in Epithelial Cells. *Journal of Cell Biology*. July 1998:1-11.

132. Weiss EE, Kroemker M, Rudiger A-H, Jockusch BM. Vinculin Is Part of the Cadherin–Catenin Junctional Complex: Complex Formation between **α**-Catenin and Vinculin. *J Biol Chem*. April 1998:1-10.

133. Xu W, Baribault H, Adamson ED. Vinculin knockout results in heart and brain defects during embryonic development. *Development*. December 1997:1-11.

134. Zemljic-Harpf AE, Ponrartana S, Avalos RT, et al. Heterozygous Inactivation of the Vinculin Gene Predisposes to Stress-Induced Cardiomyopathy. *The American Journal of Pathology*. 2004;165(3):1033-1044. doi:10.1016/S0002-9440(10)63364-0.

135. Zemljic-Harpf AE, Miller JC, Henderson SA, et al. Cardiac-Myocyte-Specific Excision of the Vinculin Gene Disrupts Cellular Junctions, Causing Sudden Death or Dilated Cardiomyopathy. *Molecular and Cellular Biology*. 2007;27(21):7522-7537. doi:10.1128/MCB.00728-07.

136. Shiraishi I, Simpson DG, Carver W, et al. Vinculin is an Essential Component for Normal Myofibrillar Arrangement in Fetal Mouse Cardiac Myocytes. *Journal of Molecular and Cellular Cardiology*. August 1997:1-12.

137. Vasile VC, Ommen SR, Edwards WD, Ackerman MJ. A missense mutation in a ubiquitously expressed protein, vinculin, confers susceptibility to hypertrophic cardiomyopathy. *Biochemical and Biophysical Research Communications*. May 2006:1-6. doi:10.1016/j.bbrc.2006.04.151.

138. Rangarajan ES, Izard T. The Cytoskeletal Protein **α**-Catenin Unfurls upon Binding to Vinculin. *J Biol Chem*. 2012;287(22):18492-18499. doi:10.1074/jbc.M112.351023.

139. Peng X, Nelson ES, Maiers JL, DeMali KA. New Insights into Vinculin Function and Regulation. *Internal Review of Cell and Molecular Biology*. May 2011:1-39. doi:10.1016/B978-0-12-386043-9.00005-0.

140. Bakolitsa C, Cohen DM, Bankston LA, et al. Structural basis for vinculin activation at sites of cell adhesion. *Nature*. July 2004:1-4.

141. Carisey A, Tsang R, Greiner AM, et al. Vinculin Regulates the Recruitment and Release of Core Focal Adhesion Proteins in a Force-Dependent Manner. *Current Biology*. 2013;23(4):271-281. doi:10.1016/j.cub.2013.01.009.

142. Gumbiner BM. Regulation of cadherin-mediated adhesion in morphogenesis. *Nat Rev Mol Cell Biol*. 2005;6(8):622-634. doi:10.1038/nrm1699.

143. Collinet C, Lecuit T. Stability and Dynamics of Cell-Cell Junctions. *Progress in Molecular Biology and Translation Science*. June 2013.

144. Nelson WJ. Rugulation of cell-cell adhesion by the cadherin-catenin complex. *Biochemical Society Transactions*. June 2008:1-12. doi:10.1042/BST0360149.

145. Ratheesh A, Yap AS. A bigger picture: classical cadherins and the dynamic actin cytoskeleton. *Nat Rev Mol Cell Biol*. September 2012:1-7. doi:10.1038/nrm3431.

146. Brasch J, Harrison OJ, Honig B, Shapiro L. Thinking outside the cell: how cadherins drive adhesion. *Trends in Cell Biology*. June 2012:1-23. doi:10.1016/j.tcb.2012.03.004.

147. Shapiro L, Weis WI. Structure and Biochemistry of Cadherins and Catenins. *Cold Spring Harb Perspect Biol*. August 2009:1-23. doi:10.1101/cshperspect.a003053.

148. Yamada S, Pokutta S, Drees F, Weis WI, Nelson WJ. Deconstructing the Cadherin-Catenin-Actin Complex. *Cell*. 2005;123(5):889-901. doi:10.1016/j.cell.2005.09.020.

149. Yonemura S, Wada Y, Watanabe T, Nagafuchi A, Shibata M. α-Catenin as a tension transducer that induces adherens junction development. *Nature Publishing Group*. 2010;12(6):533-542. doi:10.1038/ncb2055.

150. Kim T-J, Zheng S, Sun J, et al. Dynamic Visualization of α-Catenin Reveals Rapid, Reversible Conformation Switching between Tension States. *Current Biology*. 2015;25(2):218-224. doi:10.1016/j.cub.2014.11.017.

151. Lyon RC, Zanella F, Omens JH, Sheikh F. Mechanotransduction in Cardiac Hypertrophy and Failure. *Circulation Research*. April 2015:1-15. doi:10.1161/CIRCRESAHA.116.304937.).

152. Li J, Gao E, Goossens S, van Roy F, Radice GL. Alpha-Catenins Control Cardiomyocyte Proliferation by Regulating Yap Activity. *Integrative Physiology*. December 2014:1-25. doi:10.1161/CIRCRESAHA.116.304472/-/DC1.

153. Folmsbee SS, Morales-Nebreda L, van Hengel J, et al. The cardiac protein αT-catenin contributes to chemical induced asthma. *American Journal of Physiology*. December 2014:1-6. doi:10.1152/ajplung.00331.2014.

154. Barry AK, Tabdili H, Muhamed I, et al. α-Catenin cytomechanics – role in cadherin-dependent adhesion and mechanotransduction. *Journal of Cell Science*. April 2014:1-31. doi:10.1242/jcs.139014.

155. Kwiatkowski AV, Pokutta S, Choi H-J, Nelson WJ, Weis WI. In vitro and in vivo reconstitution of the cadherin– catenin–actin complex from Caenorhabditis elegans. *Proc Natl Acad Sci USA*. January 2016:1-10. doi:10.1073/pnas.1007349107/-/DCSupplemental/pnas.1007349107_SI.pdf.

156. Miller PW, Pokutta S, Ghosh A, et al. Danio rerio αE-catenin Is a Monomeric F-actin Binding Protein with Distinct Properties from Mus musculus αE-catenin. *J Biol Chem*. 2013;288(31):22324-22332. doi:10.1074/jbc.M113.458406.

157. Siegel LM, Monty KJ. Determination of Molecular Weights and Frictional Ratios of Proteins in Impure Systems by use of Gel Filtration and Density Gradient Centrifugation. Application to Crude Preparations of Sulfite and Hydroxylamine Reductases. *Biochimica et Biophysica Acta (BBA) - Molecular Cell Research*. March 2003:1-17.

158. Choi SH, Estaras C, Moresco JJ, Yates JR, Jones KA. a-Catenin interacts with APC to regulate b-catenin proteolysis and transcriptional repression of Wnt target genes. *Genes and Development*. November 2013:1-17. doi:10.1101/gad.229062.113.

159. Hansen SD, Kwiatkowski AV, Ouyang C-Y, et al. αE-catenin actin-binding domain alters actin filament conformation and regulates binding of nucleation and disassembly factors. *Molecular Biology of the Cell*. November 2013:1-11. doi:10.1091/mbc.E13-07-0388).

160. Janssen MEW, Kim E, Liu H, et al. Three-Dimensional Structure of Vinculin Bound to Actin Filaments. *Molecular Cell*. January 2006:1-11. doi:10.1016/j.molcel.2005.11.020.

161. Bianchini JM, Kitt KN, Gloerich M, Pokutta S, Weis WI, Nelson WJ. Reevaluating αE-catenin monomer and homodimer functions by characterizing E-cadherin/αE-catenin chimeras. *J Cell Biol*. 2015;210(7):1065-1074. doi:10.1083/jcb.201411080.

162. Frank D, Frey N. Cardiac Z-disc Signaling Network. *J Biol Chem*. 2011;286(12):9897-9904. doi:10.1074/jbc.R110.174268.

163. Knudsen KA, Soler AP, Wheelock MJ. Interaction of a-Actinin with the Cadherin/Catenin Cell-Cell Adhesion Complex via a-Catenin. *J Cell Biol*. 1995:1-11.

164. Maki K, Han S-W, Hirano Y, Yonemura S, Hakoshima T, Adachi T. Mechano-adaptive sensory mechanism of α-catenin under tension. *Nature Publishing Group*. April 2016:1-9. doi:10.1038/srep24878.

165. Needham PG, Trumbly RJ. In vitro characterization of the Mig1 repressor from Saccharomyces cerevisiae reveals evidence for monomeric and higher molecular weight forms. *Yeast*. June 2006:1-16. doi:10.1002/yea.1429.

166. Fowler VM. Identification and purification of a novel Mr 43,000 tropomyosin-binding protein from human erythrocyte membranes. *J Biol Chem*. 1987;262(26):12792-12800. doi:10.1016/S0021-9258(18)45276-3.

167. Ehler E, Moore-Morris T, Lange S. Isolation and Culture of Neonatal Mouse Cardiomyocytes. *JoVE*. 2013;(79):1-10. doi:10.3791/50154.

168. Rubsam M, Broussard JA, Wickstrom SA, Nekrasova O, Green KJ, Niessen CM. Adherens Junctions and Desmosomes Coordinate Mechanics and Signaling to

Orchestrate Tissue Morphogenesis and Function: An Evolutionary Perspective. *Cold Spring Harb Perspect Biol*. October 2018:1-23. doi:10.1101/cshperspect.a029207.

169. Priest AV, Shafraz O, Sivasankar S. Biophysical basis of cadherin mediated cell-cell adhesion. *Experimental Cell Research*. 2017;358(1):10-13. doi:10.1016/j.yexcr.2017.03.015.

170. Meng W, Takeichi M. Adherens Junction: Molecular Architecture and Regulation. *Cold Spring Harb Perspect Biol*. November 2009:1-15. doi:10.1101/cshperspect.a002899.

171. Imamura Y, Nagafuchi A, Itoh M. Functional Domains of a-Catenin Required for the Strong State of Cadherin-based Cell Adhesion. *Journal of Cell Biology*. March 1999:1-12.

172. le Duc Q, Shi Q, Blonk I, et al. Vinculin potentiates E-cadherin mechanosensing and is recruited to actin-anchored sites within adherens junctions in a myosin II–dependent manner. *J Cell Biol*. 2010;189(7):1107-1115. doi:10.1083/jcb.201001149.

173. Maki K, Han S-W, Hirano Y, Yonemura S, Hakoshima T, Adachi T. Real-time TIRF observation of vinculin recruitment to stretched α-catenin by AFM. *Scientific Reports*. January 2018:1-8. doi:10.1038/s41598-018-20115-8.

174. Twiss F, le Duc Q, van der Horst S, et al. Vinculin-dependent Cadherin mechanosensing regulates efficient epithelial barrier formation. *Biology Open*. November 2012:1-15. doi:10.1242/bio.20122428.

175. Hulpiau P, Gul IS, van Roy F. New Insights into the Evolution of Metazoan Cadherins and Catenins. *Progress in Molecular Biology and Translation Science*. June 2013:1-1.

176. Pang SM, Le S, Kwiatkowski AV, Yan J. Mechanical stability of αT-catenin and its activation by force for vinculin binding. *Molecular Biology of the Cell*. July 2019:1-8. doi:10.1091/mbc.E19-02-0102).

177. Li Y, Merkel CD, Zeng X, et al. The N-Cadherin Interactome in Primary Cardiomyocytes as Defined Using Quantitative Proximity Proteomics. *Journal of Cell Science*. 2019;132(3):jcs229757–16. doi:10.1242/jcs.229757.

178. Wood MN, Ishiyama N, Singaram I, et al. α-Catenin homodimers are recruited to phosphoinositide-activated membranes to promote adhesion. *J Cell Biol*. 2017;54:jcb.201612006-jcb.201612017. doi:10.1083/jcb.201612006.

179. Huveneers S, Oldenburg J, Spanjaard E, et al. Vinculin associates with endothelial VE-cadherin junctions to control force-dependent remodeling. *Journal of Cell Biology*. March 2012:1-12. doi:10.1083/jcb.201108120.

180. Guo Z, Neilson LJ, Zhong H, et al. E-cadherin interactome complexity and robustness resolved by quantitative proteomics. *Science Signaling*. November 2014:1-28. doi:10.1126/scisignal.2005473.

181. Sakakibara S, Mizutani K, Sugiura A, et al. Afadin regulates actomyosin organization through αE-catenin at adherens junctions. *J Cell Biol*. 2020;219(5):549–16. doi:10.1083/jcb.201907079.

182. Oldenburg J, van der Krogt G, Twiss F, et al. VASP, zyxin and TES are tension-dependent members of Focal Adherens Junctions independent of the α-catenin-vinculin module. *Scientific Reports*. November 2015:1-14. doi:10.1038/srep17225.

183. Kobielak A, Fuchs E. α-Catenin: At the Junction of Intercellular Adhesion and Actin Dynamics. *Nat Rev Mol Cell Biol*. August 2004:1-28.

184. Abe K, Takeichi M. EPLIN mediates linkage of the cadherin–catenin complex to F-actin and stabilizes the circumferential actin belt. *Proc Natl Acad Sci USA*. January 2008:1-7.

185. Giannini AL, Vivanco MDM, Kypta RM. α-Catenin Inhibits β-Catenin Signaling by Preventing Formation of a β-Catenin·T-cell Factor·DNA Complex. *J Biol Chem*. 2000;275(29):21883-21888. doi:10.1074/jbc.M001929200.

186. Neuber S, Muhmer M, Wratten D, Koch PJ, Moll R, Schmidt A. The Desmosomal Plaque Proteins of the Plakophilin Family. *Dermatology Research and Practice*. April 2010:1-11. doi:10.1155/2010/101452.

187. Cerrone M, Montnach J, Lin X, et al. Plakophilin-2 is required for transcription of genes that control calcium cycling and cardiac rhythm. *Nature Communications*. July 2017:1-16. doi:10.1038/s41467-017-00127-0.

188. Pollard TD. Actin and Actin-Binding Proteins. *Cold Spring Harb Perspect Biol*. July 2016:1-19. doi:10.1101/cshperspect.a018226.

189. Hansen MDH, Kwiatkowski AV. Control of Actin Dynamics by Allosteric Regulation of Actin Binding Proteins. *Internal Review of Cell and Molecular Biology*. June 2013.

190. Lappalainan P. Actin-binding proteins: the long road to understanding the dynamic landscape of cellular actin networks. *Molecular Biology of the Cell*. August 2016:1-4. doi:10.1091/mbc.E15-10-0728.

191. Mullins RD, Hansen SD. In vitro studies of actin filament and network dynamics. *Current Opinion in Cell Biology*. 2013;25(1):6-13. doi:10.1016/j.ceb.2012.11.007.

192. Simpson RJ, Adams PD, Golemis E. *Basic Methods in Protein Purification and Analysis*. 2009.

193. Laemmli UK. Cleavage of structural proteins during the assembly of the head of bacteriophage T4. *Nature*. 1970;227(5259):680-685. doi:10.1038/227680a0.

194. Pollard TD. A Guide to Simple and Informative Binding Assays. *Molecular Biology of the Cell*. 2010;21(23):4061-4067. doi:10.1091/mbc.E10-08-0683.

195. Perrin BJ, Ervasti JM. The Actin Gene Family: Function Follows Isoform. *Cytoskeleton*. September 2010:1-5. doi:10.1002/cm.20475).

196. Tondeleir D, Vandamme D, Vandekerckhove J, Ampe C, Lambrechts A. Actin isoform expression patterns during mammalian development and in pathology: insights from mouse models. *Cell Motil Cytoskeleton*. 2009;66(10):798-815. doi:10.1002/cm.20350.

197. Prochniewicz E, Janson N, Thomas DD, La Cruz De EM. Cofilin Increases the Torsional Flexibility and Dynamics of Actin Filaments. *Journal of Molecular Biology*. October 2005:1-11. doi:10.1016/j.jmb.2005.09.021.

198. Kuhn JR, Pollard TD. Real-Time Measurements of Actin Filament Polymerization by Total Internal Reflection Fluorescence Microscopy. *Biophysj*. 2005;88(2):1387-1402. doi:10.1529/biophysj.104.047399.

199. Hansen SD, Zuchero JB, Mullins RD. Cytoplasmic Actin: Purification and Single Molecule Assembly Assays. In: Coutts AS, ed. *Adhesion Protein Protocols: Purification and Single Molecule*. Adhesion Protein Protocols. Totowa, NJ: Humana Press; 2013:145-170.